Immersed Interface Methods for Hyperbolic Systems of Partial Differential Equations with Discontinuous Coefficients

by

Chaoming Zhang

A dissertation submitted in partial fulfillment of
the requirements for the degree of

Doctor of Philosophy

University of Washington

1996

Approved by ______________________________

(Chairperson of Supervisory Committee)

____

____

Program Authorized
to Offer Degree ______________________________

Date ______________________________

University of Washington

Abstract

Immersed Interface Methods for Hyperbolic Systems of Partial Differential Equations with Discontinuous Coefficients

by Chaoming Zhang

Chairperson of Supervisory Committee: *Professor Randall J. LeVeque*
Department of Applied Mathematics

Numerical methods of second order accuracy are developed to solve hyperbolic systems of partial differential equations in heterogeneous media, containing sharp interfaces between different wave speeds. The solution to these equations exhibit nonsmoothness and/or discontinuities at the interfaces. High resolution multi-dimensional flux-limiter methods are used on a Cartesian grid. Near the interface, special formulas are developed using the Immersed Interface Method that incorporate the jump conditions and give pointwise second order accuracy even when the interface is not aligned with the grid. Applications to acoustics, elasticity and seismology are studied.

TABLE OF CONTENTS

List of Figures **iv**

List of Tables **ix**

Chapter 1: Introduction **1**

1.1 Wave Equations in Heterogeneous Media 1

1.2 Acoustics 2

1.3 Elasticity 4

1.4 The Immersed Interface Method 5

1.5 Immersed Interface Method for Wave Equations with Discontinuous Coefficients 7

1.6 Other Numerical Approaches for Wave Equations in Heterogeneous Media 10

1.7 Contributions of This Work 13

1.8 Overview of the Thesis 16

Chapter 2: Advection Equation **18**

Chapter 3: One Dimensional Acoustic Wave Equations **27**

Chapter 4: Two Dimensional Acoustic Wave Equations **32**

4.1 The Numerical Method 32

4.2 Computational Examples 42

4.3 Non-smooth Interface Problems 55

Chapter 5: Jump Conditions at the Interface for Acoustics **65**

5.1 One Dimensional Problem 65

5.2 Two Dimensional Problem 66

Chapter 6: Two Dimensional Elasticity **72**

6.1 Equations of Elasticity 72

6.2 P-wave and S-wave 74

6.3 Eigenvalues and Eigenvectors of A 77

6.4 Exact Solutions of Plane Waves for Elasticity 78

6.5 The Numerical Method 82

6.6 Coordinate Transformation 89

6.7 Computational Examples 92

Chapter 7: Jump Conditions at the Interface for Elasticity **109**

7.1 Linear Interface 109

7.2 Curved Interfaces 119

Chapter 8: Conclusions **137**

8.1 Current Work 137

8.2 Future Work 139

Bibliography **142**

Appendix A: Equations of Acoustics **149**

A.1 Equations of Acoustics 149

Appendix B: Conservation LAWs PACKage **151**

B.1 High resolution methods 151

Appendix C: Some Discussion about the Implementations **154**
C.1 Six Point Stencil 154

LIST OF FIGURES

1.1 Cartesian grids 6

2.1 1-D interface 19

2.2 1-D advection with $c^- = 2$ and $c^+ = 1$. The plots are the exact solutions at $t = 0$ (top), $t = 0.2$ (middle) and $t = 0.4$ (bottom) respectively. On the left is for jump condition $[U] = 0$ and on the right for jump condition $[cU] = 0$. 25

2.3 1-D advection with $c^- = 2$ and $c^+ = 1$. The plots are the computed solutions at $t = 0.2$ (top) and $t = 0.4$ (bottom) respectively. On the left is for jump condition $[U] = 0$ and on the right for jump condition $[cU] = 0$. The mesh size for the computation is $h = 1/100$. 26

3.1 A wave of three humps moving rightward in 1-D. After the wave hits the interface at $\alpha = 1/3$, it is transmitted and reflected. Solutions of velocity (top) and pressure (bottom) are plotted, with $c^- = 3$, $c^+ = 1$, $\rho^- = 2$, $\rho^+ = 3$. 31

4.1 2-D interface 33

4.2 Acoustic Plane Wave Reflected and Transmitted at an Interface . . . 42

4.3 Plane wave hitting an interface at an angle. Pressure contours of the exact solution at $t = 0$ (left) and $t = 0.45$ (right). The upward moving incident wave is split at the interface into a slower transmitted wave and a reflected wave. 46

4.4 Plane wave hitting an interface at an angle, as computed by CLAWPACK alone. Top: contours of velocity u (left) and pressure p (right). Bottom: slices of velocity u along $x = 0.6$ (left) and pressure p along $x = 0.35$ (right). The solid lines in the slices are the exact solutions. 46

4.5 Log-log plot of L_∞ errors for p and u with no limiter (plotted in o) and minmod limiter (plotted in *). (a) computed with CLAWPACK alone, with high lines for u, and low lines for p; (b) using Immersed Interface formula, with low lines for u, and high lines for p. 47

4.6 Plane wave hitting an interface at an angle, as computed by CLAWPACK with modified stencils near the interface based on the Immersed Interface Method. Top: contours of velocity u (left) and pressure p (right). Bottom: slices of velocity u along $x = 0.6$ (left) and pressure along $x = 0.35$ (right). The solid lines in the slices are the exact solutions. 48

4.7 Scatter pressure plots of the solution to the Example 4.2 using the immersed interface formulas. The true and computed pressure at each grid point is shown as a function of r, distance from the center of the radially-symmetric initial data. The vertical line marks the circular interface. (a) On a 120×120 grid. (b) On a 240×240 grid. 53

4.8 Log-log plots of L_1 (plotted in o) and of L_∞ (plotted in *) errors in p for Example 4.2. 53

4.9 Oscillatory plane wave hitting a lens-like region inside of which the sound speed is larger. Shown on the top is the contour plot of the pressure and on the bottom is the mesh plot (on a 100×100 grid). It is imputed on a 200×200 grid 56

4.10 Oscillatory plane wave hitting a lens-like region inside of which the sound speed is larger. Shown on the left is the contour plot of x-velocity and on the right is the slice of u at $x = 0.5$. 57

4.11 Oscillatory plane wave hitting a lens region inside of which the sound speed is larger. Shown on the top is the contour plot of the pressure and on the bottom is the mesh plot (on a 200×200 grid). 58

4.12 Oscillatory plane wave hitting a lens region inside of which the sound speed is larger. Shown on the left is the contour plot of x-velocity and on the right is the slice of u at $x = 0.3$. 59

4.13 Oscillatory plane wave of three humps hitting a region consisting of two media separated by a piecewise smooth interfaces. Shown are the contour plots of the pressure p at $t = 0.5$ (left) and $t = 0.7$ (right). . . 60

4.14 Oscillatory plane wave of three humps hitting a region consisting of two media separated by two interfaces. Shown are the contour plots of x-velocity u at $t = 0.5$ (left) and $t = 0.7$ (right). 61

4.15 Oscillatory plane wave of three humps hitting a region consisting of three media separated by two interfaces. Shown on the top is the contour plot of the pressure and on the bottom is the mesh plot. . . . 63

4.16 Oscillatory plane wave of three humps hitting a region consisting of three media separated by two interfaces. Shown on the left is the contour plot of x-velocity u and on the right is the slice of u at $x = 0.6$. 64

6.1 Elastic Plane Wave Reflected and Transmitted at an Interface 79

6.2 Oscillatory plane P-wave hump hitting a linear interface, creating four waves: reflected and transmitted P-waves and S-waves. Shown on the left is the contour plot of the exact solution of σ_{22} and on the right is that of computed σ_{22}. 93

6.3 Oscillatory plane P-wave hump hitting a linear interface, creating four waves: reflected and transmitted P-waves and S-waves. Shown on the top is the mesh plot of σ_{22} and on the bottom is that of y-velocity v_2. All the five waves are clearly shown. 94

6.4 Oscillatory plane P-wave hump hitting a linear interface, creating four waves: reflected and transmitted P-waves and S-waves. Shown on the left is the contour plot of the exact solution of y-velocity v and on the right is that of computed v. 95

6.5 Oscillatory plane P-wave hump hitting a linear interface. Slice plot of σ_{22} at $y = 0.25$ and $y = 0.6$, the former of which shows four waves; the latter is discontinuous at the interface. Solid lines denote the exact solutions; the 'o' symbol denote the computed solutions. 95

6.6 Oscillatory plane P-wave hump hitting a linear interface. Slice plots of y-velocity v at $y = 0.25$ and $y = 0.6$. The solid lines denote the exact solutions; 'o' symbol denote the computed solutions. 96

6.7 Oscillatory plane S-wave hump hitting a linear interface, creating four waves: reflected and transmitted P-waves and S-waves. Shown on the left is the contour plot of the exact solution of σ_{12} and on the right that of computed σ_{12}. 101

6.8 Slice plot of σ_{12} for an oscillatory plane S-wave hump hitting a linear interface. Four waves are captured at $y = 0.2$ (left), and at $y = 0.75$ (right), the solution is discontinuous at the interface. Solid lines denote the exact solutions, 'o' symbols denote computed solutions. 101

6.9 Oscillatory plane S-wave hump hitting a linear interface. Mesh plots of σ_{22} (top) and y-velocity v_2 (bottom), where for the latter the view for the transmitted P-wave is blocked by the transmitted S-wave. . . 102

6.10 Oscillatory plane S-wave hump hitting a linear interface, creating four waves: reflected and transmitted P-waves and S-waves. Shown on the left is the contour plot of the exact solution of y-velocity v_2 and on the right is that of computed v_2. 104
6.11 Oscillatory plane S-wave hump hitting a linear interface. Slice plot of y-velocity v_2 at $y = 0.2$ (left) and $y = 0.75$ (right). Solid lines denote the exact solution; 'o' symbols denote computed solutions. 105
6.12 Oscillatory plane S-wave hump hitting a linear interface, creating four waves: reflected and transmitted P-waves and S-waves. Solutions are obtained with the Lax-Wendroff method on regular points away from the interface. Shown on the left is the contour plot of σ_{12} and on the right is that of y-velocity v_2. 105
6.13 Oscillatory plane S-wave hump hitting a linear interface, creating four waves: reflected and transmitted P-waves and S-waves. Solutions are obtained with the Lax-Wendroff method on regular points away from the interface. Shown on the left is the slice plot of σ_{12} at $y = 0.2$ and on the right is that of y-velocity v_2. 106
6.14 Oscillatory plane wave of a hump hitting a circular interface. Shown on the left is the contour plot of σ_{12} and on the right is that of σ_{22}. . 107
6.15 Oscillatory plane wave of a hump hitting a circular interface. Shown on the left is the contour plot of x-velocity u and on the right is that of y-velocity v. 108

LIST OF TABLES

4.1 Errors in u at Slice $x = 0.6$ minmod Limiter 49

4.2 Errors in u at Slice $x = 0.6$ with no Limiter 49

4.3 Errors in p at Slice $x = 0.35$ with minmod Limiter 50

4.4 Errors in p at Slice $x = 0.35$ with no Limiter 50

4.5 Computational Cost Comparison 51

4.6 Errors in p for the Radially Symmetric Problem with no Limiter . . . 54

6.1 Errors in σ_{22} at Slice $y = 0.6$ 96

6.2 Errors in σ_{22} at Slice $y = 0.25$ 97

6.3 Errors in v_2 at Slice $y = 0.6$ 97

6.4 Errors in v_2 at Slice $y = 0.25$ 98

6.5 Computational Cost Comparison 99

6.6 Errors in σ_{12} at Slice $y = 0.75$ 103

6.7 Errors in σ_{12} at Slice $y = 0.2$ 103

ACKNOWLEDGMENTS

I am grateful to my advisor Professor Randy LeVeque for his invaluable guidance, assistance, countless corrections, and frequent encouragement. He not only introduced me to numerical analysis, but also guided me, with great insight and patience, into the depth and breadth of my research subjects. He has been an unparalleled advisor, mentor and friend.

I would like to thank my supervisory committee for their support and time. In particular, professors Loyce Adams and Ken Bube both read my manuscript closely and had valuable comments; professors K.K. Tung and George Turkiyyah gave me constructive suggestions and encouragement.

I would also like to express my appreciation to professor Fred Wan for his inspirational support in my early years of study.

Thanks also to my officemates Ted Stern, Wendy Welch, Donna Calhoun and Dave Salinger for reading and correcting this manuscript and for their help with my English and knowledge of the American culture.

I am thankful to the faculty, staff and students in the Department of Applied Mathematics for providing me with a first class education, quality facilities and a stimulating and cooperative environment.

My wife Ying and son Jimmy know but do not hear often enough that their unlimited support throughout the years are vital to my success.

This work was supported in part by NSF grants DMS-9204329 and DMS-9303404 and DOE grant DE-FG06-93ER25181.

Chapter 1

INTRODUCTION

Linear wave equations are used in many applications such as acoustics, elasticity, and seismology to model the propagation of small disturbances in fluids or solids. In the study of wave equations for some physical problems, such as acoustic or elastic waves traveling through heterogeneous media, there can be discontinuities in the coefficients of the equations. The study of wave equations with discontinuous coefficients draws significant attention in a variety of fields, such as the oil exploration industry and mineral finding, as well as the study of earthquakes. In this dissertation we study the problem of accurately modeling such wave propagation phenomena on uniform Cartesian grids using second order finite difference methods that are specially developed near interfaces where the coefficients are discontinuous.

1.1 Wave Equations in Heterogeneous Media

Wave equations in heterogeneous media arise in many physical problems. As one example, consider the problem of transverse vibrations of an infinite string, with a discontinuity in density at a location $x = \alpha$. For $x < \alpha$ the string has a density ρ_1 and for $x > \alpha$ the density is ρ_2. The string is initially displaced to $f(x)$ at $t = 0$, with tension $\tau_0 =$ constant. Let ψ represent the nondimensionalized displacement normal to the string. We have the wave equation

$$\rho\psi_{tt} - (\tau_0\psi_x)_x = 0.$$

This is equivalent to the problem

$$\psi_{tt} - c^2\psi_{xx} = 0$$
$$\psi(x,0) = f(x), \quad \psi_t(x,0) = 0,$$

with

$$c^2 = \begin{cases} (c^-)^2 = \dfrac{\tau_0}{\rho_1} & \text{if} \quad x < \alpha, \\ (c^+)^2 = \dfrac{\tau_0}{\rho_2} & \text{if} \quad x > \alpha. \end{cases}$$

This equation has a discontinuous coefficient c. For the jump conditions at the interface $x = \alpha$, note that the normal component of the tension in the deflected string at any point (x,t) is $\tau_0\psi_x(x,t)$. This component must be continuous everywhere, including at the interface $x = \alpha$. Obviously, the displacement at $x = \alpha$ must also be continuous. So, for this physical model, we have the following jump conditions at the interface $x = \alpha$:

$$\psi(\alpha^-,t) = \psi(\alpha^+,t), \qquad \psi_x(\alpha^-,t) = \psi_x(\alpha^+,t),$$

where

$$\psi(\alpha^-,t) = \lim_{x\to\alpha-0} \psi(x,t), \qquad \psi(\alpha^+,t) = \lim_{x\to\alpha+0} \psi(x,t)$$

are the limiting values at $x = \alpha$ from left side and right side respectively. Using the square brackets $[\cdot]$ to express the jump (which we will use throughout this dissertation), we have

$$[\psi] = 0, \qquad [\psi_x] = 0.$$

1.2 Acoustics

Different physical problems lead to different wave equations and jump conditions at the interface. For example, consider the one-dimensional acoustic wave equation (see Appendix A):

$$\begin{aligned} \rho u_t + p_x &= 0 \\ p_t + \kappa u_x &= 0, \end{aligned} \tag{1.1}$$

where ρ is the density of the medium, u is the velocity, p is the pressure and κ is the compression (bulk) modulus. For the case of a heterogeneous medium, ρ and/or κ can be discontinuous at the interfaces between different media. Let $x = \alpha$ be the point separating the different media; then the coefficients are given as

$$(\rho,\ \kappa) = \begin{cases} (\rho^-,\ \kappa^-) & \text{if } \ x < \alpha, \\ (\rho^+,\ \kappa^+) & \text{if } \ x > \alpha. \end{cases}$$

The velocity and pressure must be continuous across the interface, and therefore the jump conditions at the interface are

$$[u] = 0, \quad [p] = 0.$$

This one-dimensional problem is often used as a model in seismology. The space coordinate z is usually used in place of x, representing the depth below the surface of the earth, and the discontinuities in the coefficients occur at interfaces between different layers in a vertically stratified earth.

Acoustic equations with discontinuous coefficients also arise in the study of ocean acoustics, where the interfaces between layers of water with different properties can cause reflections, as in the seismic case (*e.g.* [26]). Other applications include the study of acoustic lenses or waveguides and ultrasound imaging (*e.g.* [63, 64]).

1.3 Elasticity

A more complicated problem is the wave equation for elasticity, which in two spatial dimensions is governed by the equations (see Chapter 6.1)

$$\begin{aligned} v_{1t} &= \frac{1}{\rho}\left(\sigma_{11x} + \sigma_{12y}\right) \\ v_{2t} &= \frac{1}{\rho}\left(\sigma_{12x} + \sigma_{22y}\right) \\ \sigma_{11t} &= (\lambda + 2\mu)v_{1x} + \lambda v_{2y} \\ \sigma_{12t} &= \mu(v_{1y} + v_{2x}) \\ \sigma_{22t} &= \lambda v_{1x} + (\lambda + 2\mu)v_{2y}, \end{aligned}$$

with discontinuous coefficients

$$(\rho,\ \lambda,\ \mu) = \begin{cases} (\rho^-,\ \lambda^-,\ \mu^-) & \text{in} \quad \text{medium 1,} \\ (\rho^+,\ \lambda^+,\ \mu^+) & \text{in} \quad \text{medium 2} \end{cases}$$

at the interface $\mathcal{C}$ defined by $\mathcal{F}_{\text{int}}(x, y) = 0$. Here, v_i is the ith component of the velocity, σ_{ij} is the ijth component of the stress tensor, ρ is the density and λ and μ are Lamé constants. For the special case where the coordinate system is in the directions normal and tangential to the interface, the jump conditions are

$$[v_1] = [v_2] = [\sigma_{11}] = [\sigma_{12}] = 0.$$

The proper physical jump conditions for a general interface are derived in Chapter 7. Like acoustic wave equations, elasticity equations with discontinuous coefficients arise in many applications. Our original motivation was the study of acoustic or elastic waves in the earth. Material properties can change abruptly at interfaces between different geological materials. The acoustic wave equation is sometimes used as a simplified model for seismic modeling of the earth. The equations of linear elasticity theory are more properly used for modeling seismic waves. Here we develop techniques for solving the *forward* problem of modeling wave propagation in a known medium. Solving forward problems in heterogeneous media is extremely important in understanding the wave propagation behavior, including how waves are reflected and transmitted across the interface, especially across multiple interfaces. Furthermore, solution of the forward problem is an important ingredient in many methods for solving the *inverse* problem of determining the internal structure from boundary measurements. Solving inverse problems is critical in determining the layers of the earth's crust, e.g. in oil prospecting.

1.4 The Immersed Interface Method

1.4.1 Why we use Cartesian grids

We use Cartesian grids in our computation, even when the coefficients are discontinuous across some curved interfaces, mainly for two reasons. First, for complicated interfaces, generating and refining the uniform grid is robust and convenient. Using coordinates which depend on the interface, such as a body fitted grid, requires more effort in generating and refining the grid. Also, on a Cartesian grid, we can use standard solvers for wave equations at regular points away from interface. Since the interface is one dimension less than the dimension of the full region of the problem, relatively few points lie near the interface and it is only at these points where special formula must be used, e.g. at the point shown in Figure 1.1.

1.4.2 Review of Immersed Interface Method and Related Methods

C. S. Peskin [53, 54] developed the Immersed Boundary Method to solve the incompressible Navier-Stokes equations in a region with complicated moving boundaries. The physical problem being modeled was blood flow in beating heart, where the curve modeling the wall of a heart was immersed into a Cartesian grid with discrete delta functions for singular forces at the elastic boundary (the wall of the heart). With the discrete delta function approach in two dimensions, results of first order accuracy

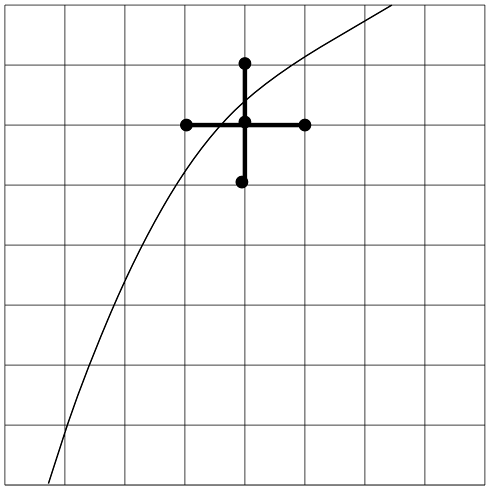

Figure 1.1: Cartesian grids

were obtained.

R. P. Beyer and R. J. LeVeque [7] analyzed a one-dimensional time-dependent model for the immersed boundary method and showed that, with an appropriate choice of the discrete delta function, second order accuracy could be obtained. This does not appear to carry over to two dimensions.

LeVeque and Li [41, 44, 46] developed an approach that gives second order accuracy in two spatial dimensions for the case of a Poisson problem, with discontinuous coefficients or singular source terms, giving rise to non-smooth solutions across an interface. The problem is to solve

$$(\beta u_x)_x + (\beta u_y)_y + \kappa(x,y)u = f(x,y) \qquad (x,y) \in \Omega$$

in some domain Ω with discontinuous β, κ and f at the interface and jump conditions in u and $\beta\dfrac{\partial u}{\partial n}$, where n is the direction normal to the specified interface. Jump conditions were built into a difference scheme near the interface, and a solution of second order accuracy was obtained.

Similar ideas have been used for the heat equation with discontinuous heat conduction coefficients [44, 45, 47, 51], for Stokes flow with immersed boundaries or free surfaces [40], and for nonlinear differential equations [62], and also coupled with multi-grid methods [2].

The term *Immersed Interface Method* was originally used in analogy to Peskin's Immersed Boundary Method, with the common theme that in both contexts some interface is immersed into a uniform grid. In contrast to the Immersed Boundary Method, which uses discrete delta function to model singularities, the Immersed Interface Method builds jump conditions into the stencil near the interface, and can also be extended to handle discontinuous coefficients as well as singular sources. In this sense, we will use the same name "Immersed Interface Method" for our method of solving wave equations with discontinuous coefficients.

The idea of modifying the coefficients of the difference scheme for differential equation with discontinuous coefficients dates back at least to Tikhonov and Samarskii in 1962 [59] who discussed methods for solving one-dimensional ordinary differential equations with discontinuous coefficients, particularly Sturm-Liouville problems. An interface (in this case, a point) lies in between two grid points, and a modified difference method was given on the two points near the interface.

1.5 Immersed Interface Method for Wave Equations with Discontinuous Coefficients

In our approach the interface of discontinuity will be *immersed* into a region of one dimension higher, which will be meshed with a Cartesian grid. Standard finite difference methods can be used away from the interface, for example the second order Lax-Wendroff method or the high resolution flux limiter methods from CLAWPACK [33] discussed in Appendix B. At grid points near the interface, however, we can not difference with any accuracy because of the discontinuity; the difference equations must be modified to take into account the discontinuity in the coefficient and resulting non-smoothness in the solution. Across such an interface some of the variables (e.g. stresses and velocity) will typically have a jump discontinuity, while the other components (e.g. pressure) will have jumps in their first derivatives.

Our main interest here is to incorporate the given jump conditions at a piecewise smooth interface into the numerical scheme to derive finite difference methods that are second order accurate at all grid points, including those adjacent to the interface. Numerical experiments presented in Section 4.2 and Section 6.7 indicate that the reflection and transmission of waves at the interface are modeled well, and second order accuracy is verified.

The approach used here relies on the fact that for these problems it is possible to determine jump conditions for the solution and its derivatives at the interface. Standard finite difference methods are typically derived using Taylor series expansions and rely on the assumption that the solution is smooth. These approximations are not valid in the neighborhood of an interface where the solution is not smooth. But if the location of the interface and the jumps in the solution and its derivatives are known at the interface, then it is possible to use this information to derive difference approximations that are accurate. We will briefly describe the procedures below.

We want to formulate a difference scheme at an irregular point near the interface. Let $U \in \mathbb{R}^m$ be the dependent vector variable of the linear hyperbolic system, then the formula for an irregular point $(i,\ j)$ near the interface is given by

$$U_{ij}^{n+1} = U_{ij}^{n} + \frac{k}{h}\sum_{l=1}^{6} \Gamma_{ij,l} U_{ij,l}^{n} \tag{1.2}$$

where the Γ's are $m \times m$ matrices, k and h are time step and spatial grid size respectively, and the $U_{ij,l}^{n}$ $(l = 1, 6)$ are values at nth time step at some set of grid points neighboring the point (i, j). The standard 5-point stencil together with one additional corner point is used.

We want to choose the Γ's so that second order accuracy is maintained. We start by analyzing the local truncation error, replacing the time derivatives with spatial derivatives by using the partial differential equations. Because the solution is smooth on both sides of the interface, we expand all terms up to second order derivatives around a nearby point P_0 on the interface using Taylor expansion. Expanding about P_0 rather than about some grid point, as frequently used in finite difference schemes, guarantees the validity of the expansion, given that solutions are smooth on both sides of the interface.

Note that U and its derivatives are discontinuous across the interface. Therefore the expression in the local truncation error of up to second order terms is a linear function of twelve terms: the values of U, U_ξ, U_η, $U_{\xi\xi}$, $U_{\xi\eta}$ and $U_{\eta\eta}$ on *both* sides of the interface at point P_0. A local coordinate system ξ-η , in the directions normal and tangential to the interface at point P_0, is introduced to simplify the computation because the physical jump conditions are specified in those directions. Then we derive jump conditions for every variable from the physical jump conditions and the hyperbolic system, and we also derive jump conditions for the first and second order derivatives of U. We can then express U and its first and second order derivatives on one side of the interface in terms of those on the other side. Therefore we are able to express all the terms of up to second order derivatives in the local truncation error by linear functions of U and its derivatives at point P_0 on *one* side of the interface, reducing the number of terms from twelve to six. This explains why we use a six point stencil in formula (1.2).

By forcing the coefficients of U, U_ξ, U_η, $U_{\xi\xi}$, $U_{\xi\eta}$ and $U_{\eta\eta}$ in the local truncation error to be zero, we obtain a system of linear algebra equations in the Γ's. The Γ's satisfying the six matrix equations make all the terms up to order two in the local truncation error zero, thereby giving a second order accurate scheme.

There are several advantages in solving hyperbolic systems of partial differential equations. First, it offers more generality. The techniques we introduce can be used for other linear first-order hyperbolic systems as well, such as Maxwell's equations.

Also, for example, consider a second order scalar wave equation such as

$$p_{tt} = c^2(p_{xx} + p_{yy}), \tag{1.3}$$

where p is the pressure of the acoustic wave with speed c. This can be rewritten as a first order hyperbolic system by introducing new variables corresponding to derivatives, so this is also a special case of a first order hyperbolic system. In addition, solving hyperbolic systems enables us to obtain multiple physical quantities simultaneously, e.g. the velocity components and the pressure in acoustics. Furthermore, working on a system gives a more natural and efficient treatment of the jump conditions for the solution at the interface (essential in applying the Immersed Interface Method), which depend strongly on the particular physical application. For the problems we analyzed, acoustics (and elasticity), there are physical jump conditions on the velocity, pressure (and stresses) which must be used.

1.6 Other Numerical Approaches for Wave Equations in Heterogeneous Media

Numerical simulation of seismic wave propagation problems in heterogeneous media can be traced back to as early as Alterman and Karal in 1968 [3] and Boore in 1972 [8]. Alterman and Karal developed a finite difference scheme to solve the equations of elasticity in one spatial dimension, and they applied their scheme to the problem of a layered half-space with a buried point source emitting a compressional pulse. The interface between different layers was placed at $z = h$ on the grid line, where z is the coordinate representing the depth below the surface of the Earth.

In two dimensions the analysis of finite difference schemes is usually limited to restricted interfaces, such as those that coincide with lines formed by the spatial grid. To model arbitrarily oriented interfaces with a Cartesian grid, one either accepts "stair-step" representations or uses schemes for averaging discontinuous coefficients to obtain intermediate grid values. Another possibility is to use a grid that is aligned with the interface. Here we list some references and their performance, focusing on the treatment and the complexity of the interface. Other related work can also be found in [1, 24, 25, 29, 42, 43, 49], and [60].

1.6.1 Staggered-grid technique

Many schemes are only able to handle simple representation of interfaces. A staggered-grid technique was introduced by Madariaga [50] to study a case of a circular fault. Virieux [61] presented a finite difference method for modeling P-SV wave propagation in heterogeneous media with an interface aligned with the grid. He decomposed the second-order elasticity wave equation into a system of two sets of first-order hyperbolic equations and obtained results of first order accuracy with the staggered-grid method.

Cao and Greenhalgh [12] decomposed the differential equations of motion for isotropic elasticity into two sets of equations which involve only first-order partial derivatives (one for the displacement fields and the other for the potential fields), which they then solved with the Leap-frog difference scheme. This work also falls into the category of staggered-grid techniques, and thus first order accuracy at the interface.

1.6.2 "Stair-step" interface method

P.P. Delsanto *et al.* [17] presented a local interaction simulation approach for the study of elastic wave propagation in two space dimensions. For the treatment of inhomogeneous media, interfaces from grid cell to grid cell were introduced. Then, taking into account the discontinuities, a special difference method was employed across the interfaces. This scheme led to a sharp interface model. However, this scheme, like many others, uses a "stair-step" to model interfaces. This will unfortunately lead to only first order accuracy across the interfaces.

1.6.3 Spectral methods

Some spectral methods are used for wave equations, but the interfaces are usually limited to simple situations.

Kosloff and Kessler *et al.* [15] used a spectral method for solving two dimensional equations of dynamic elasticity with linear interfaces aligned with the grids, based on a Chebychev expansion in the normal direction and a Fourier expansion for the horizontal direction.

Kosloff and Baysal [30] solved the two-dimensional acoustic wave equation with linear interfaces using a Fourier forward-modeling algorithm. The method utilized a spatial numerical grid to calculate spatial derivatives by the fast Fourier transform. Time derivatives are calculated by second order differencing.

1.6.4 Schemes using averaging of discontinuous coefficients

Schemes using average values of discontinuous coefficients, some of which are able to handle complicated geometry for the interface, have also been used. D. Brown [11] used an averaged wave speed and showed that it gave at least a first-order accurate approximation to the interface conditions. He also showed that, although such an averaging method was only first-order accurate, the numerical phase velocity has the same accuracy as a difference approximation. This was proved in the one-dimensional case, and demonstrated numerically for an example in two spatial dimensions with an obliquely oriented interface.

R. J. LeVeque [38] used CLAWPACK and averaged coefficients on the cells covering an arbitrary interface to deal with the discontinuity. The interface is approximated by averaging the physical parameters to obtain values in each uniform grid cell. This resulted in a good approximation, especially in the pressure p. But the solution in velocity is smeared across the interface of the discontinuity and only first order accuracy is obtained.

1.6.5 Finite element related method

Lysmer and Drake [48] solved the wave equation in the frequency domain for a non-homogeneous medium. Other examples can be found in [18] and [57]. A distinct advantage of finite elements is their flexibility to handle complicated geometries. With finite elements it is relatively straightforward to accommodate interfaces having complicated interface geometries. However, the cost for grid generation is high for complicated geometries.

The most competitive method by far, to the extent of the author's knowledge, is used by Card and Allen [13, 14], in the sense that it handles complicated interfaces and obtains second order accuracy. They used difference-like methods derived from finite-element theory for acoustic and elasticity wave equations with interfaces. They also made a good improvement in the treatment of complicated interfaces. The interface curve is approximated by piecewise linear segments, so it does not have to be aligned with any coordinate. However, this scheme appears to be very expensive. In order to get the expression for each irregular point, one needs to solve two large linear systems ($(n-1)\times(n-1)$, where n is the total number of grid points), whose elements are obtained by evaluating integrals. Therefore the cost for the expression of the irregular points appears to be significant. Moreover, in two dimensions, this approach would either yield only first order accuracy, or lose the ability to use explicit time-stepping, depending on whether or not approximation (quadrature) is used in evaluating the stiffness matrix.

1.7 Contributions of This Work

The "Immersed Interface Method" has been used previously to solve other types of equations, such as Poisson problems and the heat equation. This is the first known extension of these ideas to hyperbolic systems, resulting in an effective new method for solving wave equations in heterogeneous media. The following features distinguish the work in this dissertation from previous work.

• The problems analyzed in this dissertation are *systems* of equations, rather than scalar equations. Working on a system of equations allows us to solve for all the physical variables simultaneously, such as the components of velocity vector and stress tensor, as well as the pressure. The physical jump conditions are specified in terms of several of the physical quantities, introducing new difficulties.

• Unlike problems considered previously, for the two dimensional system of wave equations the number of physical jump conditions is less than the number of variables of the system. For example, in the acoustic equation, we have three variables (one in pressure, two in velocity), but we have only two physical jump conditions (in pressure and the normal velocity). We need to derive jump conditions for the remaining variables (the tangential velocity, in this case). This makes the derivation of the jump conditions for the system much more difficult, especially with a curved interface.

• In addition, we need to derive jump conditions for first and second derivatives of each variable as well. The difficulty of this work is significant. (See Chapters 4 and 6).

• This method has also been extended to handle some non-smooth interfaces, the first such extension for Immersed Interface Methods. Piecewise smooth interface problems, such as the acoustic lens problem, have been solved (see Chapter 4). Furthermore, this method is capable of solving problems with multiple interfaces intersecting each other, yielding the possibility of solving very interesting problems, such as the "pinch-out" problem in seismology (also see Chapter 4). This arises when two interfaces merge together into one. Examples in Section 4.2 shows that the transmitted and reflected waves are well modeled in the case where interfaces have kinks or where they intersect each other.

• Compared with other numerical schemes, solutions to wave equations obtained in this work give sharp discontinuities without smearing, regardless of the orientation, location, or complexity of the interface.

• Although the technique is a finite difference scheme, it has been successfully merged with the finite volume scheme implemented in CLAWPACK. Combining the special formula near the interface with CLAWPACK helps reduce dispersive oscillations and phase errors through the use of high resolution flux limiter methods (e.g. [35]) developed initially for capturing shock waves in compressible gas dynamics calculations. Also, this makes the treatment of boundary conditions easier.

• The Riemann solver for elasticity has been developed and successfully incorporated into CLAWPACK. This is one of the key components required by CLAWPACK.

• In contrast to other type of problems solved with the Immersed Interface Method, the work presented in this dissertation gives not only pointwise second order accuracy in the global error, but also in the local truncation error at each point.

• Furthermore, the cost of this work is relatively low because of the following. First, explicit time stepping is preserved. Second, our modified coefficients are applied only to the irregular points, which number far less than the total number of computational points. Third, we only need to compute the modified coefficients once as a pre-processing step before time-stepping. Moreover, the treatment of the interface is local. This means that at each irregular point, the size of the system we need to solve in order to obtain the modified coefficients does not depend on the mesh size. Finally, this pre-processing step has been made more efficient because the single large system that arises in determining the Γ's has been decoupled into several smaller systems (See Chapters 4 and 6). Computational cost comparisons in these chapters also confirm that the computational cost of this work is very low. The low cost should make the Immersed Interface Method practical and efficient also in solving inverse problems or moving interface problems.

• Solving hyperbolic systems offers more generality. For example, the wave equation of the acoustic pressure of the second order scalar form (1.3)

$$p_{tt} = c^2(p_{xx} + p_{yy}),$$

where $c = \sqrt{\kappa/\rho}$ is the wave speed, can simply be solved as a special case of the hyperbolic system we analyze, by introducing new variables corresponding to derivatives. This method can also be used to solve other wave equations, such as Maxwell's equations.

• The methods presented here are second order accurate, but the same ideas can be applied to derive higher order schemes near the interface for use in conjunction with higher order methods.

Using the Immersed Interface Method to solve wave equations with discontinuous coefficients is a new task. Solutions to wave equations behave very differently from solutions to other type of partial differential equations, especially with interfaces of discontinuity. When waves reach an interface of different media, they will be reflected and transmitted, creating two or more separate waves (e.g. transmitted and reflected P-waves and S-waves in elasticity). The results presented in this dissertation show that this behavior can be modeled accurately to second order.

1.8 Overview of the Thesis

Chapter 2 contains discussion of an advection equation, in order to clarify the application of the Immersed Interface Method to a hyperbolic equation with discontinuous coefficients. In Chapter 3, the one-dimensional acoustic problem is presented, followed by two-dimensional acoustics problems in Chapter 4.

The equations of elasticity in two dimensions are analyzed in Chapter 6. Detailed computational problems are presented in Chapter 4 and 6. Also, the exact solutions of acoustic plane wave and P-wave and S-wave in elasticity are obtained to verify the pointwise second order accuracy. The eigen-pairs of the matrices of the hyperbolic system are presented, and the Riemann solver algorithm needed in CLAWPACK is derived. The jump conditions of derivatives up to second order for the vector variables of the acoustics and the elasticity problems are derived in Chapters 5 and 7 respectively. The dissertation concludes in Chapter 8. Some background about acoustics is given in Appendix 6.1. Discussion about CLAWPACK and its application to acoustic and elasticity are provided in Appendix B, and some comments on the selection of the sixth point of the special formula at a point near the interface is given in Appendix C.

Chapter 2

ADVECTION EQUATION

The wave equations to which we will apply the Immersed Interface Method are systems of equations. This application is quite different from that to a scalar problem. However, we start with the simplest wave equation, a scalar advection equation (also called the one way wave equation):

$$U_t + a(x)U_x = 0$$

with

$$a(x) = c = \begin{cases} c^- & \text{if} \quad x < \alpha, \\ c^+ & \text{if} \quad x > \alpha. \end{cases}$$

Here U represents some physical quantity, $a(x)$ is the speed of the advection, with some jump condition specified. The jump condition will depend on the physical problem being studied. Suppose we are modeling the interface between two conveyor belts moving at different speeds, with U representing the density in terms of number of items per unit length on the belt. A drop in speed from the first belt to the second leads to an increase in density, so U will be discontinuous. The correct jump condition at the interface of the two conveyor belts is that the flux cU should be continuous; that is, the number of items crossing the interface per unit time must be the same on both sides. Thus the jump condition we impose is

$$[cU] = 0.$$

This is not the only possible jump condition one could impose, and different physical problems leads to different jump conditions. If U represents the concentration of a tracer in incompressible flow through a pipe with variable cross sectional area $\mathcal{A}(x)$, and hence velocity $a(x) = a_0/\mathcal{A}(x)$, where a_0 is some constant. The concentration should then be continuous and therefore the correct jump condition is

$$[U] = 0.$$

There are many ways to deal with advection equation both analytically and numerically. There is no need at all to use the Immersed Interface Method to solve this problem. We use this problem to illustrate our basic idea due to its simplicity.

The Lax-Wendroff method gives

$$U_j^{n+1} = U_j^n - \left(\frac{ka}{2h}\right)\left(U_{j+1}^n - U_{j-1}^n\right) + \frac{1}{2}\left(\frac{ka}{h}\right)^2\left(U_{j+1}^n - 2U_j^n + U_{j-1}^n\right),$$

where $U_j^n \approx U(x_j, t_n)$, h is mesh size, k is the time step, and $t_n = nk$. This is valid for all the regular points, i.e., those for which a discontinuous point does not lie in the interval of the 3-point stencil. Now consider the two irregular points J and $J+1$, with

$$x_J \leq \alpha < x_{J+1},$$

i.e., α is the interface location in between of points x_J and x_{J+1}. The Lax-Wendroff

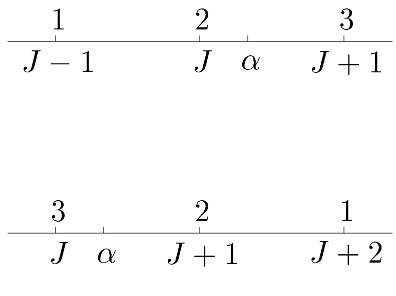

Figure 2.1: 1-D interface

method is based on the Taylor series expansion

$$\begin{aligned} U(x_j, t_{n+1}) &= U(x_j, t_n) + kU_t(x_j, t_n) + \frac{1}{2}k^2 U_{tt}(x_j, t_n) + \cdots \\ &= U(x_j, t_n) - akU_x(x_j, t_n) + \frac{1}{2}a^2k^2 U_{xx}(x_j, t_n) + \cdots, \end{aligned} \tag{2.1}$$

where the advection equation has been used repeatedly to replace U_t and U_{tt} by $-aU_x$ and a^2U_{xx} respectively. The Lax-Wendroff method results from replacing U_x and U_{xx} by centered finite difference approximations and dropping the higher order terms. This works well only if $U(x, t_n)$ is smooth in the interval from x_{j-1} to x_{j+1}. At the grid points $j = J$ and $J+1$ this is not the case, and centered approximations to these derivatives yield little or no accuracy.

We will assume that α is not exactly at a grid point, but lies strictly between points J and $J+1$ (see Figure 2.1). Then the Taylor series expansions (2.1) are still valid — the solution is smooth in both x and t at every grid point, even those near the interface. The problem comes in approximating U_x and U_{xx} by difference formulas that use values of U lying on both sides of the interface. The value $U_x(x_J, t_n)$, for example, cannot be approximated with any accuracy by $\frac{1}{2h}(U_{J+1} - U_{J-1})$. However, by taking into account the jumps in U and its derivatives at α, it is possible to find linear combinations of the grid values that do give accurate approximations to the derivatives at the grid points.

Rather than deriving expressions for U_x and U_{xx} separately, it is easiest to define a general three-point scheme of the form

$$\begin{aligned} U_J^{n+1} &= U_J^n + \frac{k}{h}(\gamma_{J,1}U_{J-1}^n + \gamma_{J,2}U_J^n + \gamma_{J,3}U_{J+1}^n) \\ U_{J+1}^{n+1} &= U_{J+1}^n + \frac{k}{h}(\gamma_{J+1,1}U_{J+2}^n + \gamma_{J+1,2}U_{J+1}^n + \gamma_{J+1,3}U_J^n), \end{aligned} \tag{2.2}$$

and then compute the proper γ coefficients so that the local truncation error gives second order accuracy.

Consider the local truncation error at J:

$$L = \frac{1}{h}(\gamma_{J,1}U_{J-1} + \gamma_{J,2}U_J + \gamma_{J,3}U_{J+1}) + aU_x - \frac{1}{2}ka^2U_{xx} + \mathrm{O}(k^2). \tag{2.3}$$

Taylor series expansion at $x = \alpha$ gives

$$
\begin{aligned}
L \;=\; & \frac{1}{h}\gamma_{J,1}\left(U^- + (x_{j-1}-\alpha)U_x^- + \frac{1}{2}(x_{j-1}-\alpha)^2 U_{xx}^-\right) \\
& + \frac{1}{h}\gamma_{J,2}\left(U^- + (x_j-\alpha)U_x^- + \frac{1}{2}(x_j-\alpha)^2 U_{xx}^-\right) \\
& + \frac{1}{h}\gamma_{J,3}\left(U^+ + (x_{j+1}-\alpha)U_x^+ + \frac{1}{2}(x_{j+1}-\alpha)^2 U_{xx}^+\right) \\
& + a\left(U_x^- + (x_J-\alpha)U_{xx}^-\right) - \frac{1}{2}ka^2 U_{xx}^- + \mathrm{O}(k^2).
\end{aligned}
\tag{2.4}
$$

Here, U^- means the limiting value of U as $x \to \alpha - 0$, and U^+ is the limiting value of U as $x \to \alpha + 0$, etc. We can eliminate U^+, U_x^+ and U_{xx}^+ by using jump conditions. For example, with the jump condition of the conveyor belt problem given by $[cU] = 0$, we can deduce the jump conditions for U_x and U_{xx} by using the advection equation:

$$
[cU] = 0 \quad \Longrightarrow \quad [cU_t] = 0 \quad \Longrightarrow \quad [c^2 U_x] = 0
$$

$$
[cU] = 0 \quad \Longrightarrow \quad [cU_{tt}] = 0 \quad \Longrightarrow \quad [c^3 U_{xx}] = 0,
$$

where advection equation has been used again to replace U_t and U_{tt} by $-cU_x$ and $c^2 U_{xx}$ respectively. Then we can express U^+, U_x^+ and U_{xx}^+ in terms of U^-, U_x^- and U_{xx}^- as follows:

$$
\begin{aligned}
U^+ &= d_1 U^- \\
U_x^+ &= d_2 U_x^- \\
U_{xx}^+ &= d_3 U_{xx}^-,
\end{aligned}
\tag{2.5}
$$

where,

$$
d_j = \left(\frac{c^-}{c^+}\right)^j, \quad (j = 1,\ 2,\ 3). \tag{2.6}
$$

Plugging (2.5) into (2.4) yields

$$
\begin{aligned}
L \;=\; & \frac{1}{h}\gamma_{J,1}\left(U^- + (x_{J-1}-\alpha)U_x^- + \frac{1}{2}(x_{J-1}-\alpha)^2 U_{xx}^-\right) \\
& + \frac{1}{h}\gamma_{J,2}\left(U^- + (x_J-\alpha)U_x^- + \frac{1}{2}(x_J-\alpha)^2 U_{xx}^-\right) \\
& + \frac{1}{h}\gamma_{J,3}\left(d_1 U^- + d_2(x_{J+1}-\alpha)U_x^- + \frac{1}{2}d_3(x_{J+1}-\alpha)^2 U_{xx}^-\right) \\
& + a\left(U_x^- + (x_J-\alpha)U_{xx}^-\right) - \frac{1}{2}ka^2 U_{xx}^- + \mathrm{O}(k^2),
\end{aligned}
\tag{2.7}
$$

or,

$$\begin{aligned}L \;=\; & \frac{1}{h}\left(\gamma_{J,1}+\gamma_{J,2}+d_1\gamma_{J,3}\right)U^- + \frac{1}{h}\Big(\,(x_{J-1}-\alpha)\gamma_{J,1} \\ & +(x_J-\alpha)\gamma_{J,2} +(x_{J+1}-\alpha)d_2\gamma_{J,3}+ha^-\Big)\,U_x^- \\ & +\frac{1}{2h}\Big(\,(x_{J-1}-\alpha)^2\gamma_{J,1}+(x_J-\alpha)^2\gamma_{J,2}+(x_{J+1}-\alpha)^2 d_3\gamma_{J,3} \\ & +2h(x_J-\alpha)a^- - kh(a^-)^2\Big)\,U_{xx}^- + \mathrm{O}(k^2).\end{aligned} \tag{2.8}$$

It will suffice for second order accuracy if we force the coefficients of U^-, U_x^- and U_{xx}^- to be zero, which leads to the 3×3 linear system for the 3 γ's

$$\begin{aligned}\alpha_{11}\gamma_{J,1}+\alpha_{12}\gamma_{J,2}+\alpha_{13}\gamma_{J,3}d_1 &= 0\\ \alpha_{21}\gamma_{J,1}+\alpha_{22}\gamma_{J,2}+\alpha_{23}\gamma_{J,3}d_2 &= -a^-\\ \alpha_{31}\gamma_{J,1}+\alpha_{32}\gamma_{J,2}+\alpha_{33}\gamma_{J,3}d_3 &= -2\alpha_{22}a^- + \frac{k}{h}(a^-)^2,\end{aligned} \tag{2.9}$$

where

$$\alpha_{ij} = \left(\frac{(x_{J+(j-2)}-\alpha)}{h}\right)^{i-1}, \quad i,j=1,2,3. \tag{2.10}$$

Similarly, at the point $J+1$ we obtain the linear equations

$$\begin{aligned}\hat\alpha_{11}\gamma_{J+1,1}+\hat\alpha_{12}\gamma_{J+1,2}+\hat\alpha_{13}\gamma_{J+1,3}d_1^{-1} &= 0\\ \hat\alpha_{21}\gamma_{J+1,1}+\hat\alpha_{22}\gamma_{J+1,2}+\hat\alpha_{23}\gamma_{J+1,3}d_2^{-1} &= -a^+\\ \hat\alpha_{31}\gamma_{J+1,1}+\hat\alpha_{32}\gamma_{J+1,2}+\hat\alpha_{33}\gamma_{J+1,3}d_3^{-1} &= -2\hat\alpha_{22}a^+ + \frac{k}{h}(a^+)^2,\end{aligned} \tag{2.11}$$

with the coefficients

$$\hat\alpha_{ij} = \left(\frac{(x_{J+1-(j-2)}-\alpha)}{h}\right)^{i-1}, \quad i,j=1,2,3. \tag{2.12}$$

The systems of linear equations (2.9) and (2.11) for γ's depend on the geometry, the media properties (coefficients of the wave equations), and the jump condition. It does not depend on the solution of the problem. Therefore we can compute the γ's once before time stepping for the problem of non-moving interface, and use the same γ's for every time step.

Previously we assumed that α is not exactly at a grid point, but lie strictly between theses points. This restriction can be lifted. For example, we can let $\alpha > x_J$ approach x_J, then equation (2.9) still holds. Therefore we can simply use the limiting value. Even if $\alpha = x_J$, and either U_x or U_{xx} is not defined at this point, both U_t and U_{tt} are well defined and continuous. Then from $U_t = -aU_x$ and $U_{tt} = a^2 U_{xx}$, either the left or the right space derivatives of U at $\alpha = x_J$ can be used. The derivation of equation (2.9) is valid with the understanding that either the left or the right space derivatives of U are used. Also note that $\alpha_{1j} = 1$ $(j = 1, 2, 3)$ in equation (2.10), which is used for concreteness. Therefore, the method and equations (2.9)-(2.12) are well defined even if $\alpha = x_J$.

For different jump conditions, we only need to make slight modification. Consider now the jump condition $[U] = 0$. We have

$$[U] = 0 \quad \Longrightarrow \quad [U_t] = 0 \quad \Longrightarrow \quad [cU_x] = 0 \tag{2.13}$$

$$[U] = 0 \quad \Longrightarrow \quad [U_{tt}] = 0 \quad \Longrightarrow \quad [c^2 U_{xx}] = 0, \tag{2.14}$$

where the advection equation has been used to replace U_t and U_{tt} by $-cU_x$ and $c^2 U_{xx}$ respectively. The expressions (2.5) for U^+, U_x^+ and U_{xx}^+ are still valid, with the modification of $d_1,\ d_2,\ d_3$ to

$$d_j = \left(\frac{c^-}{c^+}\right)^{j-1}, \quad (j = 1,\ 2,\ 3).$$

The linear equations for the γ's remain the same, but with these new value of $d_1,\ d_2,\ d_3$.

Here we will show two examples. Figure 2.2 gives the exact solutions to the advection equation with jump $[U] = 0$ (left) and $[cU] = 0$ (right) at $\alpha = 5/9$, at $t = 0$ (top), $t = 0.2$ (middle) and $t = 0.4$ (bottom) respectively. The initial data is a single hump given by

$$U(x,0) = \begin{cases} \dfrac{1}{2}\left(1 + \cos\left((x - 0.28)\pi/0.24\right)\right) & \text{if } 0.04 \le x \le 0.52, \\ 0 & \text{otherwise.} \end{cases}$$

The wave speeds are $c^- = 2$ and $c^+ = 1$. After reaching the interface, the wave speed changes accordingly on the other side. For the case of the jump condition $[U] = 0$, the solution value is continuous and the magnitude remains the same, while for the case of the jump condition $[cU] = 0$, the magnitude changes (amplified for our example) and there is a sharp jump in the solution,

Figure 2.3 gives the solutions computed on grid size $h = 1/100$ at $t = 0.2$ (top) and $t = 0.4$ (bottom) respectively. The symbols 'o' give the computed solutions and the solid lines give the exact solutions. On the left is for the jump condition $[U] = 0$ and on the right is for the jump condition $[cU] = 0$. The oscillations visible near the hump at time $t = 0.4$ are due to the use of Lax-Wendroff method. When the high-resolution methods of CLAWPACK are used instead, this dispersive error is greatly reduced (see examples in Chapters 4 and 6). Pointwise second order accuracy is observed.

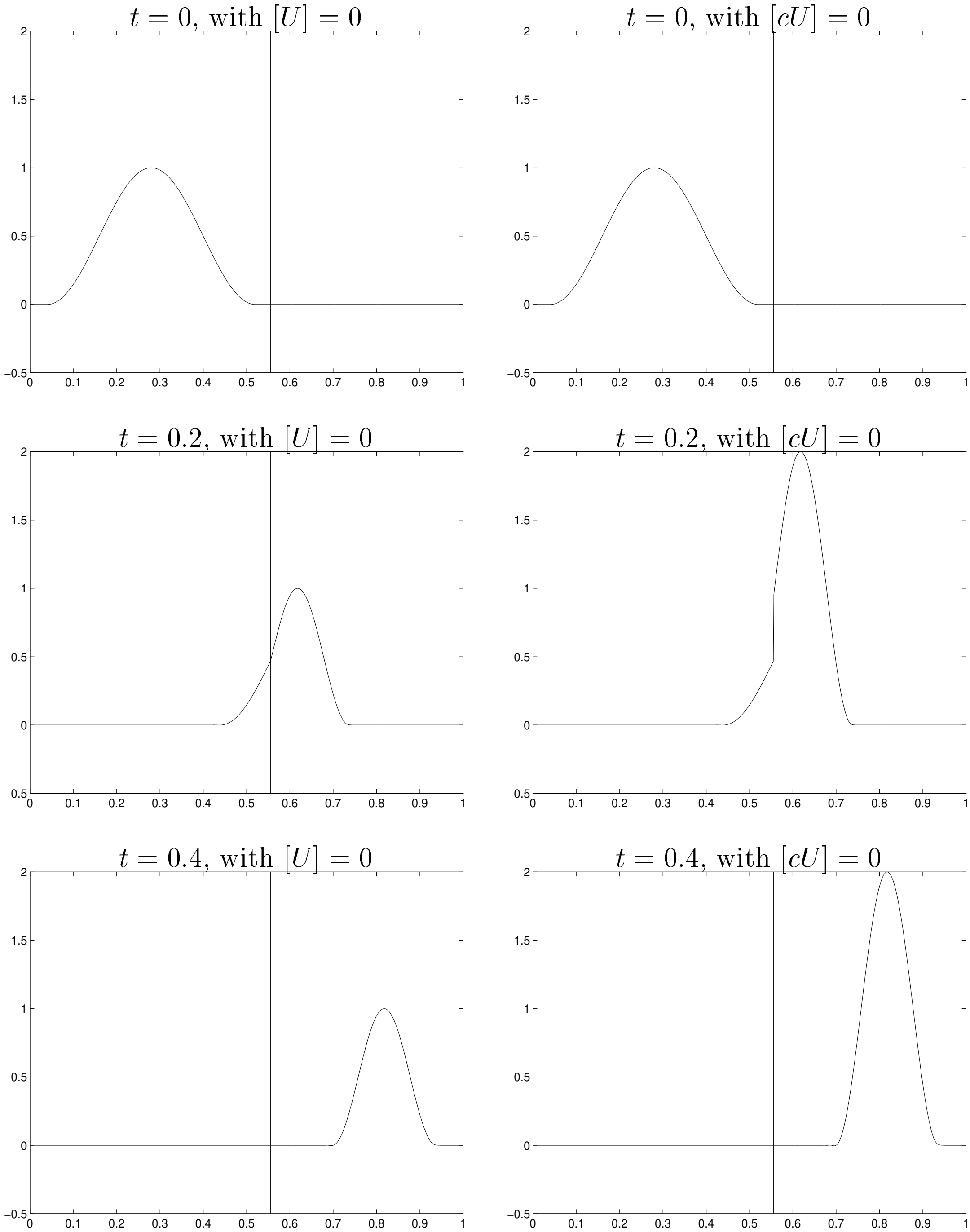

Figure 2.2: 1-D advection with $c^- = 2$ and $c^+ = 1$. The plots are the exact solutions at $t = 0$ (top), $t = 0.2$ (middle) and $t = 0.4$ (bottom) respectively. On the left is for jump condition $[U] = 0$ and on the right for jump condition $[cU] = 0$.

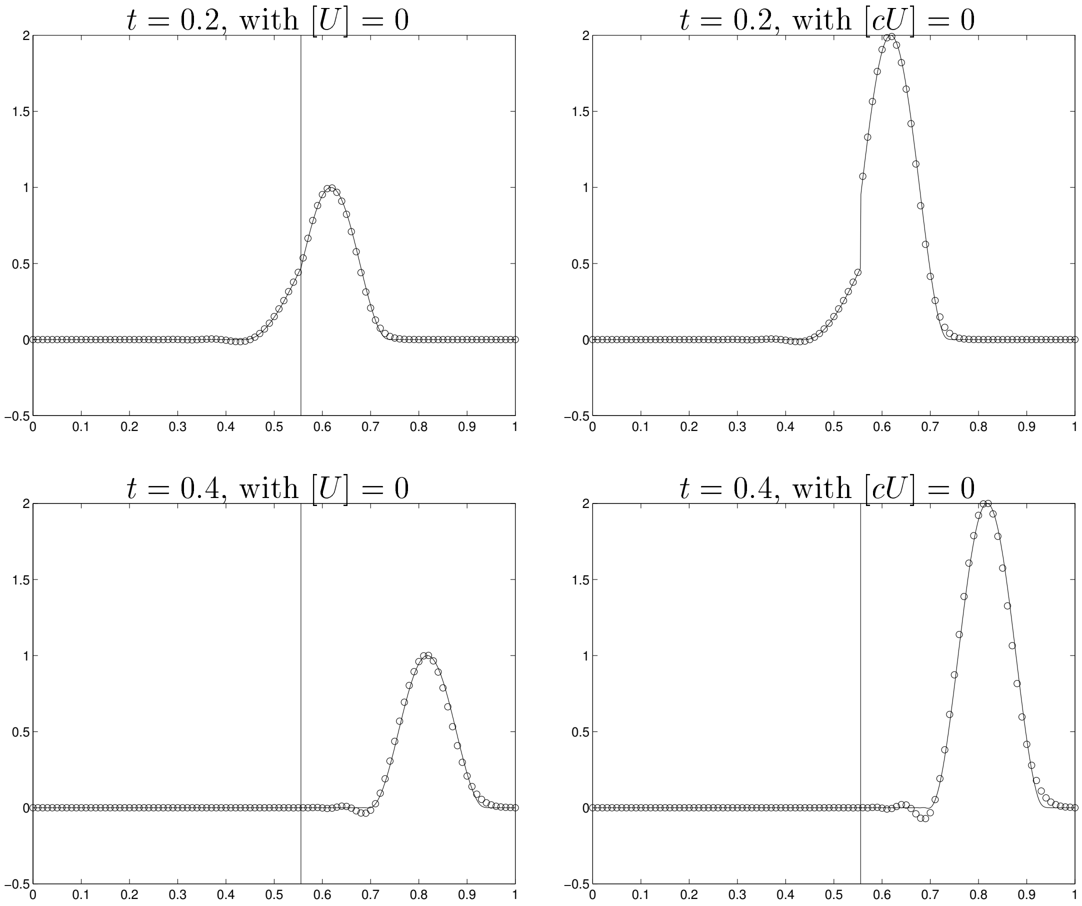

Figure 2.3: 1-D advection with $c^- = 2$ and $c^+ = 1$. The plots are the computed solutions at $t = 0.2$ (top) and $t = 0.4$ (bottom) respectively. On the left is for jump condition $[U] = 0$ and on the right for jump condition $[cU] = 0$. The mesh size for the computation is $h = 1/100$.

Chapter 3

ONE DIMENSIONAL ACOUSTIC WAVE EQUATIONS

The main interest of this thesis is to use the Immersed Interface Method to solve a system of wave equations with discontinuous coefficients, with acoustics and elasticity as the major applications. The acoustic wave equation in three spatial dimensions is given by (see Appendix A)

$$\begin{aligned} \rho \vec{v}_t + \bigtriangledown p &= 0 \\ p_t + \kappa \bigtriangledown \cdot \vec{v} &= 0, \end{aligned} \tag{3.1}$$

where ρ is the density of the medium, $\vec{v}$ is the velocity field, p is the pressure and κ is the compression (bulk) modulus. For the case of a heterogeneous medium, ρ and/or κ can be discontinuous at the interface between different media:

$$(\rho,\ \kappa) = \begin{cases} (\rho^-,\ \kappa^-) & \text{in medium 1,} \\ (\rho^+,\ \kappa^+) & \text{in medium 2.} \end{cases}$$

The jump conditions at the interfaces will be given below. In the one-dimensional case, where the velocity is only a function of x (say, the depth below the Earth's surface in seismology), we get

$$\begin{aligned} \rho u_t + p_x &= 0 \\ p_t + \kappa u_x &= 0, \end{aligned} \tag{3.2}$$

with the jump conditions given by

$$[u] = 0, \quad [p] = 0 \tag{3.3}$$

at the interface $x = \alpha$, i.e., both the velocity and the pressure are continuous. The coefficients are discontinuous across the interface $x = \alpha$:

$$(\rho,\ \kappa) = \begin{cases} (\rho^-,\ \kappa^-) & \text{if } x < \alpha, \\ (\rho^+,\ \kappa^+) & \text{if } x > \alpha. \end{cases}$$

This one-dimension problem is often used as a model in seismology. The space coordinate z is usually used in place of x, representing the depth underneath the surface of the Earth, and the discontinuities in the coefficients occur at interfaces in a vertically stratified Earth.

Let

$$U = \begin{pmatrix} u(x,t) \\ p(x,t) \end{pmatrix}, \quad A = \begin{pmatrix} 0 & (1/\rho) \\ \kappa & 0 \end{pmatrix}.$$

This yields a system of first order equations

$$U_t + AU_x = 0. \tag{3.4}$$

In the region where A is smooth, the standard Lax-Wendroff method can be used:

$$U_j^{n+1} = U_j^n - \frac{k}{2h}A(U_{j+1}^n - U_{j-1}^n) + \frac{1}{2}\left(\frac{k}{h}\right)^2 A^2(U_{j+1}^n - 2U_j^n + U_{j-1}^n). \tag{3.5}$$

This can be used at all points $j \neq J,\ J+1$, where J is such that

$$x_J \leq \alpha < x_{J+1}.$$

At the two points J and $J+1$, we can no longer use the Lax-Wendroff method because of the discontinuity at the interface. Analogous to the case of the advection equation, we will use a more general 3-point difference scheme of the form:

$$\begin{aligned} U_J^{n+1} &= U_J^n + \frac{k}{h}(\Gamma_{J,1}U_{J-1}^n + \Gamma_{J,2}U_J^n + \Gamma_{J,3}U_{J+1}^n) \\ U_{J+1}^{n+1} &= U_{J+1}^n + \frac{k}{h}(\Gamma_{J+1,1}U_{J+2}^n + \Gamma_{J+1,2}U_{J+1}^n + \Gamma_{J+1,3}U_J^n). \end{aligned} \tag{3.6}$$

But U is now a vector variable and the Γ's are 2×2 matrices, in contrast to the advection problem discussed in Chapter 2, where U and γ's are scalars. We want to choose the Γ's so that second order accuracy is maintained. Again, consider the local truncation error at J:

$$L = \frac{1}{h}(\Gamma_{J,1}U^n_{J-1} + \Gamma_{J,2}U^n_J + \Gamma_{J,3}U^n_{J+1}) + \left(AU_x - \frac{1}{2}kA^2U_{xx}\right)^n_J + \mathrm{O}(k^2). \tag{3.7}$$

Expanding each U at $x = \alpha$ gives

$$\begin{aligned} L \;=\; & \frac{1}{h}\Gamma_{J,1}\left(U^- + (x_{J-1}-\alpha)U^-_x + \frac{1}{2}(x_{J-1}-\alpha)^2U^-_{xx}\right) \\ & +\frac{1}{h}\Gamma_{J,2}\left(U^- + (x_J-\alpha)U^-_x + \frac{1}{2}(x_J-\alpha)^2U^-_{xx}\right) \\ & +\frac{1}{h}\Gamma_{J,3}\left(d_1U^+ + d_2(x_{J+1}-\alpha)U^+_x + \frac{1}{2}d_3(x_{J+1}-\alpha)^2U^+_{xx}\right) \\ & +A\left(U^-_x + (x_J-\alpha)U^-_{xx}\right) - \frac{1}{2}kA^2U^-_{xx} + \mathrm{O}(k^2). \end{aligned} \tag{3.8}$$

Here, superscripts $-$ and $+$ are the same as those defined in Chapter 2. We can express U^+, U^+_x and U^+_{xx} in terms of U^-, U^-_x and U^-_{xx} by using jump conditions. The derivation in Chapter 5 will give us the following jump conditions:

$$\begin{aligned} U^+ &= D_1U^- \\ U^+_x &= D_2U^-_x \\ U^+_{xx} &= D_3U^-_{xx}, \end{aligned} \tag{3.9}$$

where $D_1,\ D_2,\ D_3$ are now 2×2 matrices given by

$$D_1 = I, \quad D_2 = \mathrm{diag}\left(\kappa^-/\kappa^+,\ \rho^+/\rho^-\right), \quad D_3 = \left(c^-/c^+\right)^2 I. \tag{3.10}$$

Substituting the interface conditions (3.9) into (3.8) gives

$$\begin{aligned} L \;=\; & \frac{1}{h}\Gamma_{J,1}\left(U^- + (x_{J-1}-\alpha)U^-_x + \frac{1}{2}(x_{J-1}-\alpha)^2U^-_{xx}\right) \\ & +\frac{1}{h}\Gamma_{J,2}\left(U^- + (x_J-\alpha)U^-_x + \frac{1}{2}(x_J-\alpha)^2U^-_{xx}\right) \\ & +\frac{1}{h}\Gamma_{J,3}\left(D_1U^- + (x_{J+1}-\alpha)D_2U^-_x + \frac{1}{2}(x_{J+1}-\alpha)^2D_3U^-_{xx}\right) \\ & +A\left(U^-_x + (x_J-\alpha)U^-_{xx}\right) - \frac{1}{2}kA^2U^-_{xx} + \mathrm{O}(k^2), \end{aligned} \tag{3.11}$$

or,

$$
\begin{aligned}
L \;=\; & \frac{1}{h}\left(\Gamma_{J,1}+\Gamma_{J,2}+\Gamma_{J,3}D_1\right)U^- + \frac{1}{h}\Big(\,(x_{J-1}-\alpha)\Gamma_{J,1} \\
& +(x_J-\alpha)\Gamma_{J,2} +(x_{J+1}-\alpha)\Gamma_{J,3}D_2 + ha^-\Big)\,U_x^- \\
& +\frac{1}{2h}\Big(\,(x_{J-1}-\alpha)^2\Gamma_{J,1}+(x_J-\alpha)^2\Gamma_{J,2}+(x_{J+1}-\alpha)^2\Gamma_{J,3}D_3 \\
& +2h(x_J-\alpha)A^- - kh(A^-)^2\Big)\,U_{xx}^- + \mathrm{O}(k^2).
\end{aligned}
\tag{3.12}
$$

It will suffice for second order accuracy if we force the coefficients of U^-, U_x^- and U_{xx}^- to be zero, which leads to a system of matrix equations:

$$
\begin{aligned}
&\alpha_{11}\Gamma_{J,1}+\alpha_{12}\Gamma_{J,2}+\alpha_{13}\Gamma_{J,3}D_1 = 0 \\
&\alpha_{21}\Gamma_{J,1}+\alpha_{22}\Gamma_{J,2}+\alpha_{23}\Gamma_{J,3}D_2 = -A^- \\
&\alpha_{31}\Gamma_{J,1}+\alpha_{32}\Gamma_{J,2}+\alpha_{33}\Gamma_{J,3}D_3 = -2\alpha_{22}A^- + \frac{k}{h}(A^-)^2,
\end{aligned}
\tag{3.13}
$$

with α_{ij} $(i,\ j=1,2,3)$ defined in (2.10).

Similarly, at the point $J+1$ we obtain the system of equations

$$
\begin{aligned}
&\hat\alpha_{11}\Gamma_{J+1,1}+\hat\alpha_{12}\Gamma_{J+1,2}+\hat\alpha_{13}\Gamma_{J+1,3}D_1^{-1} = 0 \\
&\hat\alpha_{21}\Gamma_{J+1,1}+\hat\alpha_{22}\Gamma_{J+1,2}+\hat\alpha_{23}\Gamma_{J+1,3}D_2^{-1} = -A^+ \\
&\hat\alpha_{31}\Gamma_{J+1,1}+\hat\alpha_{32}\Gamma_{J+1,2}+\hat\alpha_{33}\Gamma_{J+1,3}D_3^{-1} = -2\hat\alpha_{22}A^+ + \frac{k}{h}(A^+)^2,
\end{aligned}
\tag{3.14}
$$

where $\hat\alpha_{ij}$ $(i,\ j=1,2,3)$ are as shown in (2.12). Equations (3.13) and (3.14) can be solved for the Γ's. Fortunately, because the matrices D_1, D_2 and D_3 are diagonal, each system (i.e. (3.13) and (3.14)) can be decoupled into four disjoint 3×3 systems of equations for the four components of the Γ matrices, each of which is 3×3. It is then very easy to get the solutions of Γ's. It can also be noticed that, not surprisingly, (2.9) and (3.13) are of the same form, with d_1, d_2, d_3 and a in (2.9) corresponding to D_1, D_2, D_3 and A in (3.13) respectively.

Figure 3.1 shows the plots of the velocity (top) and pressure (bottom) respectively, for the equation (3.2) with $c^- = 3,\ c^+ = 1,\ \rho^- = 2$ and $\rho^+ = 3$. A wave of three humps moving rightward. Without the interface of discontinuity, the wave would have moved completely rightward. With the interface (at $\alpha = 1/3$), the wave is transmitted and reflected at the interface, which can be clearly observed from the plots. Again, pointwise second order accuracy has been verified.

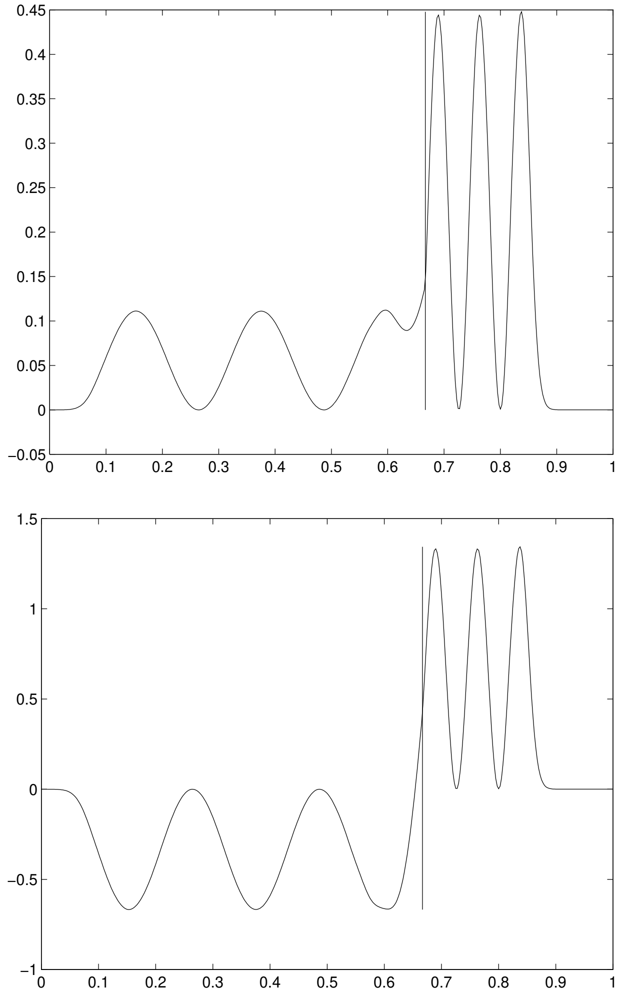

Figure 3.1: A wave of three humps moving rightward in 1-D. After the wave hits the interface at $\alpha = 1/3$, it is transmitted and reflected. Solutions of velocity (top) and pressure (bottom) are plotted, with $c^{-} = 3$, $c^{+} = 1$, $\rho^{-} = 2$, $\rho^{+} = 3$.

Chapter 4

TWO DIMENSIONAL ACOUSTIC WAVE EQUATIONS

4.1 The Numerical Method

We now consider the two-dimensional acoustic wave equations

$$\begin{aligned} &\rho u_t + p_x = 0 \\ &\rho v_t + p_y = 0 \\ &p_t + \kappa(u_x + v_y) = 0, \end{aligned} \tag{4.1}$$

where u and v are the components of the velocity in the x and y directions and p is the pressure. The density, ρ, and the bulk modulus, κ, are discontinuous

$$(\rho,\ \kappa) = \begin{cases} (\rho^-,\ \kappa^-) & \text{if } \mathcal{F}_{\text{int}}(x,y) < 0, \\ (\rho^+,\ \kappa^+) & \text{if } \mathcal{F}_{\text{int}}(x,y) > 0 \end{cases}$$

at the interface $\mathcal{C}$ defined by $\mathcal{F}_{\text{int}}(x,y) = 0$. For example, consider two layers of media below the surface of the earth separated at the depth α. By defining x as the vertical direction (downward) and y as the horizontal direction, we have $\mathcal{F}_{\text{int}}(x,y) = x - \alpha$. The physical jump conditions are similar to (3.3) from the one dimensional case:

$$[\vec{n} \cdot \vec{u}] = [p] = 0, \tag{4.2}$$

where $\vec{n}$ is the unit vector in the direction normal to the interface. That is, the velocity normal to the interface and the pressure are continuous across the interface. In contrast to the one-dimensional problem, where the number of the physical jump conditions equals the number of variables in the problem, here we have only two physical jump conditions and three variables. This naturally brings new difficulties.

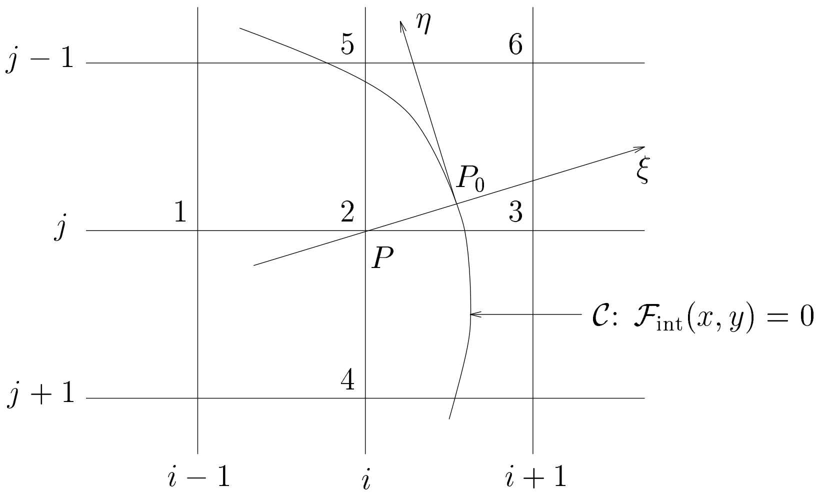

Figure 4.1: 2-D interface

The jump conditions specified in (4.2) come from the physical nature of the acoustic wave equation, and specifying additional jumps would be irrelevant physically and lead to an overdetermined problem. The fact that the number of physical jump conditions is fewer than that of the variables of the system simply makes the derivation of the derivative jump conditions more difficult. We will see these derivations in Chapter 5 (for acoustics) and Chapter 7 (for elasticity).

The jump condition for the velocity component in the direction tangential to the interface can be deduced from the jump conditions for $\vec{n} \cdot \vec{v}$ and p, together with the initial conditions. We parameterize locally the interface curve $\mathcal{C}$ with parameter τ by

$$(x(\tau), y(\tau)) \in \mathcal{C},$$

such that

$$\mathcal{F}_{\text{int}}\left(x(\tau), y(\tau)\right) = 0.$$

For any given τ such that $(x(\tau), y(\tau)) \in \mathcal{C}$, let

$$\begin{aligned} \overline{u} &= \text{component of } \vec{u} \text{ in the } \xi \text{ direction} \\ \overline{v} &= \text{component of } \vec{u} \text{ in the } \eta \text{ direction} \end{aligned}$$

and ξ and η be in the directions normal and tangential to the interface at $(x(\tau), y(\tau))$ respectively (see Figure 4.1). Note that we can then write equation (3.1) in ξ-η coordinates, which will be of the same form as (4.1) due to isotropy:

$$\begin{aligned} \rho\overline{u}_t + p_\xi &= 0 \\ \rho\overline{v}_t + p_\eta &= 0 \\ p_t + \kappa(\overline{u}_\xi + \overline{v}_\eta) &= 0. \end{aligned} \tag{4.3}$$

Note that a bar over p is not necessary as the pressure p is a scalar. From the second equation of (4.3), we have

$$[p] = 0 \quad \Longrightarrow \quad [p_\eta] = 0 \quad \Longrightarrow \quad [\rho\overline{v}_t] = 0 \quad \Longrightarrow \quad [\rho\overline{v}]_t = 0.$$

Thus $[\rho\overline{v}] = 0$, provided that it is true initially. Our jump conditions therefore are given by

$$[\overline{u}] = 0, \quad [\rho\overline{v}] = 0, \quad [p] = 0. \tag{4.4}$$

Returning to equation (4.1), let

$$U = \begin{pmatrix} u(x,y,t) \\ v(x,y,t) \\ p(x,y,t) \end{pmatrix}, \quad A = \begin{pmatrix} 0 & 0 & (1/\rho) \\ 0 & 0 & 0 \\ \kappa & 0 & 0 \end{pmatrix}, \quad B = \begin{pmatrix} 0 & 0 & 0 \\ 0 & 0 & (1/\rho) \\ 0 & \kappa & 0 \end{pmatrix}.$$

We have the 3-variable first order system

$$U_t + AU_x + BU_y = 0. \tag{4.5}$$

In the region where A and B are smooth, we can use standard numerical schemes. As in the one dimensional case, the Lax-Wendroff method can be used:

$$\begin{aligned} U_{ij}^{n+1} &= U_{ij}^n - \frac{k}{2h}\left(A(U_{i+1,j}^n - U_{i-1,j}^n) + B(U_{i,j+1}^n - U_{i,j-1}^n)\right) \\ &+ \frac{1}{2}\left(\frac{k}{h}\right)^2 \left(A^2\left(U_{i+1,j}^n - 2U_{ij}^n + U_{i-1,j}^n\right) \right. \\ &+ (AB+BA)\left(U_{i+1,j+1}^n - U_{i-1,j+1}^n - U_{i+1,j-1}^n + U_{i-1,j-1}^n\right) \\ &\left. + B^2\left(U_{i,j+1}^n - 2U_{ij}^n + U_{i,j-1}^n\right)\right). \end{aligned} \tag{4.6}$$

This is valid at regular points, where all *nine* points in the stencil lie on the same side of the interface, i.e.

$$\mathcal{F}_{\text{int}}(x_i, y_j)\mathcal{F}_{\text{int}}(x_{\tilde{i}}, y_{\tilde{j}}) \geq 0, \tag{4.7}$$

for $\tilde{i} = i-1,\ i,\ i+1$; $\tilde{j} = j-1,\ j,\ j+1$.

A careful investigation will give us a simpler form in applying the standard Lax-Wendroff method. Note that $U_{tt} = c^2\left(U_{xx} + U_{yy}\right)$, with $c = \sqrt{\kappa/\rho}$, which is really what we need in the formation of the second order derivative term in this method. Then we have

$$\begin{aligned} U_{ij}^{n+1} &= U_{ij}^n - \frac{k}{2h}\bigg(A(U_{i+1,j}^n - U_{i-1,j}^n) + B(U_{i,j+1}^n - U_{i,j-1}^n)\bigg) \\ &\quad + \frac{1}{2}\left(\frac{k}{h}\right)^2 c^2\left(U_{i+1,j}^n + U_{i-1,j}^n + U_{i,j+1}^n + U_{i,j-1}^n - 4U_{ij}^n\right). \end{aligned} \tag{4.8}$$

This is valid at regular points, where all $five$ points in the stencil lie on the same side of the interface, that is, the inequality (4.7) holds for $\tilde{i} = i$ and $\tilde{j} = j-1,\ j,\ j+1$; $\tilde{j} = j$ and $\tilde{i} = i-1,\ i+1$. Equation (4.8) is better than (4.6). There are no cross derivatives in (4.8), and therefore a 5-point instead of 9-point stencil is employed, which reduces the number of irregular points and computational cost on both regular and irregular points. As our computation indicates, (4.8) gives better results than (4.6) as well.

At irregular points, where some of the points of the 5-point stencil are on opposite sides of the interface, the Lax-Wendroff method is no longer valid. At these points a 6-point difference scheme of the form

$$U_{ij}^{n+1} = U_{ij}^n + \frac{k}{h}\sum_{l=1}^{6}\Gamma_{ij,l}U_{ij,l}^n \tag{4.9}$$

is used. The Γ's are 3×3 matrices, and the $U_{ij,l}^n$ $(l = 1, 6)$ are values at some set of grid points neighboring the point (i,j). The standard 5-point stencil together with one additional corner point is used, as indicated in Figure 4.1. We want to choose the Γ's so that second order accuracy is maintained. Consider the local truncation error

$$L = \frac{1}{h}\sum_{l=1}^{6}\Gamma_{ij,l}U_l - \left(U_t(x_i,y_j) + \frac{1}{2}kU_{tt}(x_i,y_j)\right) + \mathrm{O}(k^2). \tag{4.10}$$

There will be a different set of six Γ matrices for each point (i,j). These must be derived at each point, based on the geometry of the interface near this point. We will now concentrate on a particular point (i,j) and discuss the derivation of the corresponding Γ matrices. From the derivation of the jump conditions in $\overline{v}$ in this section, we know that it is convenient to introduce local coordinates normal and tangential to the interface, respectively. We write the coordinate transformation as

$$\begin{pmatrix} x \\ y \end{pmatrix} = \begin{pmatrix} \cos\beta & \sin\beta \\ -\sin\beta & \cos\beta \end{pmatrix}\begin{pmatrix} \xi \\ \eta \end{pmatrix} + \begin{pmatrix} x_0 \\ y_0 \end{pmatrix}, \tag{4.11}$$

where ξ and η are in the directions normal and tangential to the interface at point $(x_0,y_0) \in \mathcal{C}$ respectively, which is a point on the interface near the point (i,j), and β is the rotation angle. In the example of $\mathcal{F}_{\mathrm{int}}(x,y) = x - \alpha$, the rotation angle is 0, and $\xi = x,\ \eta = y$. Let

$$\overline{U}(\xi,\eta,t) = \begin{pmatrix} \overline{u}(\xi,\eta,t) \\ \overline{v}(\xi,\eta,t) \\ p(\xi,\eta,t) \end{pmatrix}, \quad Q_0 = \begin{pmatrix} \cos\beta & -\sin\beta & 0 \\ \sin\beta & \cos\beta & 0 \\ 0 & 0 & 1 \end{pmatrix}, \tag{4.12}$$

Then we have

$$U(x,y,t) = Q_0\overline{U}(\xi,\eta,t). \tag{4.13}$$

and (4.3) gives the transformed equation

$$\overline{U}_t + A\overline{U}_\xi + B\overline{U}_\eta = 0. \tag{4.14}$$

We want to also transform (4.10) to ξ-η coordinates. Now, expressing the derivatives of U with respect to t in terms of those of $\overline{U}$ with respect to ξ and η, we obtain

$$\begin{aligned} U_t &= Q_0\overline{U}_t = -Q_0\left(A\overline{U}_\xi + B\overline{U}_\eta\right) \\ U_{tt} &= Q_0\overline{U}_{tt} = c^2Q_0\left(\overline{U}_{\xi\xi} + \overline{U}_{\eta\eta}\right). \end{aligned} \tag{4.15}$$

Also, we have

$$\sum_{l=1}^{6} \Gamma_{ij,l} U_{ij,l}^n = \sum_{l=1}^{6} \Gamma_{ij,l} Q_0 \overline{U}_{ij,l}^n. \tag{4.16}$$

To simplify the notation, we will now concentrate on a particular point (i,j) and drop these subscripts, and also incorporate the necessary rotation into the Γ's, now defining the following Γ's and U's as shorthand:

$$\Gamma_l = Q_0^{-1} \Gamma_{ij,l} Q_0, \quad \overline{U}_l = \overline{U}_{ij,l}^n. \tag{4.17}$$

Then with (4.15), (4.16) and (4.17) the local truncation error (4.10) at point (i,j) has the form

$$L = Q_0 \left\{ \frac{1}{h} \sum_{l=1}^{6} \Gamma_l \overline{U}_l - \left(\overline{U}_t(x_i, y_j) + \frac{1}{2} k \overline{U}_{tt}(x_i, y_j) \right) \right\} + \mathrm{O}(k^2). \tag{4.18}$$

Expanding $\overline{U}_l$ ($l = 1, 2, \ldots, 6$) about point (x_0, y_0) and setting $U^* = \overline{U}(x_0, y_0)$, we get

$$\overline{U}_l = U^* + (\xi_l U_\xi^* + \eta_l U_\eta^*) + \frac{1}{2} \left(\xi_l^2 U_{\xi\xi}^* + 2\xi_l \eta_l U_{\xi\eta}^* + \eta_l^2 U_{\eta\eta}^* \right) + \mathrm{O}(k^3), \tag{4.19}$$

where ξ_l and η_l are coordinates of point l under ξ-η coordinates, and $* = -$ or $+$ depending on whether the lth point is on the $-$ or on the $+$ side of the interface. Also, with (4.15), expanding its right hand side about point (x_0, y_0) also, we have

$$\begin{aligned} \overline{U}_t &= -AU_\xi^* - BU_\eta^* - \left(A\xi_2 U_{\xi\xi}^* + (A\eta_2 + B\xi_2) U_{\xi\eta}^* + B\eta_2 U_{\eta\eta}^* \right) + \mathrm{O}(k^2) \\ \overline{U}_{tt} &= c^2 \left(\overline{U}_{\xi\xi} + \overline{U}_{\eta\eta} \right) = c^2 \left(U_{\xi\xi}^* + U_{\eta\eta}^* \right) + \mathrm{O}(k). \end{aligned} \tag{4.20}$$

Note that the center point is marked as Point 2. Plugging equations (4.19) and (4.20) into the local truncation error (4.18), we get

$$\begin{aligned} L \;=\; & Q_0 \left\{ \frac{1}{h} \sum_{l=1}^{6} \Gamma_l \left(U^* + (\xi_l U_\xi^* + \eta_l U_\eta^*) + \frac{1}{2} \left(\xi_l^2 U_{\xi\xi}^* + 2\xi_l \eta_l U_{\xi\eta}^* + \eta_l^2 U_{\eta\eta}^* \right) \right) \right. \\ & + AU_\xi^* + BU_\eta^* + \left(A\xi_2 U_{\xi\xi}^* + (A\eta_2 + B\xi_2) U_{\xi\eta}^* + B\eta_2 U_{\eta\eta}^* \right) \\ & \left. - \frac{1}{2} kc^2 \left(U_{\xi\xi}^* + U_{\eta\eta}^* \right) \right\} + \mathrm{O}(k^2). \end{aligned} \tag{4.21}$$

Expression (4.21) shows that the local truncation error L is a linear function of U^*, U_ξ^*, U_η^*, $U_{\xi\xi}^*$, $U_{\xi\eta}^*$, and $U_{\eta\eta}^*$. Since for a irregular point near the interface, some of the points of the stencil are on different sides, L depends on twelve terms: the values of the above six terms on *each* side of the interface. We can express these values on one side of the interface in terms of those on the other side. With the jump conditions specified (see Chapter 5), we have the following

$$
\begin{aligned}
U^+ &= Q_1 U^- \\
U_\eta^+ &= Q_1 U_\eta^- \\
U_\xi^+ &= Q_2 U_\xi^- + Q_3 U_\eta^- \\
U_{\eta\eta}^+ &= Q_1 U_{\eta\eta}^- - \chi''(0)\left(\left(Q_2 - Q_1\right) U_\xi^- + Q_3 U_\eta^-\right) \\
U_{\xi\xi}^+ &= \left(c^-/c^+\right)^2 Q_1 U_{\xi\xi}^- + \left(\left(c^-/c^+\right)^2 - 1\right) Q_1 U_{\eta\eta}^- \\
&\quad + \chi''(0)\left(\left(Q_2 - Q_1\right) U_\xi^- + Q_3 U_\eta^-\right) \\
U_{\xi\eta}^+ &= Q_2 U_{\xi\eta}^- + Q_3 U_{\eta\eta}^- + \chi''(0) Q_4 \left(\left(Q_2 - Q_1\right) U_\xi^- + Q_3 U_\eta^-\right),
\end{aligned}
\tag{4.22}
$$

where the Q's are given as follows

$$
\begin{aligned}
Q_1 &= \operatorname{diag}\left(1,\ \rho^-/\rho^+,\ 1\right) \\
Q_2 &= \operatorname{diag}\left(\kappa^-/\kappa^+,\ 1,\ \rho^+/\rho^-\right) \\
Q_3 &= \left(\rho^-/\rho^+\right)\left(\left(c^-/c^+\right)^2 - 1\right)\begin{pmatrix} 0 & 1 & 0 \\ 0 & 0 & 0 \\ 0 & 0 & 0 \end{pmatrix} \\
Q_4 &= \begin{pmatrix} 0 & 1 & 0 \\ -1 & 0 & 0 \\ 0 & 0 & 0 \end{pmatrix},
\end{aligned}
\tag{4.23}
$$

and $\chi''(0)$ is the curvature of the interface at point $(x_0,\ y_0)$. Exchanging $+$ and $-$ sign in the superscripts of all terms (including the Q's) in (4.22), we can express $U^-, U_\eta^-, ..., U_{\xi\xi}^-$ in terms of $U^+, U_\eta^+, ..., U_{\xi\xi}^+$. Similar to the one-dimensional case, substituting (4.19) and (4.20) into (4.18), and replacing $U^+, U_\eta^+, ..., U_{\xi\xi}^+$ with the jump condition (4.22), we will obtain the local truncation error expressed in terms of

$U^-, U^-_\eta, ..., U^-_{\xi\xi}$, reducing the dependent variables from twelve to six. This explains why a six point stencil is adopted in this method. For second order accuracy it will suffice to make all the coefficients of U^-, U^-_ξ, U^-_η, $U^-_{\xi\xi}$, $U^-_{\xi\eta}$, $U^-_{\eta\eta}$ equal zero in the local truncation error L. Then we have the following six equations

$$\begin{aligned} &\sum_{l=1}^{6} \Gamma_l \hat{Q}_1 = 0 && \sum_{l=1}^{6} \Gamma_l \hat{Q}_4 = hkc^2 - 2h\xi_2 A \\ &\sum_{l=1}^{6} \Gamma_l \hat{Q}_2 = -hA && \sum_{l=1}^{6} \Gamma_l \hat{Q}_5 = -2h(\eta_2 A + \xi_2 B) \\ &\sum_{l=1}^{6} \Gamma_l \hat{Q}_3 = -hB && \sum_{l=1}^{6} \Gamma_l \hat{Q}_6 = hkc^2 - 2h\eta_2 B, \end{aligned} \tag{4.24}$$

where the Q's are 3×3 matrices. If point l is on the same side as the center point, then

$$\hat{Q}_1 = I,\ \hat{Q}_2 = \xi_l I,\ \hat{Q}_3 = \eta_l I,\ \hat{Q}_4 = \xi_l^2 I,\ \hat{Q}_5 = 2\xi_l \eta_l I,\ \hat{Q}_6 = \eta_l^2 I. \tag{4.25}$$

Otherwise

$$\begin{aligned} \hat{Q}_{1l} &= Q_1 \\ \hat{Q}_{2l} &= \frac{\xi_l}{h} Q_2 + \frac{1}{2h^2}\chi''(0)\left(\xi_l^2 - \eta_l^2 + 2\xi_l\eta_l Q_4\right)(Q_2 - Q_1) \\ \hat{Q}_{3l} &= \frac{\eta_l}{h} Q_1 + \frac{\xi_l}{h} Q_3 + \frac{1}{2h^2}\chi''(0)\left(\xi_l^2 - \eta_l^2 + 2\xi_l\eta_l Q_4\right) Q_3 \\ \hat{Q}_{4l} &= \left(\frac{\xi_l c^-}{hc^+}\right)^2 Q_1 \\ \hat{Q}_{5l} &= 2\frac{\xi_l\eta_l}{h^2} Q_2 \\ \hat{Q}_{6l} &= \left(\frac{\eta_l}{h}\right)^2 Q_1 + 2\frac{\xi_l\eta_l}{h^2} Q_3 + \left(\frac{\xi_l}{h}\right)^2 \left(\left(\frac{c^-}{c^+}\right)^2 - 1\right) Q_1. \end{aligned} \tag{4.26}$$

The six matrix equations can be used to solve for Γ_l ($l = 1, ..., 6$). Since each Γ is 3×3, we have 54 equations for 54 unknowns. Normally we do not need to solve for the 54 unknowns simultaneously, but instead we decouple the system into smaller systems of equations. Note that the $\hat{Q}$'s in (4.25) are always diagonal; therefore how to decouple equation (4.24) depends on the structure of the $\hat{Q}$'s in (4.26), which in turn depends on the application, including the interface and jump conditions.

In the special case of a linear interface, where $\chi''(0) = 0$, and $\hat{Q}_{1l}$, $\hat{Q}_{2l}$ and $\hat{Q}_{3l}$ in (4.26) are diagonal or upper-triangular matrices, the system can be decoupled into nine systems of equations, each of which is 6×6. In this case, Q_1 and Q_2 are diagonal. But since $Q_3(1,2)$ is nonzero, and thus so are $\hat{Q}_{3l}(1,2)$ and $\hat{Q}_{6l}(1,2)$, we see that $\Gamma(1,j)$ and $\Gamma(2,j)$ $(j = 1,2,3)$ are coupled to each other. We must solve for $\Gamma(1,j)$ before we can determine $\Gamma(2,j)$ $(j = 1,2,3)$.

If not all the Q's are diagonal, but instead are triangular matrices, the nine systems of equations are coupled together. Thus they have to be solved sequentially. More typically, as in the case of a curved interface, the Q's will not be of any particular form, such as diagonal or triangular form. In our case, Q_4 (see equation (5.27)) is not of any particular form, and therefore neither is $\hat{Q}_{2l}$ or $\hat{Q}_{3l}$ due to the non-zero $\chi''(0)$. Then we will need to solve a system of equations, from (4.24), of the form

$$\sum_{l=1}^{6} \Gamma_l \hat{Q}_{jl} = F_j, \quad j = 1,2,...,6,$$

where $F_j \in \mathbb{R}^{3\times 3}$ $(j = 1,2,...,6)$ are the right hand sides of equations (4.24). Taking the transpose of the system, we get

$$\sum_{l=1}^{6} \hat{Q}'_{jl} \Gamma'_l = F'_j, \quad j = 1,2,...,6,$$

which is equivalent to

$$\hat{Q}\hat{\Gamma} = \hat{F}. \tag{4.27}$$

Here $\hat{Q}$ is a 6×6 block matrix, with block element (j,l) being $\hat{Q}'_{jl}$, and $\hat{\Gamma}$ and $\hat{F}$ are block matrices of dimension 6×1, with block element l of $\hat{\Gamma}$ and j of $\hat{F}$ being Γ'_l and F'_j, respectively. Solving the system of equation (4.27) is equivalent to solving 3 systems of 18 linear equations, with the 3 systems each having the same coefficient matrix $\hat{Q}$. The treatment of the interface is local, this means that at each irregular point, the size of the system we need to solve for the Γ's does not depend on the mesh size. Also note that the calculation of the Γ's for each irregular point is independent of all other points, lending itself to parallel computing. More importantly, since the forward time stepping is preserved, the procedure of determining the finite difference formulas at the irregular points need be done only once as a preprocessing stage. The same formulas can then be used in every time step in solving the wave equation.

Let us compare three computational costs: the cost for the preprocessing step to obtain the Γ's (one-time cost), the cost for updating values at irregular points near the interface, and the cost for the entire computation. We need to solve three 18×18 linear systems to obtain Γ's for each irregular point, and solving such a system takes C_1, a large constant number, operations (*e.g.*, $\mathrm{O}(18^3)$ assuming Gauss elimination is used). Since the size of the linear systems do not grow when we refine the grid, the operations needed to obtain Γ's for each irregular point remains the same. Since the total number of irregular points is $\mathrm{O}(m)$, where $m = 1/h$ and h is the grid size, the cost to compute all the Γ's is $\mathrm{O}(C_1 m)$. Note also that we need to determine whether a point is regular or irregular at cost C_2, a constant, then the cost for $\mathrm{O}(m^2)$ total points is $\mathrm{O}(C_2 m^2)$. Therefore the total cost to for the preprocessing step is $\mathrm{O}(C_1 m + C_2 m^2)$, where $C_1 \gg C_2$. The cost to update U values at all irregular points near the interface is $\mathrm{O}(m)\times\mathrm{O}(n)$, or $\mathrm{O}(mn)$, where n is the number of time steps. The cost to use a standard solver over all grid points is $\mathrm{O}(m^2)\times\mathrm{O}(n)$, or $\mathrm{O}(m^2 n)$, where $\mathrm{O}(m^2)$ comes from the total number of computation points, and n is the total number of time steps we use in the computation. Note that the cost analysis remains valid in elasticity (see Chapter 6) as well.

In summary, the cost of using the Immersed Interface Method is low. Table 4.5 in Section 4.2 will confirm the above analysis. Table 4.5 will also show that, with CLAWPACK being our standard solver, the cost of using the Immersed Interface Method is very low compared with the total computational cost.

Note that in the special case that the material properties are the same of both sides of the interface (the interface actually disappears), $\Gamma_6 = 0$ and the special formula of the six-point stencil recovers the original scheme of the five-point stencil. The result is the same as applying a Lax-Wendroff scheme.

4.2 Computational Examples

In this section we present some numerical results to illustrate this method and verify second order accuracy in some simple cases.

4.2.1 Plane Wave for Acoustics

Example 4.1. A typical example is to consider a plane wave hitting a linear interface at incident angle α_I. It will reflect and transmit at the interface, at the angles of α_r and α_t, respectively (see Figure 4.2). Let c_1 and c_2 be the wave speeds in media 1

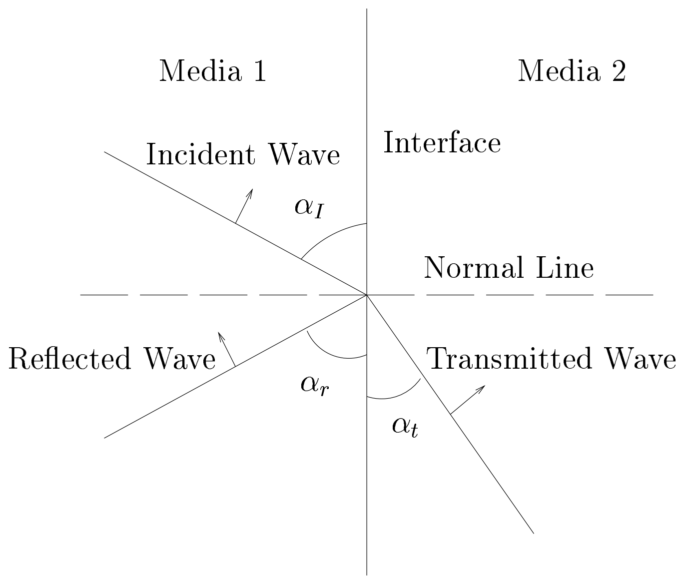

Figure 4.2: Acoustic Plane Wave Reflected and Transmitted at an Interface

and 2, respectively. By the law of reflection and Snell's law, we have

$$\alpha_r = \alpha_I, \quad \sin\alpha_t = \frac{c_2}{c_1}\sin\alpha_I, \quad \cos\alpha_t = \sqrt{1-\sin^2\alpha_t}.$$

The arrows in Figure 4.2 represent the directions in which the waves propagate. Let our local coordinates ξ_I-η_I be such that the origin is a point on the interface at $t = 0$, and positive ξ_I is in the direction of the incident wave propagation. Then the incident wave can be written as

$$\overline{U}_I = f(\xi_I - c_1 t)U_E(\rho_1 c_1),$$

where, the bar notation indicates a local coordinate system, f is a scalar function propagating in the ξ_I direction, and

$$U_E(\rho c) = \begin{pmatrix} 1/(\rho c) \\ 0 \\ 1 \end{pmatrix}$$

is the eigenvector of A corresponding to eigenvalue c. The incident wave under x-y coordinates then is given by

$$U_I = P(\alpha_I)\overline{U}_I,$$

where

$$P(\alpha) = \begin{pmatrix} \cos\alpha & -\sin\alpha & 0 \\ \sin\alpha & \cos\alpha & 0 \\ 0 & 0 & 1 \end{pmatrix}.$$

Similarly, the reflected and transmitted waves are given by

$$U_R = A_r f(\xi_r - c_1 t)P(\pi - \alpha_r)U_E(\rho_1 c_1)$$
$$U_T = A_t f(\xi_t - c_2 t)P(\alpha_t)U_E(\rho_2 c_2).$$

Where, A_r (A_t) is the amplified factor of the reflected (transmitted) wave, ξ_r (ξ_t) is the first components of the local coordinates, whose origin is the same as that of ξ_I-η_I coordinates, and whose positive direction is in the direction of propagation of the reflected (transmitted) wave. Jump conditions at the interface can be used to determine A_r and A_t. The jump conditions

$$[p] = 0, \quad [u] = 0$$

are valid for any function f at the interface, which yields

$$1 + A_r = A_t$$

$$(1 - A_r)(\cos\alpha_I/\rho_1 c_1) = A_t(\cos\alpha_t/\rho_2 c_2).$$

Solving for A_r and A_t, we have

$$A_r = (\rho_2 c_2 \cos\alpha_I - \rho_1 c_1 \cos\alpha_t) / (\rho_2 c_2 \cos\alpha_I + \rho_1 c_1 \cos\alpha_t)$$

$$A_t = (2\rho_2 c_2 \cos\alpha_I) / (\rho_2 c_2 \cos\alpha_I + \rho_1 c_1 \cos\alpha_t).$$

Note that if we multiply $1 + A_r = A_t$ and $\sin\alpha_I/c_1 = \sin\alpha_t/c_2$, which is from Snell's law, we obtain

$$(1 + A_r)(\sin\alpha_I/c_1) = A_t(\sin\alpha_t/c_2),$$

or,

$$\rho_1\{(1 + A_r)\sin\alpha_I/\rho_1 c_1\} = \rho_2\{A_t \sin\alpha_t/\rho_2 c_2\}.$$

Not surprisingly, this is equivalent to $[\rho v] = 0$, the derived jump condition for v.

Now we consider a plane wave striking an interface at an angle. The interface is given by

$$y = 0.3 + \tan(0.4)x.$$

The wave consists of a single pulse with

$$p(x,y,t) = \begin{cases} \dfrac{A_p}{2}(1 - \cos(2\pi\omega\xi)) & \text{for} 0 \le \xi \le 1/\omega, \\ 0 & \text{otherwise.} \end{cases}$$

Where

$$\xi = a(x - x_0) + b(y - y_0) - ct$$

with (a, b) a unit vector giving the direction of propagation, A_p the amplitude of the plane wave, and c the sound speed. The parameter ω determines the width of the pulse. The incident plane-wave velocities u and v are then given by

$$u(x,y,t) = \left(\frac{a}{\rho c}\right) p(x,y,t), \qquad v(x,y,t) = \left(\frac{b}{\rho c}\right) p(x,y,t).$$

After hitting the interface the incident wave is split into a reflected wave and a transmitted wave, as we have seen in this section.

Figure 4.3 shows contour plots of the exact pressure at $t = 0$ (left) and $t = 0.45$ (right). Figure 4.4 shows the solution at $t = 0.45$ as computed using CLAWPACK alone. Contour plots of both p and u are shown, along with slices of the solutions along $x = 0.35$ in the case of p and along $x = 0.6$ for u. The slice of p shows that both the transmitted and reflected wave are well captured. The slice of p is chosen to include both the transmitted and the reflected waves, while the slice of u is chosen to go through the point where the wave is currently interacting with the interface since it is only here that u is discontinuous.

Figure 4.5(a) shows errors in the computed solution as measured along these slices on a series of different grids. The max-norm (the maximum error on this slice) with no limiter (plotted in o) and with minmod limiter (plotted in *) are shown. We see that first order accuracy is observed in pressure while the discontinuous velocity has worse errors.

We consider the error only along these slices rather than over the full domain to minimize contamination from the effect of computational boundary conditions, which is not our intent to study here. With CLAWPACK we have simply specified the exact solution along all boundaries, which is stable in spite of the apparent over-specification because of the fact that the wave-propagation algorithms used in CLAWPACK are based on solving Riemann problems at each cell interface and using only the incoming waves, which is tantamount to specifying the correct incoming characteristic variables.

Figure 4.6 and Figure 4.5(b) show analogous results for the case where the Immersed Interface Method developed here is used near the interface. In the plots an improvement is seen primarily in the velocity u near the discontinuity. The observed orders of accuracy with no limiter for p and v are approximately 1.83 and 1.80 (1-norm) and 1.76 and 2.30 (max-norm) respectively. Using the limiter helps to dampen out the oscillation, but it may reduce the order of accuracy.

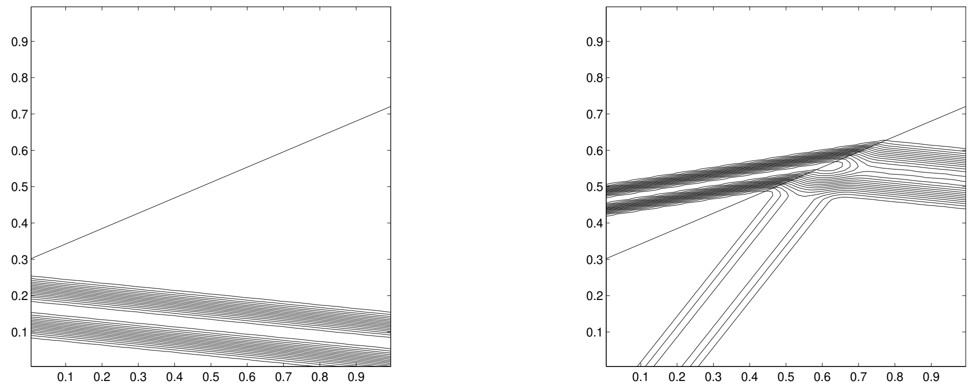

Figure 4.3: Plane wave hitting an interface at an angle. Pressure contours of the exact solution at $t = 0$ (left) and $t = 0.45$ (right). The upward moving incident wave is split at the interface into a slower transmitted wave and a reflected wave.

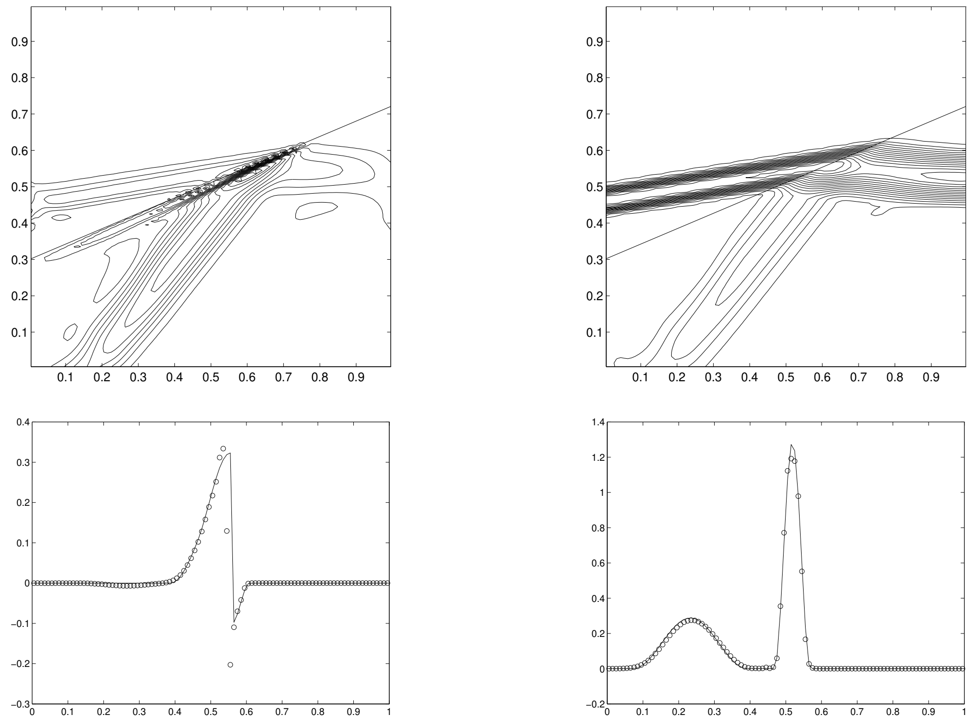

Figure 4.4: Plane wave hitting an interface at an angle, as computed by CLAWPACK alone. Top: contours of velocity u (left) and pressure p (right). Bottom: slices of velocity u along $x = 0.6$ (left) and pressure p along $x = 0.35$ (right). The solid lines in the slices are the exact solutions.

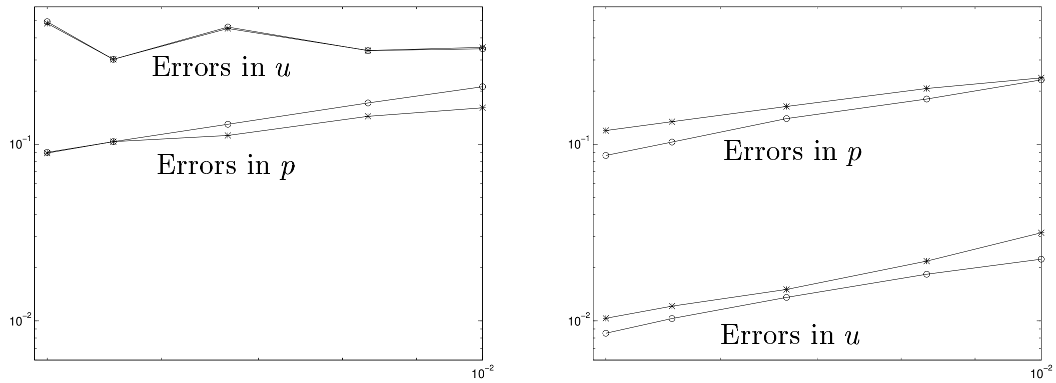

(a) (b)

Figure 4.5: Log-log plot of L_∞ errors for p and u with no limiter (plotted in o) and minmod limiter (plotted in *). (a) computed with CLAWPACK alone, with high lines for u, and low lines for p; (b) using Immersed Interface formula, with low lines for u, and high lines for p.

Tables 4.1 and 4.2 are the 1-norm and max-norm errors in u at slice $x = 0.6$ with minmod limiter and with no limiter respectively. Tables 4.3 and 4.4 are the similar errors in p at slice $x = 0.35$ with minmod limiter and with no limiter respectively. Piecewise second order accuracy is observed.

Table 4.5 shows three computational costs, C_{prep}, C_{irr} and C_{total}, for this problem with different grid sizes. All are measured in seconds on a DEC 3000/650 workstation with 32 MB main memory. Here C_{prep} is the cost for the preprocessing step (one time cost for computing the Γ's), C_{irr} is the cost for updating solutions at irregular points near the interface using the special finite difference formula, and C_{total} is the total cost for the entire computation. We compute the solutions at the same stopping time with different grid sizes. Note that with fixed CFL number, time steps will be proportional to $m = 1/h$, where h is the grid size. For example, if we compute a solution at $n_1 = 100$ time steps with $m = 100$ (grid size $h_1 = 1/100$), then we need

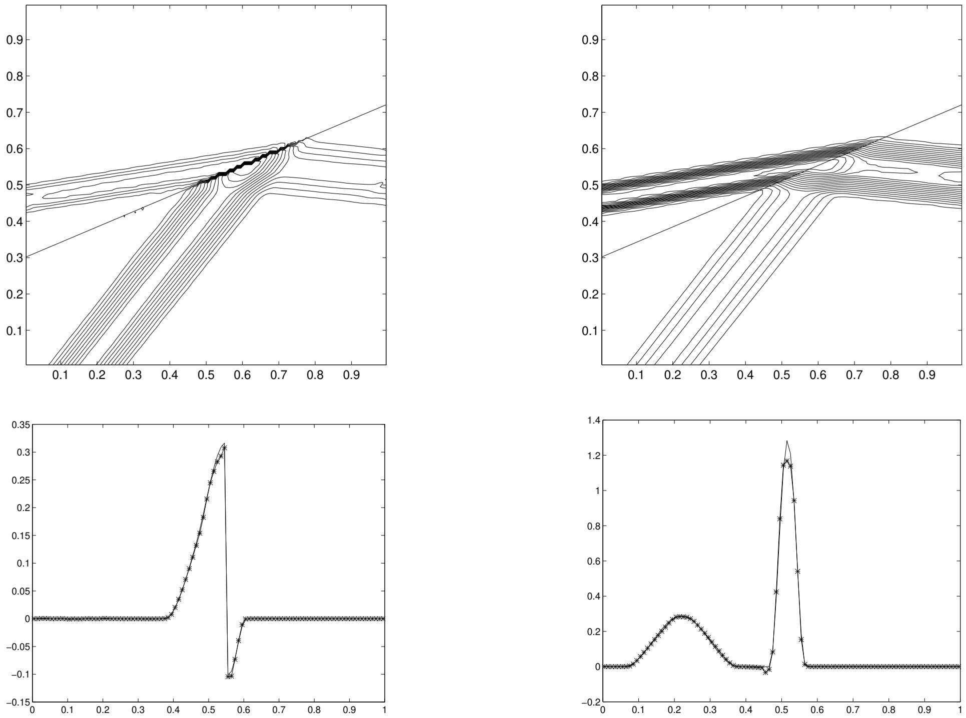

Figure 4.6: Plane wave hitting an interface at an angle, as computed by CLAWPACK with modified stencils near the interface based on the Immersed Interface Method. Top: contours of velocity u (left) and pressure p (right). Bottom: slices of velocity u along $x = 0.6$ (left) and pressure along $x = 0.35$ (right). The solid lines in the slices are the exact solutions.

Table 4.1: Errors in u at Slice $x = 0.6$ minmod Limiter

grid	1-norm	rate	max-norm	rate
100	0.00280430		0.0315573	
120	0.00221109	1.30	0.0217942	2.03
150	0.00154761	1.60	0.0150680	1.65
180	0.00120481	1.37	0.0121123	1.20
200	0.00107253	1.10	0.0103475	1.49
250	0.00073893	1.67	0.0074343	1.48
300	0.00052143	1.91	0.0062032	0.99

Table 4.2: Errors in u at Slice $x = 0.6$ with no Limiter

grid	1-norm	rate	max-norm	rate
100	0.00262742		0.0223439	
120	0.00196896	1.83	0.0183772	1.53
150	0.00134386	1.71	0.0135829	1.35
180	0.00095317	1.88	0.0103158	1.51
200	0.00077523	1.96	0.0085156	1.82
250	0.00051664	1.82	0.0052552	2.16
300	0.00037210	1.80	0.0034557	2.30

Table 4.3: Errors in p at Slice $x = 0.35$ with minmod Limiter

grid	1-norm	rate	max-norm	rate
100	0.0167565		0.2377209	
120	0.0121189	1.78	0.2068515	0.76
150	0.0082937	1.70	0.1637440	1.05
180	0.0063211	1.49	0.1342996	1.09
200	0.0056491	1.07	0.1196488	1.10
250	0.0042738	1.25	0.0925774	1.15
300	0.0034535	1.17	0.0755290	1.12

Table 4.4: Errors in p at Slice $x = 0.35$ with no Limiter

grid	1-norm	rate	max-norm	rate
100	0.0208377		0.2313843	
120	0.0150229	1.79	0.1802906	1.37
150	0.0105806	1.57	0.1396992	1.14
180	0.0076363	1.79	0.1029557	1.67
200	0.0063073	1.81	0.0864820	1.65
250	0.0042078	1.81	0.0597291	1.66
300	0.0030156	1.83	0.0433146	1.76

to compute the same solution for $n_2 = 2n_1 = 200$ time steps with $m_2 = 2m_1 = 200$. We start with $m = 50$ and $n = 50$ in this table.

This table confirms our analysis of the computation cost in Section 4.1. Cost C_{prep} is proportional to $\mathrm{O}(C_1 m + C_2 m^2)$, where $C_1 \gg C_2$, cost C_{irr} is proportional to mn, and cost C_{total} is proportional to $m^2 n$. It shows that both C_{prep} and C_{irr} are very small compared with the total cost of the entire computation. When we refine the grid, the computational cost for using the Immersed Interface Method is relatively negligible.

Note that if we multiply C_{prep} by the number of time steps n, nC_{prep} will still be very small compared with C_{total}. This means that the relative cost to compute the Γ's for each time step, which is needed in moving interface problems, will still be small. The low cost should make the Immersed Interface Method practical and efficient also in solving moving interface problems. For inverse problems, we need to solve the full forward problem with each guess at the interface, so C_{prep} again occurs only at the beginning of each forward solve.

Table 4.5: Computational Cost Comparison

grid m	C_{prep} (sec)	C_{irr} (sec)	C_{total} (sec)
50	0.0283	0.1426	5.86
100	0.0674	0.6025	43.19
150	0.0909	1.2666	143.50
200	0.1494	2.3311	355.54
250	0.2023	3.6582	654.25
300	0.2519	5.4561	1137.47
400	0.3886	9.6719	2482.12

4.2.2 Radially Symmetric Problem

Example 4.2. As a second example we consider a radially symmetric pressure disturbance moving through a circular interface. The solution remains radially symmetric and hence a highly accurate solution can be computed by solving a one-dimensional problem with appropriate source terms on a very fine grid. This is a good test problem because the interface is curved so that the curvature terms come into the jump conditions. Also the interface cuts through the grid at every possible angle as we move around the circle. The computational results show that the method works well at all angles and indeed the results are isotropic. Contour lines of the computed solution are nearly circular and appear indistinguishable from circles on the finer grid used below. Instead of displaying these plots, we show scatter plots of the solution that are more revealing of the isotropy and accuracy at the interface.

The initial data has $u = v = 0$ and

$$p(x, y, t) = \begin{cases} \frac{1}{2}(1 + \cos(15\pi r)) & \text{if } r < 0.2, \\ 0 & \text{otherwise.} \end{cases}$$

Where $r = \sqrt{(x - 0.5)^2 + (y - 0.5)^2}$. These "humps" moves out radially and are partially reflected at the interface, which we set at $r = 0.25$. A one-dimensional simulation on a fine grid produces a reference solution $P(r, t)$.

The scatter plots in Figure 4.7 show the function $P(r, t)$ at $t = 0.46$ plotted as a function of r, as a solid line. The dots in the figures are the values of p_{ij} from the two-dimensional calculation, plotted against $r_{ij} = \sqrt{(x_i - 0.5)^2 + (y_j - 0.5)^2}$. Ideally all of these points would fall on the curve, and the degree of scatter shows both the magnitude of the error at different radii, and also the degree of anisotropy in the computed results.

Figures 4.7(a) and 4.7(b) show results on two different grids in the case where the CLAWPACK algorithms and with no limiters are used away from the interface.

Figure 4.8 shows log-log plots of the L_1 (plotted with o) and L_∞ (plotted with *)

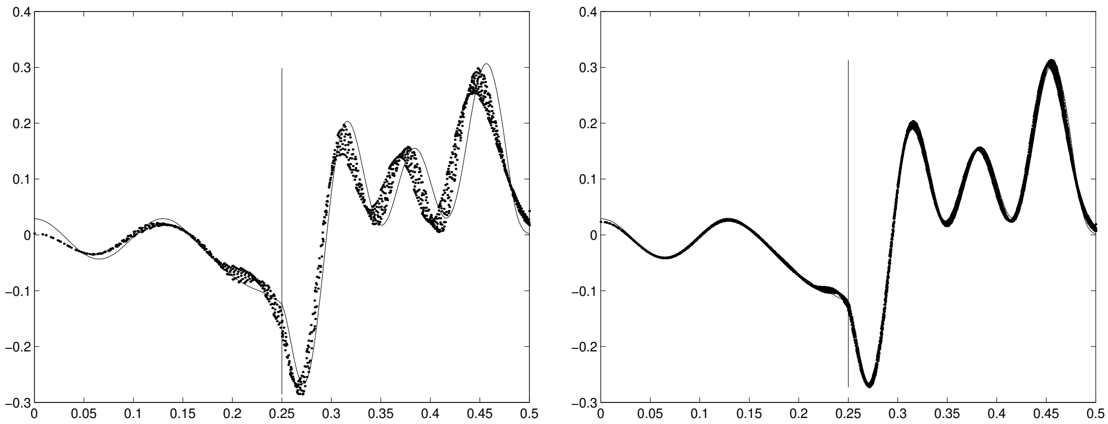

Figure 4.7: Scatter pressure plots of the solution to the Example 4.2 using the immersed interface formulas. The true and computed pressure at each grid point is shown as a function of r, distance from the center of the radially-symmetric initial data. The vertical line marks the circular interface. (a) On a 120×120 grid. (b) On a 240×240 grid.

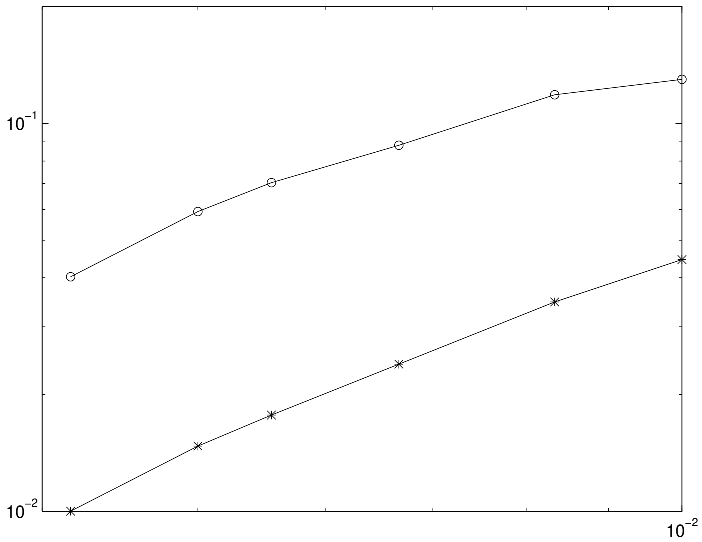

Figure 4.8: Log-log plots of L_1 (plotted in o) and of L_∞ (plotted in *) errors in p for Example 4.2.

errors in the pressure for a mesh refinement study that includes both of these grids and intermediate grids. The observed orders of accuracy in p on the finest grids are 2.1 and 1.7 respectively. Note that the velocity is continuous at the interface in this problem since the wave motion is orthogonal to the interface. The following table gives the error in p, the error in u behaves similarly.

Table 4.6: Errors in p for the Radially Symmetric Problem with no Limiter

grid	1-norm	rate	max-norm	rate
100	0.0445491		0.1298722	
120	0.0346586	1.38	0.1185258	0.50
150	0.0239425	1.66	0.0878421	1.34
180	0.0177070	1.65	0.0703263	1.22
200	0.0147277	1.75	0.0592739	1.62
240	0.0100042	2.12	0.0402248	1.73

4.2.3 Acoustic Lens Problem

Example 4.3. In the third example we show a more interesting test case. We consider a plane oscillation striking a half-circular lens which leads to a focusing of the wave. The material parameters are $\rho = 1, c = 1$ in Region 1 and $\rho = 0.8, c = 1.25$ in Region 2. Here Region 2 consists of the set $\{(x-0.3)^2 + (y-0.5)^2 < 0.15\} \cup \{0.35 < y < 0.65 \text{ and } x > 0.3\}$ and Region 1 is the exterior of this lens. The solution is forced by an oscillatory solid wall at $x = 0$, where we set

$$u(0, y, t) = 1 - \cos(\omega t)$$

with $\omega = 11.17$. Figures 4.9 (left) and 4.10 (left) show contours of p and u at $t = 2$, after a steady oscillatory solution has been reached. This solution was calculated on a 400×400 grid. Figure 4.9 (right) shows a mesh plot of the pressure p. We can clearly see the focusing of the wave. Figure 4.10 (right) shows a cross-section of u along $x = 0.5$ (the solid line is for the same computed solution). Note that u is discontinuous at the interfaces but smooth on either side, as expected. This is also visible on the contour plot of u.

4.3 Non-smooth Interface Problems

4.3.1 Piece-wise Smooth Interface Problems

In the derivation of the derivative jump condition in Chapter 5, we require the interface to be smooth. This is because we need the curvature at a point on the interface which is chosen as the origin of a local coordinate system. Actually, we only require piece-wise smooth. On irregular points near one smooth curve, the process remains the same. At an irregular point near the connecting point of two smooth curve segments, we can pick a point on either curve (preferably a closer one to the irregular point) as the origin of the local coordinates, and we will set up the local coordinates in the directions of normal and tangential to the curve. Then the remaining work is the same as for the case of smooth interface.

Example 4.4. We consider a plane oscillation striking a full lens which focuses the wave. This problem is interesting because of the physical meaning of the full lens, and the fact that the interface is only piecewise smooth with two corners. In this example the material parameters are $\rho = 0.8, c = 1.25$ inside the lens and $\rho = 1, c = 1$ outside the lens. The lens, centered at $(0.3, 0.5)$, is formed by two arc of the same radius $r = \left(0.3154^2 + 0.6^2\right)/0.3154/4 = 0.3642$, i.e., its thickness is 0.3154 and its width is 0.6. Mathematically the region for the lens is given by the set $\{(x - 0.3 - a)^2 + (y - 0.5)^2 < r^2\} \cup \{(x - 0.3 + a)^2 + (y - 0.5)^2 < r^2\}$, with $a = r - 0.3154/2 = 0.2065$. The solution is forced by an oscillatory solid wall at

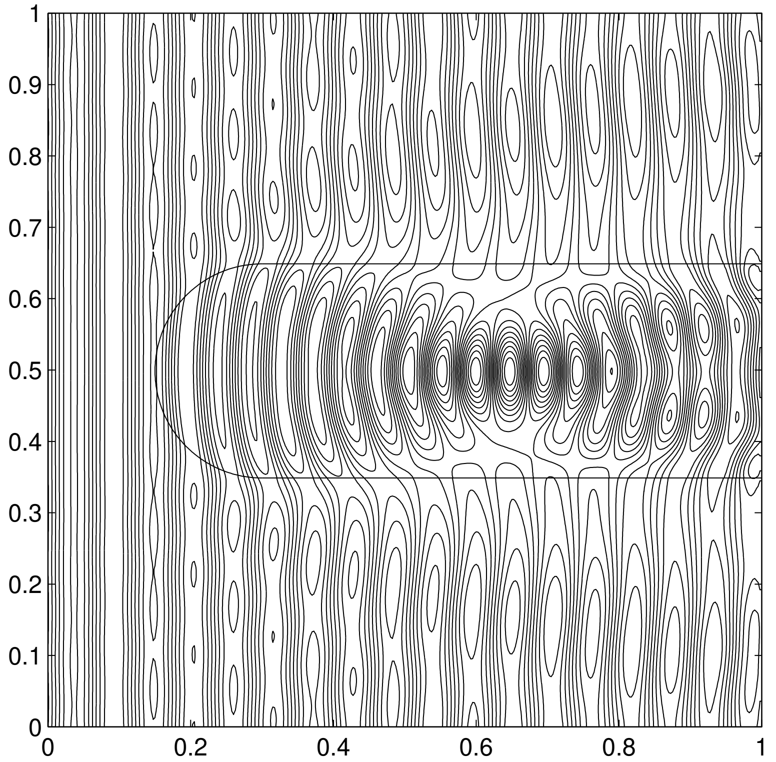

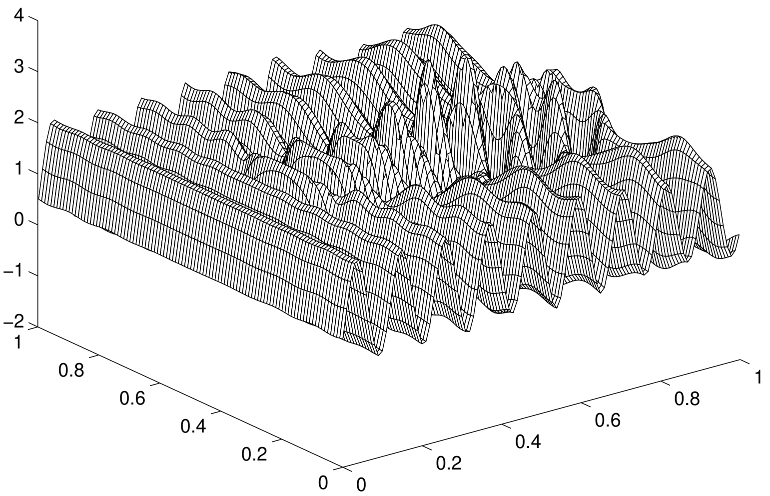

Figure 4.9: Oscillatory plane wave hitting a lens-like region inside of which the sound speed is larger. Shown on the top is the contour plot of the pressure and on the bottom is the mesh plot (on a 100×100 grid). It is imputed on a 200×200 grid

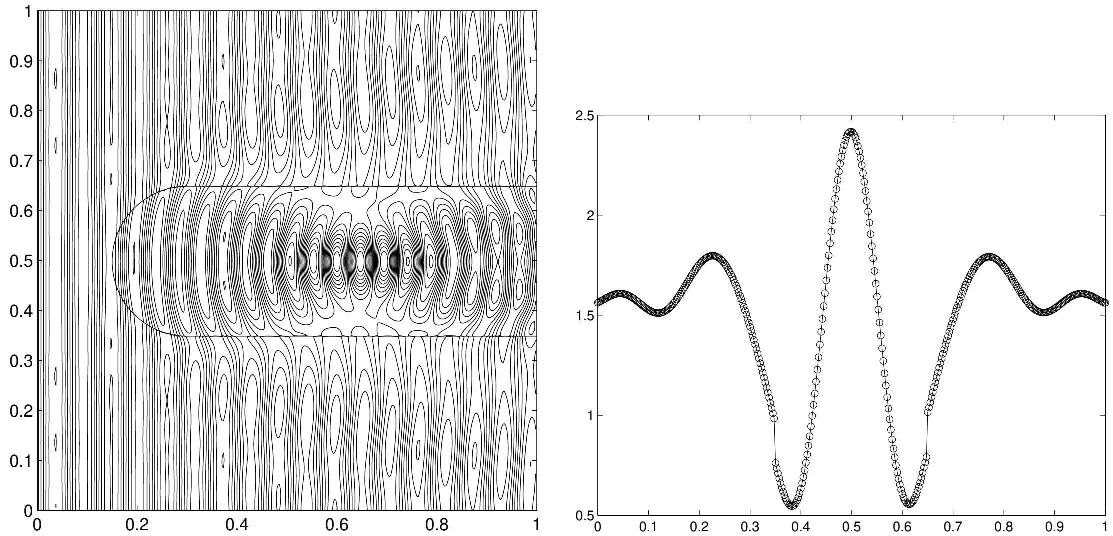

Figure 4.10: Oscillatory plane wave hitting a lens-like region inside of which the sound speed is larger. Shown on the left is the contour plot of x-velocity and on the right is the slice of u at $x = 0.5$.

$x = 0$, where we set

$$u(0, y, t) = 1 - \cos(\omega t)$$

with $\omega = 11.17$. Figure 4.11 (left) and 4.12 show contours of p and u at $t = 2$, after a steady oscillatory solution has been reached. This solution was calculated on a 400×400 grid. Figure 4.11 (right) shows a mesh plot of the pressure p. We can clearly see the focusing of the wave. Figure 4.12 (right) shows a cross-section of u along $x = 0.3$ (the solid line is for the same computed solution), which is also the location of the edge of the lens. Note that u is discontinuous at the interfaces but smooth on either side, as expected. This is also visible on the contour plot of u. Compared with Example 4.3, the focusing effect is stronger in the full lens example.

Example 4.5. In this example we have two media separated by piece-wise smooth interface (or equivalently, two interfaces joining together). Medium one is given by

$$\left\{(x - 0.5)^2 + (y - 0.5)^2 < 0.25^2\right\} \cup \{y - x\tan(\pi/3) < 0\}$$

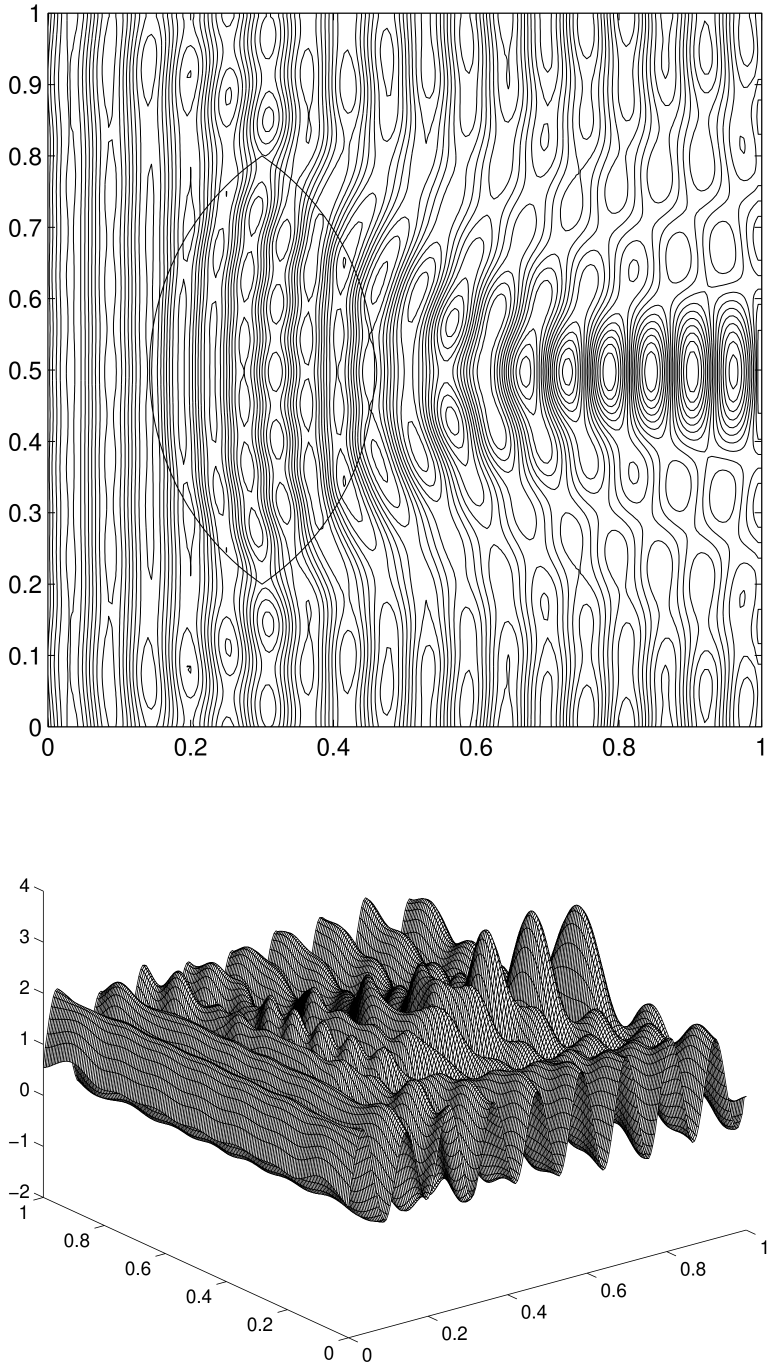

Figure 4.11: Oscillatory plane wave hitting a lens region inside of which the sound speed is larger. Shown on the top is the contour plot of the pressure and on the bottom is the mesh plot (on a 200×200 grid).

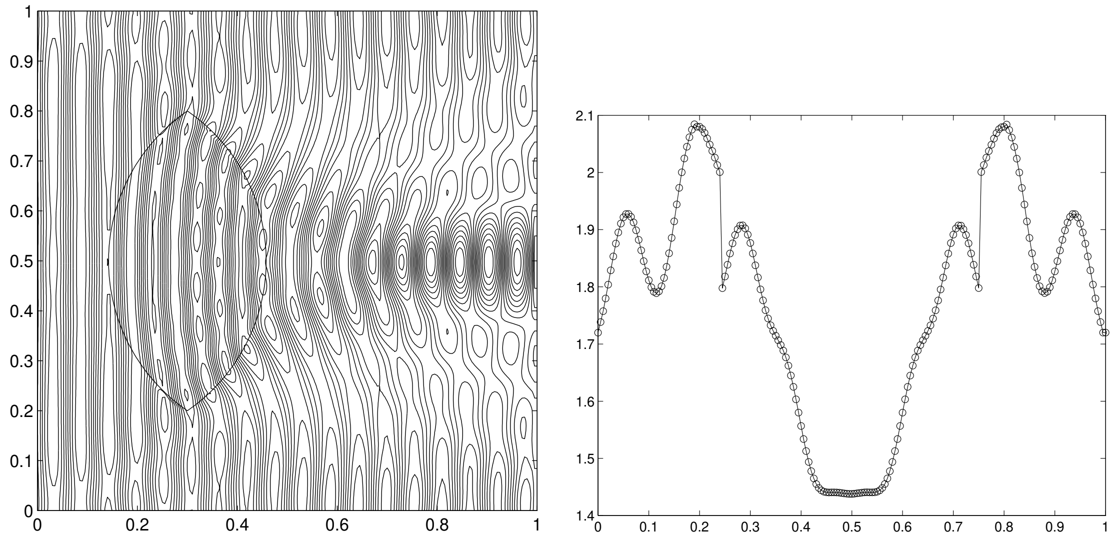

Figure 4.12: Oscillatory plane wave hitting a lens region inside of which the sound speed is larger. Shown on the left is the contour plot of x-velocity and on the right is the slice of u at $x = 0.3$.

and medium two is the exterior of medium one. The initial data is

$$p(x, y, 0) = \begin{cases} 1 + \cos(\omega(x - 0.12)) & \text{if } \; 0.04 \leq x \leq 0.24, \\ 0 & \text{otherwise.} \end{cases}$$

$$u(x, y, 0) = p(x, y, 0)/(\rho c)$$

$$v(x, y, 0) = 0,$$

with $\omega = 30\pi$, which will give a right moving wave before it hits the interface and gets reflected and transmitted. The wave speeds and densities are $c_1 = 1$ and $\rho_1 = 1$, and $c_2 = 1.5$ and $\rho_2 = 2$.

Figure 4.13 are the contour plots of pressure p at time $t = 0.5$ and $t = 0.7$ and Figure 4.14 are similar plots for the x-velocity u. Pressure p is smoothly connected across the interfaces, while the discontinuity in u is visible. The wave get transmitted and reflected at the interfaces (both linear and curved), creating clear patterns at $t = 0.5$ (left). At $t = 0.7$ (right), the transmitted wave from the linear interface and the reflected wave from the curved interface interact with each other. The waves reflected from the linear interface travel parallelly away from the interface, and those transmitted from the linear interface continue traveling in region one until they hit the curved interface part. Then the waves are transmitted and reflected at the curved interface again. Waves leaving region one into region two will travel in region two forever; while waves traveling in region one will form the pattern of transmission and reflection at the interface again.

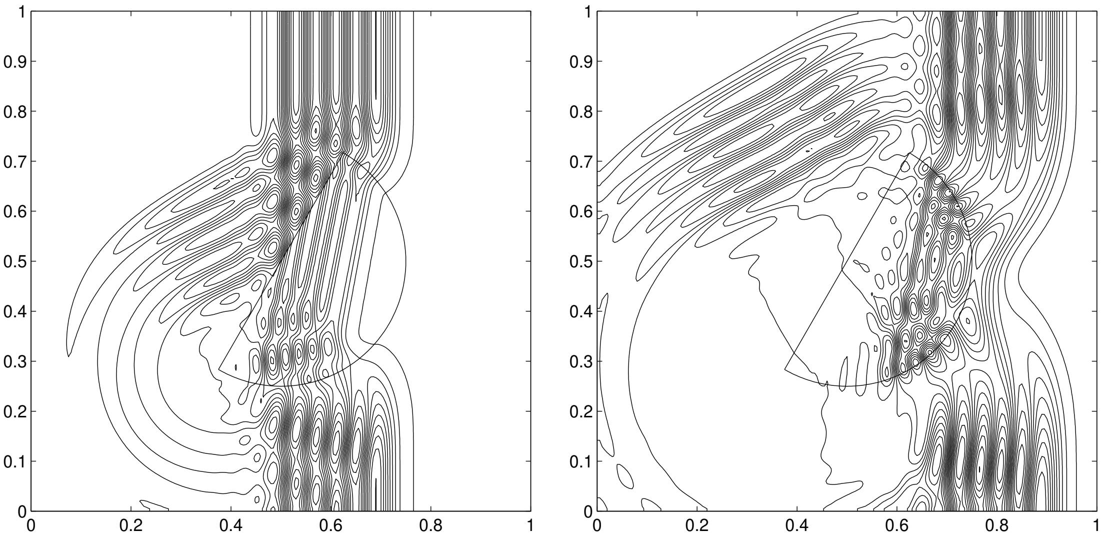

Figure 4.13: Oscillatory plane wave of three humps hitting a region consisting of two media separated by a piecewise smooth interfaces. Shown are the contour plots of the pressure p at $t = 0.5$ (left) and $t = 0.7$ (right).

4.3.2 Intersecting Interfaces

We now use this method in problems of multiple interfaces intersecting each other, yielding the possibility of solving very interesting problems, such as *pinch-out* problem in seismology. Pinch-out problem arises when two interfaces merge together into one. In an intersecting interface problem, for irregular points near the intersection

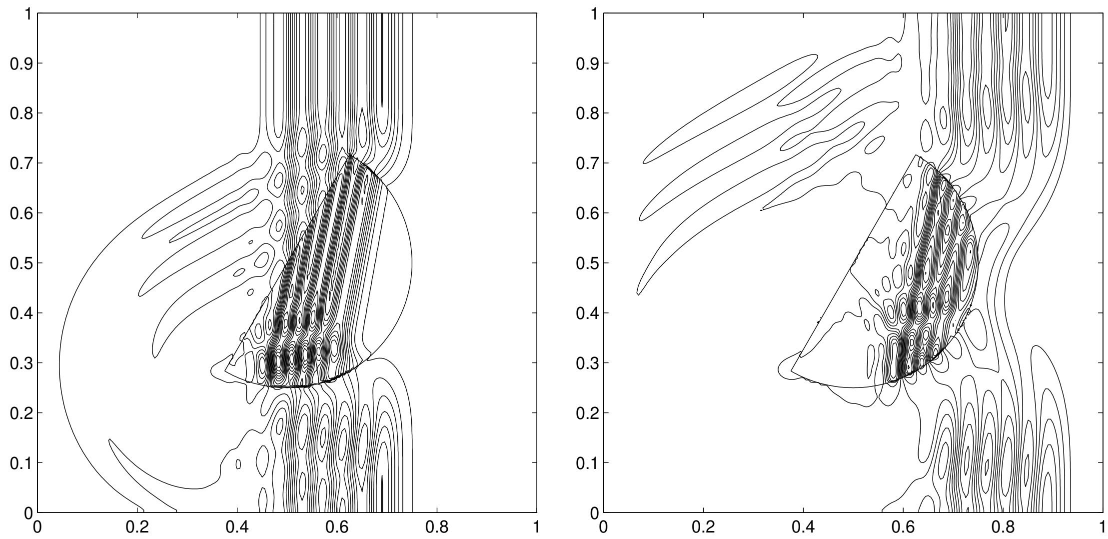

Figure 4.14: Oscillatory plane wave of three humps hitting a region consisting of two media separated by two interfaces. Shown are the contour plots of x-velocity u at $t = 0.5$ (left) and $t = 0.7$ (right).

of interfaces, three or more material properties and jumps across the interfaces are involved. We need to keep track of which medium each point is in, and which Taylor series expansion should be used bringing in the appropriate jump conditions. Since the six points of our stencil may be in three different media, it makes the problem more complicated. As for our implementation, we expand points on different media on the side where the center point of the stencil is located. In order to expand the function values and the derivatives for each point of the six-point stencil about the point of the interface (the origin of the local coordinates) near the center point, it may be necessary to expand across two interfaces for some of the points. We may choose the intersection as the origin of the local coordinates for convenience. To express the values of U^+, U^+_ξ, U^+_η, ... in terms of the values on the $-$ side in (4.22), we need two local coordinate systems for the two interfaces separating three different media. In addition, we will transform the data expressed on one of the local coordinate system into the other, leaving only one local coordinate system. The following example shows that the waves are well modeled.

Example 4.6. In this example, we have two intersecting interfaces which separate three different region, which are given as:

$$\begin{aligned}
&\text{Region 1:} \qquad \left\{(x-0.5)^2+(y-0.5)^2<0.25^2\right\} \cup \{x<y\}\,,\\
&\text{Region 2:} \qquad \left\{(x-0.5)^2+(y-0.5)^2<0.25^2\right\} \cup \{x>y\}\,,\\
&\text{Region 3:} \qquad \left\{(x-0.5)^2+(y-0.5)^2>0.25^2\right\}.
\end{aligned}$$

The initial data is

$$\begin{aligned}
p(x,y,0) &= \begin{cases} 1+\cos(\omega(x-0.12)) & \text{if } \ 0.04 \le x \le 0.24, \\ 0 & \text{otherwise,} \end{cases}\\
u(x,y,0) &= p(x,y,0)/(\rho c)\\
v(x,y,0) &= 0,
\end{aligned}$$

with $\omega = 30\pi$, which will give a right moving wave before it hits the interface and gets reflected and transmitted. The wave speeds and densities on the three parts are $c_1 = 1$, $c_2 = 1.4$ and $c_3 = 1.8$, and $\rho_1 = 1$, $\rho_2 = 1.2$ and $\rho_3 = 1.5$. The pressure p is smoothly connected across the interfaces, while the discontinuity in u is visible in both the contour plot and the slice plot across $x = 0.6$. After the waves reach the curved interface, they are transmitted and reflected. Those reflected travel in region three forever, and those transmitted keep traveling in region one until they hit the linear interface. Then the transmission and reflection happen again. In region one, we can see the effect of two waves clearly: waves initially transmitted at the curved interface, and waves reflected from the linear interface.

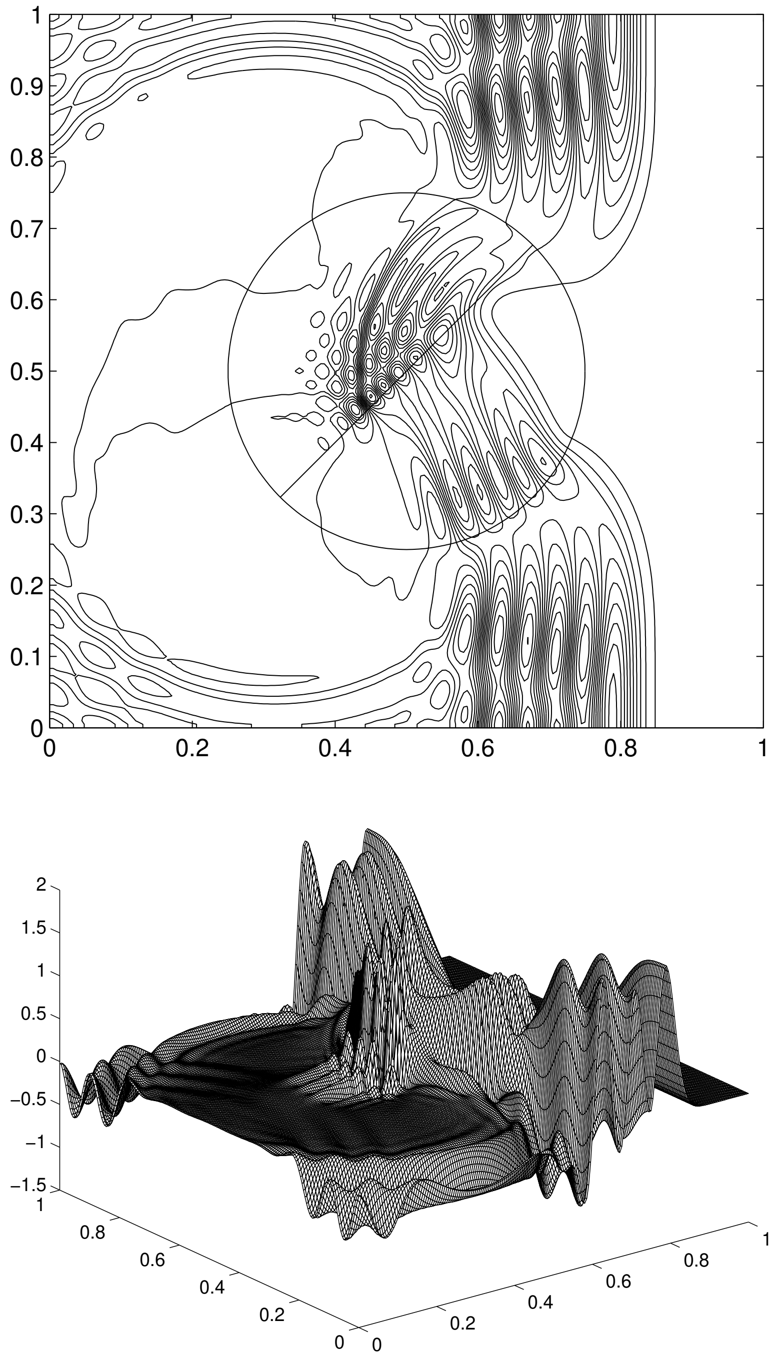

Figure 4.15: Oscillatory plane wave of three humps hitting a region consisting of three media separated by two interfaces. Shown on the top is the contour plot of the pressure and on the bottom is the mesh plot.

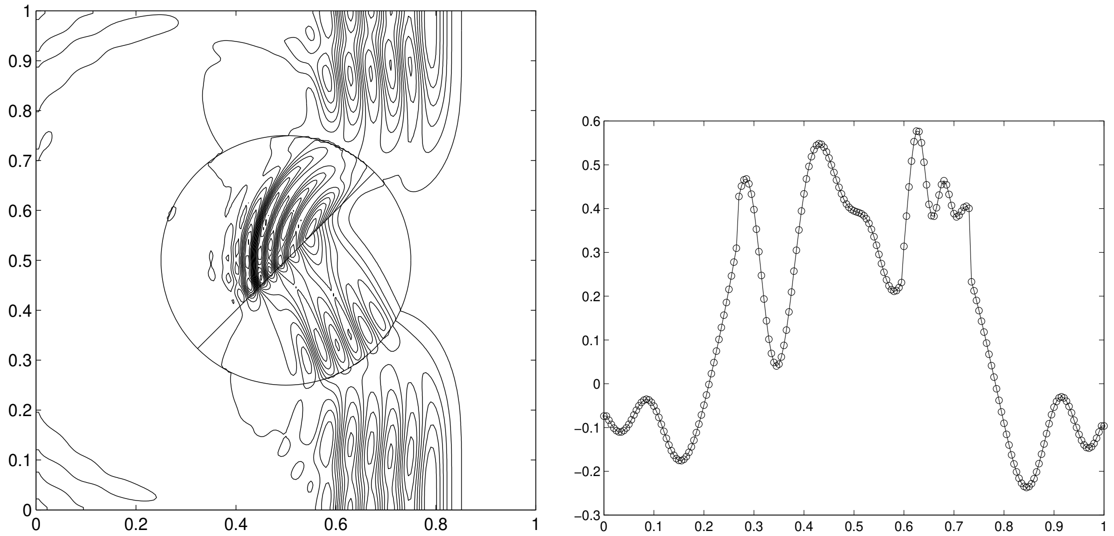

Figure 4.16: Oscillatory plane wave of three humps hitting a region consisting of three media separated by two interfaces. Shown on the left is the contour plot of x-velocity u and on the right is the slice of u at $x = 0.6$.

Chapter 5

JUMP CONDITIONS AT THE INTERFACE FOR ACOUSTICS

In chapters 3 and 4 we used the jump conditions for vector variable U and its first and second order derivatives. We have already seen that those jump conditions are extremely important in formulating the special finite difference scheme at the irregular points near the interface. Here we will give the derivation of the jump conditions in the case of one spatial dimension first, followed by those for two spatial dimensions with a linear interface and finally, the more complicated case, with a curved interface.

5.1 One Dimensional Problem

We will derive the one dimensional jump condition (3.9) first. The jump conditions (3.3) give

$$[U] = 0 \quad \Longrightarrow \quad U^+ = D_1 U^-. \tag{5.1}$$

From (2.3) we get

$$[u] = 0 \quad \Longrightarrow \quad [u_t] = 0 \quad \Longrightarrow \quad \left[\frac{1}{\rho} p_x\right] = 0$$

$$[p] = 0 \quad \Longrightarrow \quad [p_t] = 0 \quad \Longrightarrow \quad [\kappa u_x] = 0,$$

or,

$$U_x^+ = D_2 U_x^-. \tag{5.2}$$

We can deduce $U_{tt} = c^2 U_{xx}$ from (2.3), then

$$[U] = 0 \quad \Longrightarrow \quad [U_{tt}] = 0 \quad \Longrightarrow \quad [c^2 U_{xx}] = 0 \quad \Longrightarrow \quad U_{xx}^+ = D_3 U_{xx}^-. \tag{5.3}$$

The combination of (5.1), (5.2) and (5.3) gives (3.9), with D_1, D_2 and D_3 given in (3.10).

5.2 Two Dimensional Problem

5.2.1 Linear Interface

Now we derive the jump conditions in two spatial dimensions, starting with the case of a linear interface. Given the interface conditions (4.4) for the scalar variable $\overline{u}$, $\overline{v}$, and p, we can obtain the corresponding interface conditions for the vector variable $\overline{U}$ (or equivalently, U). We get jump conditions at the interface for $\overline{U}$ immediately from equation (4.4) and find that

$$\overline{U}^+ = Q_1\overline{U}^-.$$

Dropping the bar notation for simplicity, noting that the definition and derivation are based on the local coordinate system ξ-η, we have

$$U^+ = Q_1 U^-. \tag{5.4}$$

Differentiating this twice with respect to η gives

$$\begin{aligned} U_\eta^+ &= Q_1 U_\eta^- \\ U_{\eta\eta}^+ &= Q_1 U_{\eta\eta}^-. \end{aligned} \tag{5.5}$$

Next, we will derive the jump conditions for U_ξ, $U_{\xi\eta}$ and $U_{\xi\xi}$. We will also drop the bar notation in u and v for simplicity. The first equation of (4.1) gives

$$[u]_t = 0 \quad \Longrightarrow \quad \left[\frac{1}{\rho}p_\xi\right] = 0 \quad \Longrightarrow \quad p_\xi^+ = \frac{\rho^+}{\rho^-}p_\xi^-. \tag{5.6}$$

Combining the first and second equations of (4.1) we get

$$u_{t\eta} - v_{t\xi} = 0 \quad \Longrightarrow \quad (u_\eta - v_\xi)_t = 0$$

and therefore

$$u_\eta - v_\xi \equiv 0$$

is true provided that it is true of the initial data. Physically, this means that for acoustic waves, the deformation is irrotational, as is generally assumed. Then we have

$$[v_\xi] = [u_\eta] \equiv 0 \quad \Longrightarrow \quad v_\xi^+ = v_\xi^- . \tag{5.7}$$

From the third equation of (4.1) it follows that

$$[\kappa u_\xi] = -[\kappa v_\eta] \quad \Longrightarrow \quad u_\xi^+ = \frac{\kappa^-}{\kappa^+} u_\xi^- - v_\eta^+ + \frac{\kappa^-}{\kappa^+} v_\eta^- . \tag{5.8}$$

Expressing v_η^+ in terms v_η^-:

$$[\rho v] = 0 \quad \Longrightarrow \quad [\rho v_\eta] = 0 \quad \Longrightarrow \quad v_\eta^+ = \frac{\rho^-}{\rho^+} v_\eta^- . \tag{5.9}$$

Then we have

$$u_\xi^+ = \frac{\kappa^-}{\kappa^+} u_\xi^- - \frac{\rho^-}{\rho^+} v_\eta^- + \frac{\kappa^-}{\kappa^+} v_\eta^- = \frac{\kappa^-}{\kappa^+} u_\xi^- + \frac{\rho^-}{\rho^+} \left(\left(\frac{c^-}{c^+} \right)^2 - 1 \right) v_\eta^- . \tag{5.10}$$

Combining (5.6) (5.7) (5.10) we have as expression for U_ξ^+ in terms of U_ξ^- and U_η^-:

$$U_\xi^+ = Q_2 U_\xi^- + Q_3 U_\eta^- . \tag{5.11}$$

It follows, by differentiating the above with respect to η, that

$$U_{\xi\eta}^+ = Q_2 U_{\xi\eta}^- + Q_3 U_{\eta\eta}^- . \tag{5.12}$$

We can obtain a system of decoupled second order equations from (4.1):

$$\begin{aligned} u_{tt} &= c^2 \left(u_{\xi\xi} + u_{\eta\eta} \right) \\ v_{tt} &= c^2 \left(v_{\xi\xi} + v_{\eta\eta} \right) \\ p_{tt} &= c^2 \left(p_{\xi\xi} + p_{\eta\eta} \right) . \end{aligned} \tag{5.13}$$

Since $[u] = [\rho v] = [p] = 0$, we have

$$\begin{aligned} \left[c^2\left(u_{\xi\xi}+u_{\eta\eta}\right)\right] &= 0 \\ \left[\kappa\left(v_{\xi\xi}+v_{\eta\eta}\right)\right] &= 0 \\ \left[c^2\left(p_{\xi\xi}+p_{\eta\eta}\right)\right] &= 0. \end{aligned} \tag{5.14}$$

With $[u_{\eta\eta}] = [\rho v_{\eta\eta}] = [p_{\eta\eta}] = 0$, and noting that $\kappa = \rho c^2$, we get

$$\begin{aligned} u^+_{\xi\xi} &= \left(\frac{c^-}{c^+}\right)^2 u^-_{\xi\xi} + \left(\left(\frac{c^-}{c^+}\right)^2 - 1\right) u^-_{\eta\eta} \\ v^+_{\xi\xi} &= \frac{\kappa^-}{\kappa^+} v^-_{\xi\xi} + \frac{\rho^-}{\rho^+}\left(\left(\frac{c^-}{c^+}\right)^2 - 1\right) v^-_{\eta\eta} \\ p^+_{\xi\xi} &= \left(\frac{c^-}{c^+}\right)^2 p^-_{\xi\xi} + \left(\left(\frac{c^-}{c^+}\right)^2 - 1\right) p^-_{\eta\eta}, \end{aligned} \tag{5.15}$$

which is

$$U^+_{\xi\xi} = \left(\frac{c^-}{c^+}\right)^2 Q_1 U^-_{\xi\xi} + \left(\left(\frac{c^-}{c^+}\right)^2 - 1\right) Q_1 U^-_{\eta\eta}. \tag{5.16}$$

The jump conditions (5.4), (5.5), (5.11), (5.12) and (5.16), form the set (4.22) (in the special case of $\chi''(0) \equiv 0$), with the Q's being those defined in (4.23).

5.2.2 Curved Interface

We now consider the case of a curved interface. Since ξ and η are chosen in the directions normal and tangential to the interface respectively, the interface can be expressed locally by

$$\begin{aligned} \xi &= \chi(\eta) \\ \eta &= \eta. \end{aligned} \tag{5.17}$$

Choosing the origin of the coordinate system to be at a point on the interface, we have

$$\chi(0) = \chi'(0) = 0.$$

Again, with the jump conditions given as in (4.4), which in matrix form will be

$$[SU] = 0, \tag{5.18}$$

where $S = \text{diag}(1,\ \rho,\ 1)$, or equivalently, as we have in (5.5)

$$U^+ = Q_1 U^-. \tag{5.19}$$

Apparently the jump conditions for U_ξ and U_η are the same as for the linear interface[1], i.e.,

$$\begin{aligned} U_\eta^+ &= Q_1 U_\eta^- \\ U_\xi^+ &= Q_2 U_\xi^- + Q_3 U_\eta^-. \end{aligned} \tag{5.20}$$

Differentiating (5.18) with respect to η, we get

$$\left[S\left(U_\xi \chi' + U_\eta\right)\right] = 0,$$

from which (**??**) follows naturally by letting $\eta = 0$ and with the fact that $\chi'(0) = 0$. One more differentiation yields

$$\left[S\left(U_{\xi\xi}\chi'^2 + 2U_{\xi\eta}\chi' + U_\xi \chi'' + U_{\eta\eta}\right)\right] = 0.$$

At $\eta = 0$ we have

$$\left[S\left(U_\xi \chi''(0) + U_{\eta\eta}\right)\right] = 0,$$

which gives us

$$U_{\eta\eta}^+ = Q_1 U_{\eta\eta}^- - \chi''(0)\left(\left(Q_2 - Q_1\right)U_\xi^- + Q_3 U_\eta^-\right). \tag{5.21}$$

As for $U_{\xi\xi}$, we start with

$$\begin{aligned} u_{tt} &= c^2\left(u_{\xi\xi} + u_{\eta\eta}\right) \\ v_{tt} &= c^2\left(v_{\xi\xi} + v_{\eta\eta}\right) \\ p_{tt} &= c^2\left(p_{\xi\xi} + p_{\eta\eta}\right). \end{aligned}$$

given $[u_{tt}] = [\rho v_{tt}] = [p_{tt}] = 0$, we have

$$\begin{aligned} &\left[c^2\left(u_{\xi\xi} + u_{\eta\eta}\right)\right] = 0 \\ &\left[\rho c^2\left(v_{\xi\xi} + v_{\eta\eta}\right)\right] = 0 \\ &\left[c^2\left(p_{\xi\xi} + p_{\eta\eta}\right)\right] = 0, \end{aligned}$$

[1] Actually, the derivations for linear interface for U_ξ and U_η are still valid here

or,

$$\begin{aligned} u^+_{\xi\xi} &= \left(\frac{c^-}{c^+}\right)^2 \left(u^-_{\xi\xi} + u^-_{\eta\eta}\right) - u^+_{\eta\eta} \\ v^+_{\xi\xi} &= \frac{\kappa^-}{\kappa^+} \left(v^-_{\xi\xi} + v^-_{\eta\eta}\right) - v^+_{\eta\eta} \\ p^+_{\xi\xi} &= \left(\frac{c^-}{c^+}\right)^2 \left(p^-_{\xi\xi} + p^-_{\eta\eta}\right) - p^+_{\eta\eta}, \end{aligned}$$

this yields

$$U^+_{\xi\xi} = \left(\frac{c^-}{c^+}\right)^2 Q_1 \left(U^-_{\xi\xi} + U^-_{\eta\eta}\right) - U^+_{\eta\eta}.$$

Substituting (5.21) into the above we get

$$U^+_{\xi\xi} = \left(\frac{c^-}{c^+}\right)^2 Q_1 U^-_{\xi\xi} + \left(\left(\frac{c^-}{c^+}\right)^2 - 1\right) Q_1 U^-_{\eta\eta} + \chi''(0) \left(\left(Q_2 - Q_1\right) U^-_\xi + Q_3 U^-_\eta\right). \quad (5.22)$$

Now we come to $U^+_{\xi\eta}$. From the irrotational condition $u_\eta - v_\xi \equiv 0$, we have

$$\left(u_\eta - v_\xi\right)_\eta = 0 \quad \Longrightarrow \quad v^+_{\xi\eta} = v^-_{\xi\eta} + u^+_{\eta\eta} - u^-_{\eta\eta}. \quad (5.23)$$

From $p_t + \rho c^2 \left(u_\xi + v_\eta\right) = 0$, using $[p_{t\eta}] = 0$, we get

$$p_{t\eta} + \rho c^2 \left(u_{\xi\eta} + v_{\eta\eta}\right) = 0 \quad \Longrightarrow \quad u^+_{\xi\eta} = \left(\frac{\rho^-}{\rho^+}\right) \left(\frac{c^-}{c^+}\right)^2 \left(u^-_{\xi\eta} + v^-_{\eta\eta}\right) - v^+_{\eta\eta}. \quad (5.24)$$

Also from the differential equation $u_t + \frac{1}{\rho} p_\xi = 0$, we have

$$u_{t\eta} + \frac{1}{\rho} p_{\xi\eta} = 0 \quad \Longrightarrow \quad p^+_{\xi\eta} = \frac{\rho^+}{\rho^-} p^-_{\xi\eta}. \quad (5.25)$$

Equations (5.23), (5.24) and (5.25) give us

$$U^+_{\xi\eta} = Q_2 U^-_{\xi\eta} + Q_3 U^-_{\eta\eta} + \chi''(0) Q_4 \left(\left(Q_2 - Q_1\right) U^-_\xi + Q_3 U^-_\eta\right), \quad (5.26)$$

where

$$Q_4 = \begin{pmatrix} 0 & 1 & 0 \\ -1 & 0 & 0 \\ 0 & 0 & 0 \end{pmatrix}. \quad (5.27)$$

Combining (5.19), (5.20), (5.21), (5.22) and (5.26) we obtain

$$\begin{aligned}
U^+ &= Q_1U^- \\
U^+_\eta &= Q_1U^-_\eta \\
U^+_\xi &= Q_2U^-_\xi + Q_3U^-_\eta \\
U^+_{\eta\eta} &= Q_1U^-_{\eta\eta} - \chi''(0)\left((Q_2 - Q_1)\,U^-_\xi + Q_3U^-_\eta\right) \\
U^+_{\xi\xi} &= \left(c^-/c^+\right)^2 Q_1U^-_{\xi\xi} + \left(\left(c^-/c^+\right)^2 - 1\right) Q_1U^-_{\eta\eta} \\
&\quad +\chi''(0)\left((Q_2 - Q_1)\,U^-_\xi + Q_3U^-_\eta\right) \\
U^+_{\xi\eta} &= Q_2U^-_{\xi\eta} + Q_3U^-_{\eta\eta} + \chi''(0)Q_4\left((Q_2 - Q_1)\,U^-_\xi + Q_3U^-_\eta\right),
\end{aligned} \tag{5.28}$$

which is the same as (4.22).

We can see that the numerical jump conditions (5.28) depend on the physical jump conditions, the material properties, and the geometry of the interface.

Chapter 6

TWO DIMENSIONAL ELASTICITY

We have applied the Immersed Interface Method to systems of acoustic wave equations in one and two space dimensions. This method can be effectively applied to problems of elasticity as well. In contrast to the mode of exposition in Chapter 3, we will address the case of two spatial dimensions directly. In addition to taking advantage of the similarities in applying the Immersed Interface Method to the elasticity vs. the acoustic problem, we also pay attention to the differences between these different applications. We start with a brief derivation of the elasticity equation and introduce the P-waves and S-waves, more details of which can be found in many references [22, 23]. We will solve the problem of a P-wave and S-wave hitting an interface between two media at an angle and will obtain the exact solutions analytically, before applying the Immersed Interface Method to solve the equations of elasticity numerically.

6.1 Equations of Elasticity

The motion of the body must obey the equation of continuity

$$\frac{\partial \rho}{\partial t} + \frac{\partial (\rho v_i)}{\partial x_i} = 0 \tag{6.1}$$

and the equation of motion

$$\rho \left(\frac{\partial v_i}{\partial t} + v_j \frac{\partial v_i}{\partial x_j} \right) = \frac{\partial \sigma_{ij}}{\partial x_j} + X_i, \tag{6.2}$$

and the strain tensors and the particle velocity are given by

$$e_{ij} = \frac{1}{2} \left(\frac{\partial u_j}{\partial x_i} + \frac{\partial u_i}{\partial x_j} - \frac{\partial u_k}{\partial x_i} \frac{\partial u_k}{\partial x_j} \right), \tag{6.3}$$

and

$$v_i = \frac{\partial u_i}{\partial t} + \frac{\partial u_i}{\partial x_j}\frac{\partial x_j}{\partial t}. \tag{6.4}$$

Where ρ is the density, v_i the ith component of the velocity, x_j the jth component of the coordinates, σ_{ij} and e_{ij} the ijth component of the stress tensors and strain tensors respectively, X_i the ith component of the body force, and u_i the ith component of the displacement. Repeated indices mean the term is summed over all values of the index, e.g.

$$\frac{\partial (\rho v_i)}{\partial x_i} = \sum_{i=1}^{3} \frac{\partial (\rho v_i)}{\partial x_i}$$

in three dimensional space. For linear elasticity, we can simplify the problem by considering small displacements and small velocities, i.e. by restricting ourselves to values of u_i, v_i small enough that the nonlinear terms in equation (6.2), (6.3) and (6.4) may be neglected. In such a linearized theory, we have

$$\rho \frac{\partial v_i}{\partial t} = \frac{\partial \sigma_{ij}}{\partial x_j} + X_i \tag{6.5}$$

$$e_{ij} = \frac{1}{2}\left(\frac{\partial u_j}{\partial x_i} + \frac{\partial u_i}{\partial x_j}\right) \tag{6.6}$$

$$v_i = \frac{\partial u_i}{\partial t}. \tag{6.7}$$

The theory of linear elasticity is also based on Hooke's law. For a homogeneous isotropic material, this is

$$\sigma_{ij} = \lambda e_{kk}\delta_{ij} + 2\mu e_{ij}, \tag{6.8}$$

where δ_{ij} is the Kronecker delta, i.e.

$$\delta_{ij} = \begin{cases} 1 & \text{if } i = j, \\ 0 & \text{otherwise,} \end{cases}$$

and λ and μ are Lamé constants. In many books, G is used in place of μ. Other constants can be used as an alternative, such as *Young's modulus* E, *Poisson's ratio* ν and *bulk modulus* κ, with

$$E = \frac{\mu(3\lambda + 2\mu)}{\lambda + \mu}, \qquad \nu = \frac{\lambda}{2(\lambda + \mu)}, \qquad \kappa = \lambda + \frac{2}{3}\mu.$$

Differentiating equation (6.8) with respect to t, and with (6.6) and (6.7) gives

$$\frac{\partial \sigma_{ij}}{\partial t} = \lambda \frac{\partial v_k}{\partial x_k} + \mu \left(\frac{\partial v_j}{\partial x_i} + \frac{\partial v_i}{\partial x_j} \right). \tag{6.9}$$

Together with equation (6.5), we have a system of equations containing only σ's and v's:

$$\begin{aligned} \rho \frac{\partial v_i}{\partial t} &= \frac{\partial \sigma_{ij}}{\partial x_j} + X_i \\ \frac{\partial \sigma_{ij}}{\partial t} &= \lambda \frac{\partial v_k}{\partial x_k} + \mu \left(\frac{\partial v_j}{\partial x_i} + \frac{\partial v_i}{\partial x_j} \right). \end{aligned} \tag{6.10}$$

This gives nine equations for nine unknowns: v_i $(i = 1,\ 2,\ 3)$ and six independent σ's in three dimensions. In two dimensions, omitting body force terms for simplicity, and using the notation of x and y instead of x_1 and x_2, equation (6.10) yields

$$\begin{aligned} v_{1t} &= \frac{1}{\rho}\left(\sigma_{11x} + \sigma_{12y}\right) \\ v_{2t} &= \frac{1}{\rho}\left(\sigma_{12x} + \sigma_{22y}\right) \\ \sigma_{11t} &= (\lambda + 2\mu) v_{1x} + \lambda v_{2y} \\ \sigma_{12t} &= \mu(v_{1y} + v_{2x}) \\ \sigma_{22t} &= \lambda v_{1x} + (\lambda + 2\mu) v_{2y}, \end{aligned} \tag{6.11}$$

where we use v_{1t} to express $\dfrac{\partial v_1}{\partial t}$ and σ_{11x} to express $\dfrac{\partial \sigma_{11}}{\partial x}$ and so on.

6.2 P-wave and S-wave

We will derive the *Navier equation*, which governs small displacements from an equilibrium state of zero elastic stress. For small displacements of a linear elastic solid, we may neglect the term $(\vec{v} \cdot \bigtriangledown)\vec{v}$, which is a quadratic function of the small quantity $\vec{v}$ compared with $\partial \vec{v}/\partial t$. Furthermore the difference between Lagrangian and Eulerian derivatives is also small and we may replace $\partial \vec{v}/\partial t$ with $\partial^2 \vec{u}/\partial t^2$. Using Hooke's law

(6.8) and equation (6.6) gives

$$\begin{aligned}\frac{\partial \sigma_{ij}}{\partial x_j} &= \frac{\partial}{\partial x_j}\left(\lambda e_{kk}\delta_{ij} + 2\mu e_{ij}\right) \\ &= \frac{\partial}{\partial x_j}\left(\lambda \bigtriangledown \cdot \vec{u}\right) + \mu\left(\bigtriangledown^2 u_i + \frac{\partial}{\partial x_i}\bigtriangledown \cdot \vec{u}\right) + 2\frac{\partial \mu}{\partial x_j}e_{ij}.\end{aligned} \tag{6.12}$$

In the simplest case of wave propagation in a homogeneous medium, we take ρ, λ and μ to be constant, then (6.12) becomes

$$\frac{\partial \sigma_{ij}}{\partial x_j} = \lambda \frac{\partial}{\partial x_i}\left(\bigtriangledown \cdot \vec{u}\right) + \mu\left(\bigtriangledown^2 u_i + \frac{\partial}{\partial x_i}\bigtriangledown \cdot \vec{u}\right), \tag{6.13}$$

or

$$\frac{\partial \sigma_{ij}}{\partial x_j} = \left\{(\lambda + \mu)\bigtriangledown\left(\bigtriangledown \cdot \vec{u}\right) + \mu \bigtriangledown^2 \vec{u}\right\}_i. \tag{6.14}$$

Then ignoring body force, (6.5) and (6.14) give

$$\rho\frac{\partial^2 \vec{u}}{\partial t^2} = (\lambda + \mu)\bigtriangledown\left(\bigtriangledown \cdot \vec{u}\right) + \mu \bigtriangledown^2 \vec{u}. \tag{6.15}$$

This is the *Navier equation* for the case of homogeneous medium and the absence of the body force. Using the vector calculus identity

$$\bigtriangledown^2 \vec{u} = \bigtriangledown\left(\bigtriangledown \cdot \vec{u}\right) - \bigtriangledown \times \bigtriangledown \times \vec{u}, \tag{6.16}$$

we transform (6.15) into the more useful form

$$\rho\frac{\partial^2 \vec{u}}{\partial t^2} = (\lambda + 2\mu)\bigtriangledown\left(\bigtriangledown \cdot \vec{u}\right) - \mu \bigtriangledown \times \bigtriangledown \times \vec{u}. \tag{6.17}$$

We can now effect a separation of (6.17) into two equations, one governing the dilatation (volume changes) and the other the rotation. We make use of the vector identities

$$\begin{aligned}&\bigtriangledown \cdot \left(\bigtriangledown \times \vec{u}\right) = 0 \\ &\bigtriangledown \times \bigtriangledown \theta = 0,\end{aligned} \tag{6.18}$$

which hold for any $\vec{u}$ and θ. The divergence of (6.17) yields

$$\rho\frac{\partial^2 \theta}{\partial t^2} = (\lambda + 2\mu)\bigtriangledown^2 \theta, \tag{6.19}$$

where

$$\theta = \bigtriangledown \cdot \vec{u}$$

is the dilatation. The curl of (6.17) yields

$$\rho \frac{\partial^2 \vec{\omega}}{\partial t^2} = \mu \bigtriangledown^2 \vec{\omega}, \tag{6.20}$$

where

$$\vec{\omega} = \bigtriangledown \times \vec{u}$$

is the rotation associated with the vorticity. The general equation (6.17) therefore contains two separate wave equations, (6.19) and (6.20). Equation (6.19) governs P-waves. The phase speed, c_p, is given by

$$c_p^2 = (\lambda + 2\mu)/\rho = \left(\kappa + \frac{4}{3}\mu\right)/\rho, \tag{6.21}$$

where κ is the adiabatic bulk modulus as we mentioned earlier. Change in volume is an essential feature of the P-wave. The notation P-wave is used here for a Pressure-wave, or compressional wave, and this wave propagates in the same direction as its movement.

Equation (6.20) governs S-waves. The phase speed, c_s, is given by

$$c_s^2 = \mu/\rho. \tag{6.22}$$

Rotation is an essential feature of S-waves. The notation S-wave is used for Shear-wave, and this wave propagates in directions perpendicular to the direction of its movement. Note the contrast to linearized gas dynamics: since liquids wave do not support shear forces, S-waves do not exist in acoustics. For normal materials $\kappa > 0$ and so (6.21) and (6.22) give $c_p > c_s$; the P-waves are the faster of the two and will therefore arrive first. For this reason, P-wave also stands for Primary-wave, and S-wave stands for Secondary-wave.

6.3 Eigenvalues and Eigenvectors of A

In the next section we will derive the exact solutions for a plane P-wave and S-wave hitting an interface with an angle, for which we need to know the eigenvalues and eigenvectors of A and B. Also, these eigen-pairs are required by CLAWPACK (for the Riemann Solver), which we will use later in this chapter to solve for the solutions away from the interface. Thanks to the isotropy of the equations, we can focus on the x-axis as the topic of our discussion. We will solve the problem with the interface perpendicular to the x-axis, and use coordinate transformation to obtain solutions to problems with interfaces in other orientations. Therefore only the eigen-pairs of A are needed, which we obtain as

$$\{-c_p, \vec{\alpha}_1\}, \quad \{c_p, \vec{\alpha}_2\}, \quad \{-c_s, \vec{\alpha}_3\}, \quad \{c_s, \vec{\alpha}_4\}, \quad \{0, \vec{\alpha}_5\},$$

where,

$$c_p = \sqrt{(\lambda + 2\mu)/\rho}, \quad c_s = \sqrt{\mu/\rho}$$

are the P-wave speed and S-wave speed respectively (see Appendix 6.1 for more details about P-wave and S-wave), and

$$\begin{pmatrix} \vec{\alpha}_1 & \vec{\alpha}_2 & \vec{\alpha}_3 & \vec{\alpha}_4 & \vec{\alpha}_5 \end{pmatrix} = \begin{pmatrix} c_p & -c_p & 0 & 0 & 0 \\ 0 & 0 & 1 & 1 & 0 \\ \rho c_p^2 & \rho c_p^2 & 0 & 0 & 0 \\ 0 & 0 & \rho c_s & -\rho c_s & 0 \\ \lambda & \lambda & 0 & 0 & 1 \end{pmatrix}.$$

Note that since the last eigenvalue is zero, we have the freedom of choosing the corresponding eigenvector $\vec{\alpha}_5$. We have chosen $\vec{\alpha}_5$ simply to make the five eigenvectors span the whole space.

In the Riemann solver used in CLAWPACK , we need to split the jump in U across each interface of two adjacent cells into waves in the directions of eigenvectors. Let

$\vec{\Delta} = (\delta_1 \quad \delta_2 \quad \delta_3 \quad \delta_4 \quad \delta_5)'$ be the jump in U across each interface, then we can split it into waves. Letting

$$\sum_{j=1}^{5} a_j \vec{\alpha}_j = \vec{\Delta},$$

we can solve for the coefficients

$$\begin{aligned}
a_1 &= \frac{1}{2}\left(\frac{\delta_3}{\rho c_p^2} + \frac{\delta_1}{c_p}\right) \\
a_2 &= \frac{1}{2}\left(\frac{\delta_3}{\rho c_p^2} - \frac{\delta_1}{c_p}\right) \\
a_3 &= \frac{1}{2}\left(\delta_2 + \frac{\delta_4}{\rho c_s}\right) \\
a_4 &= \frac{1}{2}\left(\delta_2 - \frac{\delta_4}{\rho c_s}\right) \\
a_5 &= \delta_5 - \frac{\lambda}{\rho c_p^2}\delta_3.
\end{aligned}$$

Note that in the implementation of CLAWPACK, a_5 is not needed because the corresponding wave speed is zero. This is consistent with the fact that the selection of $\vec{\alpha}_5$ should not matter.

6.4 Exact Solutions of Plane Waves for Elasticity

A typical test problem is a plane P-wave or S-wave hitting an interface at some angle. We will derive the exact solutions for the problem of a P-wave or S-wave hitting an interface at an angle, which will be used as computational examples in Section 6.5. Given a plane P-wave (or S-wave), it will generate four waves at the interface: a reflected P-wave, a reflected S-wave, a transmitted P-wave and a transmitted S-wave. In Figure 6.1, α_I is the incident angle of a P-wave (or S-wave), α_{rp} and α_{rs} are the angles of reflected P-wave and S-wave respectively, and α_{tp} and α_{ts} are the angles of transmitted P-wave and S-wave respectively. We will solve for the exact solution, and use it to check the order of accuracy of the numerical method.

Let c_{p_1} and c_{p_2} be the P-wave speeds, c_{s_1} and c_{s_2} be the S-wave speeds in media

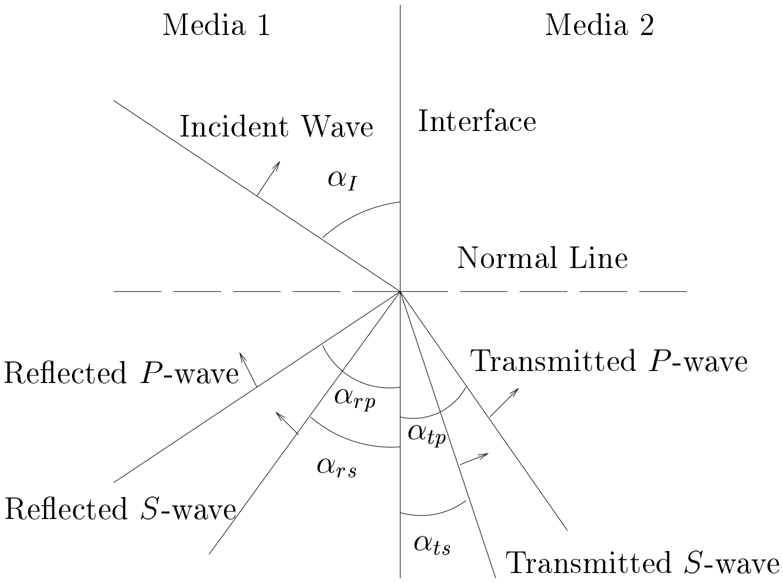

Figure 6.1: Elastic Plane Wave Reflected and Transmitted at an Interface

1 and 2 respectively and c_I be the incident wave speed. Then $c_I = c_{p_1}$ if the incident wave is a P-wave, and $c_I = c_{s_1}$ if it is an S-wave. The reflected and transmitted angles are determined by Snell's Law, which gives

$$\sin\alpha_{rp} = \frac{c_{p_1}}{c_I}\sin\alpha_I, \quad \sin\alpha_{rs} = \frac{c_{s_1}}{c_I}\sin\alpha_I,$$
$$\sin\alpha_{tp} = \frac{c_{p_2}}{c_I}\sin\alpha_I, \quad \sin\alpha_{ts} = \frac{c_{s_2}}{c_I}\sin\alpha_I,$$

and

$$\cos\beta = \sqrt{1-\sin^2\beta}, \quad \text{for} \quad \beta = \alpha_{rp},\ \alpha_{rs},\ \alpha_{tp},\ \alpha_{ts}.$$

Each of the arrows in Figure 6.1 indicates the direction of the wave propagation. If we choose a local coordinate system ξ_I-η_I, whose origin is a point on the interface, and ξ_I is in the same direction as the propagation of the incident wave, then the incident wave can be expressed as

$$\overline{U}_I = \begin{cases} f(\xi_I - c_{p_1}t)U_P\left(c_{p_1},\ \rho_1 c_{p_1}^2,\ \lambda_1\right), & \text{for } P\text{-waves}, \\ f(\xi_I - c_{s_1}t)U_S\left(\rho_1 c_{s_1}\right), & \text{for } S\text{-waves}, \end{cases} \tag{6.23}$$

where U_P and U_S are the eigen-vectors of matrix A corresponding to eigen-values c_p (for a P-wave) and c_s (for an S-wave) respectively, as derived in Section 6.3, with

$$U_P\left(c_p,\ \rho c_p^2,\ \lambda\right) = \begin{pmatrix} c_p \\ 0 \\ -\rho c_p^2 \\ 0 \\ -\lambda \end{pmatrix}, \quad U_S\left(\rho c_p\right) = \begin{pmatrix} 0 \\ 1 \\ 0 \\ -\rho c_p \\ 0 \end{pmatrix}.$$

The bar notation for U_I in (6.23) is used to indicate that it is a function under the local coordinates ξ_I-η_I, and $f(\xi_I - c_I t)$ is a scalar function, propagating in the ξ_I direction with wave speed of c_I. The incident wave in the x-y coordinate system is determined by equation (6.58),

$$U_I = P(\alpha_I)\overline{U}_I,$$

where matrix $P(\alpha_I)$ is given by equation (6.59), i.e.

$$P(\alpha) = \begin{pmatrix} \cos\alpha & -\sin\alpha & 0 & 0 & 0 \\ \sin\alpha & \cos\alpha & 0 & 0 & 0 \\ 0 & 0 & \cos^2\alpha & -2\cos\alpha\sin\alpha & \sin^2\alpha \\ 0 & 0 & \cos\alpha\sin\alpha & (\cos^2\alpha - \sin^2\alpha) & -\cos\alpha\sin\alpha \\ 0 & 0 & \sin^2\alpha & 2\cos\alpha\sin\alpha & \cos^2\alpha \end{pmatrix}.$$

Letting the other four local coordinates originate at the origin of the ξ_I-η_I system, and each of the four first components of the local coordinates, ξ_{rp}, ξ_{rs}, ξ_{tp} and ξ_{ts}, be in the propagation direction of the reflected P-wave, reflected S-wave, transmitted

P-wave and transmitted S-wave respectively, then the four waves are given by

$$\begin{aligned}
\overline{U}_{rp} &= A_{rp} f(\xi_{rp} - c_{p_1} t) U_P \left(c_{p_1}, \rho_1 c_{p_1}^2, \lambda_1\right) \\
\overline{U}_{rs} &= A_{rs} f(\xi_{rs} - c_{s_1} t) U_S \left(c_{s_1} \rho_1\right) \\
\overline{U}_{tp} &= A_{tp} f(\xi_{tp} - c_{p_2} t) U_P \left(c_{p_2}, \rho_2 c_{p_2}^2, \lambda_2\right) \\
\overline{U}_{ts} &= A_{ts} f(\xi_{ts} - c_{s_2} t) U_S \left(c_{s_2} \rho_2\right),
\end{aligned} \tag{6.24}$$

where the bar's over the U values mean that each of them is in its own local coordinates. The corresponding amplitude factors of the four waves, A_{rp}, A_{rs}, A_{tp}, and A_{ts}, are yet to be determined. In the x-y coordinate system, we have

$$\begin{aligned}
U_{rp} &= P(\pi - \alpha_{rp}) \overline{U}_{rp} \\
U_{rs} &= P(\pi - \alpha_{rs}) \overline{U}_{rs} \\
U_{tp} &= P(\alpha_{tp}) \overline{U}_{tp} \\
U_{ts} &= P(\alpha_{ts}) \overline{U}_{ts}.
\end{aligned} \tag{6.25}$$

We can determine A_{rp}, A_{rs}, A_{tp}, and A_{ts} with the jump conditions at the interface. Partitioning matrix $P(\alpha)$ to

$$P(\alpha) = \begin{pmatrix} P_a(\alpha) \\ P_b(\alpha) \end{pmatrix},$$

where $P_a(\alpha)$, composed of the first 4 rows of $P(\alpha)$, is a 4×5 matrix, and $P_b(\alpha)$, composed of the last row of $P(\alpha)$, is a 1×5 matrix, and using the fact that v_1, v_2, σ_{11} and σ_{12} are continuous at the interface, we get

$$-P_a(\pi - \alpha_{rp}) \overline{U}_{rp} - P_a(\pi - \alpha_{rs}) \overline{U}_{rs} + P_a(\alpha_{tp}) \overline{U}_{tp} + P(\alpha_{ts}) \overline{U}_{ts} - P_a(\alpha_I) \overline{U}_I = 0$$

at the interface, or

$$-P_a(\pi - \alpha_{rp}) \overline{U}_{rp} - P_a(\pi - \alpha_{rs}) \overline{U}_{rs} + P_a(\alpha_{tp}) \overline{U}_{tp} + P(\alpha_{ts}) \overline{U}_{ts} = P_a(\alpha_I) \overline{U}_I. \tag{6.26}$$

This is a 4×4 linear system, with the left hand side containing A_{rp}, A_{rs}, A_{tp}, and A_{ts}. Since the linear system is valid for any function f, setting

$$\xi_I = \xi_{rp} = \xi_{rs} = \xi_{tp} = \xi_{ts} = t = 0,$$

and letting

$$U_1 = -P_a(\pi - \alpha_{rp})U_P\left(c_{p_1},\ \rho_1 c_{p_1}^2,\ \lambda_1\right)$$
$$U_2 = -P_a(\pi - \alpha_{rs})U_S\left(\rho_1 c_{p_1}\right)$$
$$U_3 = P_a(\alpha_{tp})U_P\left(c_{p_2},\ \rho_2 c_{p_2}^2,\ \lambda_2\right)$$
$$U_4 = P_a(\alpha_{ts})U_S\left(\rho_2 c_{p_2}\right),$$

equation (6.26) becomes

$$\left(U_1 A_{rp} + U_2 A_{rs} + U_3 A_{tp} + U_4 A_{ts}\right) f(0) = P_a(\alpha_I)U_P\left(c_{p_1},\ \rho_1 c_{p_1}^2,\ \lambda_1\right) f(0).$$

Noting that this is true for arbitrary $f(0)$, we have

$$\begin{pmatrix} U_1 & U_2 & U_3 & U_4 \end{pmatrix} \begin{pmatrix} A_{rp} \\ A_{rs} \\ A_{tp} \\ A_{ts} \end{pmatrix} = P_a(\alpha_I)U_P\left(c_{p_1},\ \rho_1 c_{p_1}^2,\ \lambda_1\right) \tag{6.27}$$

if the incident wave is a P-wave. Here $(U_1\ \ U_2\ \ U_3\ \ U_4)$ is a 4×4 matrix. Solving the linear system (6.27) will give us the four amplified factors of the reflected and transmitted P-waves and S-waves, and the four corresponding waves are given by equations (6.24) and (6.25). When the incident wave is an S-wave, we only need to replace the right hand side of equation (6.27) with $P_a(\alpha_I)U_S\left(\rho_1 c_{p_1}\right)$.

6.5 The Numerical Method

We now return to the two dimensional wave equations of linear elasticity

$$\begin{aligned}
v_{1t} &= \frac{1}{\rho}\left(\sigma_{11x} + \sigma_{12y}\right) \\
v_{2t} &= \frac{1}{\rho}\left(\sigma_{12x} + \sigma_{22y}\right) \\
\sigma_{11t} &= (\lambda + 2\mu)v_{1x} + \lambda v_{2y} \\
\sigma_{12t} &= \mu(v_{1y} + v_{2x}) \\
\sigma_{22t} &= \lambda v_{1x} + (\lambda + 2\mu)v_{2y}
\end{aligned} \tag{6.28}$$

with the discontinuous coefficients

$$(\rho,\ \lambda,\ \mu) = \begin{cases} (\rho^-,\ \lambda^-,\ \mu^-) & \text{if} \quad \mathcal{F}_{\text{int}}(x,y) < 0, \\ (\rho^+,\ \lambda^+,\ \mu^+) & \text{if} \quad \mathcal{F}_{\text{int}}(x,y) > 0 \end{cases}$$

at the interface $\mathcal{C}$, defined by $\mathcal{F}_{\text{int}}(x,y) = 0$. Here, v_1 and v_2 are the two components of the velocity in x (the first coordinate) and y (the second coordinate), respectively, σ_{11}, σ_{12} and σ_{22} are the three stress components in two dimensional problems, ρ is the density, and λ and μ are Lamé constants. For the special case where the coordinate system is in the directions normal and tangential to the interface, the jump conditions are

$$[v_1] = [v_2] = [\sigma_{11}] = [\sigma_{12}] = 0. \tag{6.29}$$

The number of these physical jump conditions is fewer than that of the variables in the system of elastic wave equations. We will see in Chapter 7 that the jump condition of σ_{22} can be deduced from the specified jump conditions, together with equation (6.28).

Let

$$U = \begin{pmatrix} v_1(x,y,t) \\ v_2(x,y,t) \\ \sigma_{11}(x,y,t) \\ \sigma_{12}(x,y,t) \\ \sigma_{22}(x,y,t) \end{pmatrix}, \quad A = -\begin{pmatrix} 0 & 0 & (1/\rho) & 0 & 0 \\ 0 & 0 & 0 & (1/\rho) & 0 \\ (\lambda+2\mu) & 0 & 0 & 0 & 0 \\ 0 & \mu & 0 & 0 & 0 \\ \lambda & 0 & 0 & 0 & 0 \end{pmatrix},$$

$$B = -\begin{pmatrix} 0 & 0 & 0 & (1/\rho) & 0 \\ 0 & 0 & 0 & 0 & (1/\rho) \\ 0 & \lambda & 0 & 0 & 0 \\ \mu & 0 & 0 & 0 & 0 \\ 0 & (\lambda+2\mu) & 0 & 0 & 0 \end{pmatrix}.$$

We have the 5-variable first order system

$$U_t + AU_x + BU_y = 0. \tag{6.30}$$

For this first order system of equations, standard numerical methods can be used in regions where A and B are smooth. For example, the Lax-Wendroff method gives

$$
\begin{aligned}
U_{ij}^{n+1} &= U_{ij}^{n} - \frac{k}{2h}\Bigg(A(U_{i+1,j}^{n} - U_{i-1,j}^{n}) + B(U_{i,j+1}^{n} - U_{i,j-1}^{n})\Bigg) \\
&\quad + \frac{1}{2}\left(\frac{k}{h}\right)^2 \Bigg(A^2\left(U_{i+1,j}^{n} - 2U_{ij}^{n} + U_{i-1,j}^{n}\right) \\
&\quad +(AB+BA)\left(U_{i+1,j+1}^{n} - U_{i-1,j+1}^{n} - U_{i+1,j-1}^{n} + U_{i-1,j-1}^{n}\right) \\
&\quad +B^2\left(U_{i,j+1}^{n} - 2U_{ij}^{n} + U_{i,j-1}^{n}\right)\Bigg).
\end{aligned}
\tag{6.31}
$$

This is valid at regular points, where all nine points in the stencil lie on the same side of the interface, i.e.

$$\mathcal{F}_{\mathrm{int}}(x_i, y_j)\mathcal{F}_{\mathrm{int}}(x_{\tilde{i}}, y_{\tilde{j}}) \geq 0, \tag{6.32}$$

for $\tilde{i} = i-1,\, i,\, i+1$; $\tilde{j} = j-1,\, j,\, j+1$. This requires a nine point stencil, unlike the acoustic equation case, where we could use a five point stencil. In practice we have used CLAWPACK as described in Appendix B.

At irregular points, where some of the points of the 9-point stencil are on the other side of the interface, the Lax-Wendroff method is not valid anymore. At these points, as with the acoustic wave equations, a 6-point difference scheme of the form

$$U_{ij}^{n+1} = U_{ij}^{n} + \frac{k}{h}\sum_{l=1}^{6}\Gamma_{ij,l}U_{ij,l}^{n} \tag{6.33}$$

is used. The Γ's are 5×5 matrices, and the $U_{ij,l}^{n}$ $(l = 1,6)$ are values at grid points of the standard 5-point stencil together with one additional corner point. Note that in the acoustics problem, when the discontinuity disappears, i.e. when material properties are equal on both side of the "interface", the six-point formula recovers exactly the original numerical scheme with the standard five-point stencil. This is not the case for elasticity. When the discontinuity disappears, the six-point formula will not recover the scheme on the standard nine point stencil. The difference between the six-point and the nine-point stencil will be the contributions from the higher order terms in the local truncation errors.

We want to choose the Γ's so that second order accuracy is maintained. Consider the local truncation error

$$L = \frac{1}{h}\sum_{l=1}^{6}\Gamma_{ij,l}U_l - \Big(U_t(x_i, y_j) + \frac{1}{2}kU_{tt}(x_i, y_j)\Big) + \mathrm{O}(k^2). \tag{6.34}$$

The derivation for the Γ's will be very similar to that of the acoustic problem. We will use local coordinates in the directions normal and tangential to the interface, respectively. We write the coordinate transformation as

$$\begin{pmatrix} x \\ y \end{pmatrix} = \begin{pmatrix} \cos\beta & -\sin\beta \\ \sin\beta & \cos\beta \end{pmatrix}\begin{pmatrix} \xi \\ \eta \end{pmatrix} + \begin{pmatrix} x_0 \\ y_0 \end{pmatrix}, \tag{6.35}$$

where ξ and η are in the directions normal and tangential to the interface at $(x_0, y_0) \in \mathcal{C}$ respectively, which is a point on the interface near the point (i, j), and β is the rotation angle. Let

$$\overline{U}(\xi,\eta,t) = \begin{pmatrix} \overline{v}_1(\xi,\eta,t) \\ \overline{v}_2(\xi,\eta,t) \\ \overline{\sigma}_{11}(\xi,\eta,t) \\ \overline{\sigma}_{12}(\xi,\eta,t) \\ \overline{\sigma}_{22}(\xi,\eta,t) \end{pmatrix}, \quad Q_0 = \begin{pmatrix} c & -s & 0 & 0 & 0 \\ s & c & 0 & 0 & 0 \\ 0 & 0 & c^2 & -2cs & s^2 \\ 0 & 0 & cs & (c^2 - s^2) & -cs \\ 0 & 0 & s^2 & 2cs & c^2 \end{pmatrix}, \tag{6.36}$$

where $c = \cos\beta,\ s = \sin\beta,\ \overline{v}_1(\xi,\eta,t)$ and $\overline{v}_2(\xi,\eta,t)$ are the components of $\vec{v}$ in the ξ and η directions respectively, and the $\overline{\sigma}$'s are the stress components in the ξ-η coordinates. Then the relations of the velocity vector and stress tensor between the two coordinate systems can be expressed as (see Section 6.6)

$$U(x,y,t) = Q_0\overline{U}(\xi,\eta,t). \tag{6.37}$$

We can write the system (6.28) in ξ-η coordinates and it maintains the same form due to isotropy

$$\overline{U}_t + A\overline{U}_\xi + B\overline{U}_\eta = 0. \tag{6.38}$$

We also want to transform (6.34) to ξ-η coordinates. Now, expressing the derivatives of U with respect to t in terms of those of $\overline{U}$ with respect to ξ and η, we obtain

$$\begin{aligned} U_t &= Q_0\overline{U}_t = -Q_0\left(A\overline{U}_\xi + B\overline{U}_\eta\right) \\ U_{tt} &= Q_0\overline{U}_{tt} = Q_0\left(A^2\overline{U}_{\xi\xi} + (AB+BA)U_{\xi\eta} + B^2\overline{U}_{\eta\eta}\right). \end{aligned} \tag{6.39}$$

Also, we have

$$\sum_{l=1}^{6}\Gamma_{ij,l}U^n_{ij,l} = \sum_{l=1}^{6}\Gamma_{ij,l}Q_0\overline{U}^n_{ij,l}. \tag{6.40}$$

To simplify the notation, we will now concentrate on a particular point $(i,\ j)$ and drop these subscripts, and also incorporate the necessary rotation into the Γ's, now defining the Γ's and U's below in shorthand as

$$\Gamma_l = Q_0^{-1}\Gamma_{ij,l}Q_0, \quad \overline{U}_l = \overline{U}^n_{ij,l}. \tag{6.41}$$

Then with (6.39), (6.40) and (6.41) the local truncation error (6.34) at point (i,j) has the form

$$L = Q_0\left\{\frac{1}{h}\sum_{l=1}^{6}\Gamma_l\overline{U}_l - \left(\overline{U}_t(x_i,y_j) + \frac{1}{2}k\overline{U}_{tt}(x_i,y_j)\right)\right\} + \mathrm{O}(k^2). \tag{6.42}$$

Expanding $\overline{U}_l$ $(l = 1, 2, ..., 6)$ about point (x_0, y_0) and setting $U^* = \overline{U}(x_0, y_0)$, we get

$$\overline{U}_l = U^* + (\xi_l U^*_\xi + \eta_l U^*_\eta) + \frac{1}{2}\left(\xi_l^2 U^*_{\xi\xi} + 2\xi_l\eta_l U^*_{\xi\eta} + \eta_l^2 U^*_{\eta\eta}\right) + \mathrm{O}(k^3), \tag{6.43}$$

where ξ_l and η_l are the ξ-η coordinates of point l, and $* = -$ or $+$ depending on whether the lth point is on the $-$ or on the $+$ side of the interface. Also, with (6.39) we have

$$\begin{aligned} \overline{U}_t &= -AU^*_\xi - BU^*_\eta - \left(A\xi_2U^*_{\xi\xi} + (A\eta_2 + B\xi_2)U^*_{\xi\eta} + B\eta_2U^*_{\eta\eta}\right) + \mathrm{O}(k^2) \\ \overline{U}_{tt} &= A^2\overline{U}_{\xi\xi} + (AB+BA)\overline{U}_{\xi\eta} + B^2\overline{U}_{\eta\eta} \\ &= A^2U^*_{\xi\xi} + (AB+BA)U^*_{\xi\eta} + B^2U^*_{\eta\eta} + \mathrm{O}(k). \end{aligned} \tag{6.44}$$

Note that the center point is marked as Point 2. With the jump conditions specified (see Chapter 7 for derivation), we have the following:

$$
\begin{aligned}
U^+ &= Q_1 U^- \\
U^+_\eta &= Q_1 U^-_\eta + R_1 U^- \\
U^+_\xi &= Q_2 U^-_\xi + Q_3 U^-_\eta + R_2 U^- \\
U^+_{\eta\eta} &= Q_1 U^-_{\eta\eta} + R_3 U^-_\xi + R_4 U^-_\eta + R_5 U^- \\
U^+_{\xi\eta} &= Q_2 U^-_{\xi\eta} + Q_3 U^-_{\eta\eta} + R_6 U^-_\xi + R_7 U^-_\eta + R_8 U^- \\
U^+_{\xi\xi} &= Q_4 U^-_{\xi\xi} + Q_5 U^-_{\xi\eta} + Q_6 U^-_{\eta\eta} + R_9 U^-_\xi + R_{10} U^-_\eta + R_{11} U^-,
\end{aligned}
\tag{6.45}
$$

where the Q's and R's are 5×5 matrices, functions of λ, μ and ρ. Exchanging $+$ and $-$ signs in the superscripts of all terms (including the Q's) in (6.45), we can express $U^-, U^-_\eta, ..., U^-_{\xi\xi}$ in terms of $U^+, U^+_\eta, ..., U^+_{\xi\xi}$. Similar to the acoustics problem, plugging (6.43) and (6.44) into (6.42), and replacing $U^+, U^+_\eta, ..., U^+_{\xi\xi}$ with the jump condition (6.45), we will get the local truncation error expressed in terms of $U^-, U^-_\eta, ..., U^-_{\xi\xi}$. It will suffice for second order accuracy if we can make all the coefficients of U^-, U^-_ξ, U^-_η, $U^-_{\xi\xi}$, $U^-_{\xi\eta}$, $U^-_{\eta\eta}$ be zero in the local truncation error L. Then we have the following six equations

$$
\begin{aligned}
&\sum_{l=1}^{6} \Gamma_l \hat{Q}_1 = 0, && \sum_{l=1}^{6} \Gamma_l \hat{Q}_4 = hkA^2 - 2h\xi_2 A, \\
&\sum_{l=1}^{6} \Gamma_l \hat{Q}_2 = -hA, && \sum_{l=1}^{6} \Gamma_l \hat{Q}_5 = kh(AB+BA) - 2h(\eta_2 A + \xi_2 B), \\
&\sum_{l=1}^{6} \Gamma_l \hat{Q}_3 = -hB, && \sum_{l=1}^{6} \Gamma_l \hat{Q}_6 = hkB^2 - 2h\eta_2 B,
\end{aligned}
\tag{6.46}
$$

where the Q's are 5×5 matrices. If point l is on the same side as the center point, then

$$
\hat{Q}_1 = I,\ \hat{Q}_2 = \xi_l I,\ \hat{Q}_3 = \eta_l I,\ \hat{Q}_4 = \xi_l^2 I,\ \hat{Q}_5 = 2\xi_l \eta_l I,\ \hat{Q}_6 = \eta_l^2 I. \tag{6.47}
$$

Otherwise

$$
\begin{aligned}
\hat{Q}_1 &= Q_1 + (\eta_l R_1 + \xi_l R_2) + \frac{1}{2}(\eta_l^2 R_5 + 2\xi_l \eta_l R_8 + \xi_l^2 R_{11}) \\
\hat{Q}_2 &= \xi_l Q_2 + \frac{1}{2}(\eta_l^2 R_3 + 2\xi_l \eta_l R_5 + \xi_l^2 R_9) \\
\hat{Q}_3 &= \eta_l Q_1 + \xi_l Q_3 + \frac{1}{2}(\eta_l^2 R_4 + 2\xi_l \eta_l R_7 + \xi_l R_{10}) \\
\hat{Q}_4 &= \xi_l^2 Q_4 \\
\hat{Q}_5 &= 2\xi_l \eta_l Q_2 + \xi_l^2 Q_5 \\
\hat{Q}_6 &= \eta_l^2 Q_1 + 2\xi_l \eta_l Q_3 + \xi_l^2 Q_6.
\end{aligned}
\tag{6.48}
$$

The six matrix equations can be used to solve for Γ_l $(l = 1, ..., 6)$. Since each Γ is 5×5, we have 150 equations for 150 unknowns $(6 \times 5 \times 5)$. We do not solve for the 150 unknowns simultaneously but instead decouple the problem into smaller systems of equations. Then we need to solve a system of equations, from (6.46), of the form

$$\sum_{l=1}^{6} \Gamma_l \hat{Q}_{jl} = F_j, \quad j = 1, 2, ..., 6,$$

where F_j (j = 1,2,...,6) are the 5×5 matrix right hand sides of equations (6.46). Taking the transpose of the system, we get

$$\sum_{l=1}^{6} \hat{Q}'_{jl} \Gamma'_l = F'_j, \quad j = 1, 2, ..., 6,$$

which is equivalent to

$$\hat{Q}\hat{\Gamma} = \hat{F}, \tag{6.49}$$

where Q is a block 6×6 matrix, with element (j, l) being $\hat{Q}'_{jl}$, and $\hat{\Gamma}$ and $\hat{F}$ are block 6×1 matrices, with element l being Γ'_l and F'_j respectively. Solving for the system of equations (6.49) is equivalent to solving for 5 systems of 30×30 linear equations, with the 5 systems having the same coefficient matrix $\hat{Q}$.

All the properties discussed in Chapter 4 which led to low cost for the acoustics problem are retained, with elasticity posing a larger system for the Γ's. Solving elasticity problems are certainly more expensive computationally, but the analysis of relative computational costs in Chapter 4 is still valid. That means that the computational cost to obtain the Γ's for all the irregular points near the interface is between $O(m)$ and $O(m^2)$, depending on which of the two costs dominate — the cost for computing the Γ's, or the cost for determining whether each point is regular or irregular; the cost to update U values at all irregular points near the interface is $O(mn)$; and the cost to use a standard solver over all grid points is $O(m^2 n)$; where $m = 1/h$ (h is the grid size) and n is the total number of time steps we use in the computation. Table 6.5 in Section 6.7 confirms this analysis.

A noticeable difference between acoustics and elasticity problems is that we could use a five-point stencil for regular points away from the interface for the former, but we must use a nine-point stencil for the latter because of the appearance of cross derivative terms. In the special case where the material properties are equal on both sides of the interface (i.e., the interface actually disappears), Γ_6 will be zero and the special formula will recover the original five-point stencil scheme for the acoustics problem, while it is not the case for a scheme of a nine-point stencil in solving elasticity problems. Since the contribution from the four corner points do not disappear due to cross derivative terms, a six-point stencil scheme will not give the same scheme as a nine-point stencil scheme.

6.6 Coordinate Transformation

In order to use the jump conditions efficiently, it is essential to have the proper coordinate transformation. The correct matrix form for the transformation will not be as obvious as in the acoustics problem. The first two variables u and v are the components of the velocity vector, while the last three variables σ_{11}, σ_{12} and σ_{22} are the components of the stress tensor. To derive the transformation matrix, we will work on the components of the velocity vector and stress tensor separately. Consider again the wave equations for elasticity

$$
\begin{aligned}
v_{1t} &= \frac{1}{\rho}\left(\sigma_{11x} + \sigma_{12y}\right) \\
v_{2t} &= \frac{1}{\rho}\left(\sigma_{12x} + \sigma_{22y}\right) \\
\sigma_{11t} &= (\lambda + 2\mu)v_{1x} + \lambda v_{2y} \\
\sigma_{12t} &= \mu(v_{1y} + v_{2x}) \\
\sigma_{22t} &= \lambda v_{1x} + (\lambda + 2\mu)v_{2y}.
\end{aligned}
\tag{6.50}
$$

The system of equation (6.50) maintains the same form in ξ-η coordinates due to isotropy:

$$
\begin{aligned}
\overline{v}_{1t} &= \frac{1}{\rho}\left(\overline{\sigma}_{11\xi} + \overline{\sigma}_{12\eta}\right) \\
\overline{v}_{2t} &= \frac{1}{\rho}\left(\overline{\sigma}_{12\xi} + \overline{\sigma}_{22\eta}\right) \\
\overline{\sigma}_{11t} &= (\lambda + 2\mu)\overline{v}_{1\xi} + \lambda \overline{v}_{2\eta} \\
\overline{\sigma}_{12t} &= \mu(\overline{v}_{1\eta} + \overline{v}_{2\xi}) \\
\overline{\sigma}_{22t} &= \lambda \overline{v}_{1\xi} + (\lambda + 2\mu)\overline{v}_{2\eta}.
\end{aligned}
\tag{6.51}
$$

Variables with a bar mean components of velocity and stresses in ξ-η coordinates. Let the coordinate transformation be given by

$$
\begin{pmatrix} x \\ y \end{pmatrix} = P_1 \begin{pmatrix} \xi \\ \eta \end{pmatrix} + \begin{pmatrix} x_0 \\ y_0 \end{pmatrix}, \tag{6.52}
$$

or, equivalently,

$$
\begin{pmatrix} \xi \\ \eta \end{pmatrix} = Q_1 \begin{pmatrix} x - x_0 \\ y - y_0 \end{pmatrix}, \tag{6.53}
$$

with the rotation matrices P_1 and Q_1 of the form

$$
P_1 = \begin{pmatrix} c & -s \\ s & c \end{pmatrix}, \quad Q_1 = \begin{pmatrix} c & s \\ -s & c \end{pmatrix}, \tag{6.54}
$$

where $c = \cos\beta$ and $s = \sin\beta$, with β being the rotation angle. Then we have

$$\begin{pmatrix} v_1 \\ v_2 \end{pmatrix} = P_1 \begin{pmatrix} \overline{v}_1 \\ \overline{v}_2 \end{pmatrix}. \tag{6.55}$$

The relationship for the stress tensors in the two coordinate systems is given by the equation

$$\overline{\sigma}_{mn} = q_{mj} q_{nk} \sigma_{jk}, \tag{6.56}$$

where q_{mj} and q_{nk} are the elements of rotation matrix Q_1, and the repeated indices are to be summed from 1 to 2 (or 3 in a three dimensional problem), as is the convention in tensor analysis and elasticity. We can write these equations explicitly as

$$\overline{\sigma}_{11} = q_{11}^2 \sigma_{11} + q_{11} q_{12} \sigma_{12} + q_{12} q_{11} \sigma_{21} + q_{12}^2 \sigma_{22},$$

or

$$\overline{\sigma}_{11} = c^2 \sigma_{11} + 2cs\sigma_{12} + s^2 \sigma_{22}.$$

Similarly we have

$$\overline{\sigma}_{12} = -cs\sigma_{11} + (c^2 - s^2)\sigma_{12} + cs\sigma_{22}$$

$$\overline{\sigma}_{22} = s^2 \sigma_{11} - 2cs\sigma_{12} + c^2 \sigma_{22},$$

or in matrix form, we get

$$\begin{pmatrix} \overline{\sigma}_{11} \\ \overline{\sigma}_{12} \\ \overline{\sigma}_{22} \end{pmatrix} = Q_2 \begin{pmatrix} \sigma_{11} \\ \sigma_{12} \\ \sigma_{22} \end{pmatrix}.$$

Equivalently,

$$\begin{pmatrix} \sigma_{11} \\ \sigma_{12} \\ \sigma_{22} \end{pmatrix} = P_2 \begin{pmatrix} \overline{\sigma}_{11} \\ \overline{\sigma}_{12} \\ \overline{\sigma}_{22} \end{pmatrix}, \tag{6.57}$$

where

$$P_2 = \begin{pmatrix} c^2 & -2cs & s^2 \\ cs & (c^2 - s^2) & -cs \\ s^2 & 2cs & c^2 \end{pmatrix}, \quad Q_2 = \begin{pmatrix} c^2 & 2cs & s^2 \\ -cs & (c^2 - s^2) & cs \\ s^2 & -2cs & c^2 \end{pmatrix},$$

Combining (6.55) and (6.57), we get the relation for $\overline{U}$ and U

$$\overline{U} = QU, \quad U = P\overline{U}, \tag{6.58}$$

where

$$Q = \begin{pmatrix} Q_1 & 0 \\ 0 & Q_2 \end{pmatrix}, \quad P = \begin{pmatrix} P_1 & 0 \\ 0 & P_2 \end{pmatrix}, \tag{6.59}$$

and Q, obtainable by replacing s with $-s$ in P, is the inverse matrix of P.

6.7 Computational Examples

Example 6.7.1. The first example is a plane P-wave hitting an linear interface at an incident angle of $\alpha_I = \text{Arctan}(1.3)$. The initial data is

$$\begin{aligned} \sigma_{11} &= -\rho c_p^2 f(\xi) \\ \sigma_{12} &= 0 \\ \sigma_{22} &= -\lambda f(\xi) \\ v_1 &= c_p f(\xi) \\ v_2 &= 0 \end{aligned}$$

under ξ-η coordinates, which are given by

$$\begin{aligned} \xi &= (x - 0.5)\cos(0.05\pi) - (y + 0.2)\sin(0.05\pi) \\ \eta &= (x - 0.5)\sin(0.05\pi) + (y + 0.2)\cos(0.05\pi). \end{aligned}$$

The interface is at $\xi = 0$ and the function $f(\xi)$ is a single hump given by

$$f(\xi) = \begin{cases} \dfrac{1}{2}(1 - \cos(\omega\xi)) & \text{if } \; -0.2 \le \xi \le 0, \\ 0 & \text{otherwise,} \end{cases}$$

with $\omega = 10\pi$. This initial data gives an oscillatory plane P-wave. The coefficients of the elasticity equations are $\lambda_1 = 1.8$, $\mu_1 = 1.5$, and $\rho = 0.5$ (for $\xi < 0$) and $\lambda_1 = 1$, $\mu_1 = 1$, and $\rho = 1$ (for $\xi > 0$). CLAWPACK with superbee limiter is used on regular points away from the interface. Figure 6.2 and 6.4 show the contour plots of the solutions at $t = 0.75$ of σ_{22} and v_2 respectively. On the left is the exact solution and on the right is the computed solution. When the incident wave (upper-left) hits the interface of the discontinuity, it generates transmitted (lower-left) and reflected (right side of the interface) P-waves and S-waves. Figure 6.3 shows the mesh plots of σ_{22} (top) and y-velocity v_2 (bottom). The transmitted and reflected P-waves and S-waves are displayed as well as the incident P wave.

Table 6.1 shows the 1-norm and max-norm errors in σ_{22} at slice $y = 0.6$, at which the solution is discontinuous. Table 6.2 shows the errors at slice $y = 0.25$, where reflected and transmitted P-waves and S-waves are captured. Similar errors for y-velocity v_2 are shown in tables 6.3 and 6.4 respectively. Second order accuracy is observed, the max-norm error in σ_{22} at slice $y = 0.6$ is not quite as good as the rest of other errors.

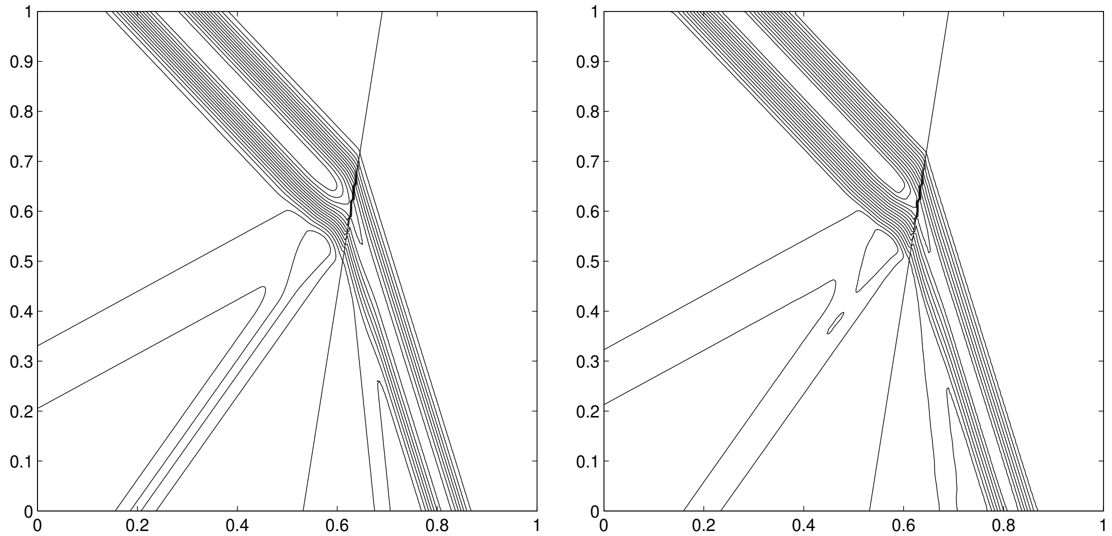

Figure 6.2: Oscillatory plane P-wave hump hitting a linear interface, creating four waves: reflected and transmitted P-waves and S-waves. Shown on the left is the contour plot of the exact solution of σ_{22} and on the right is that of computed σ_{22}.

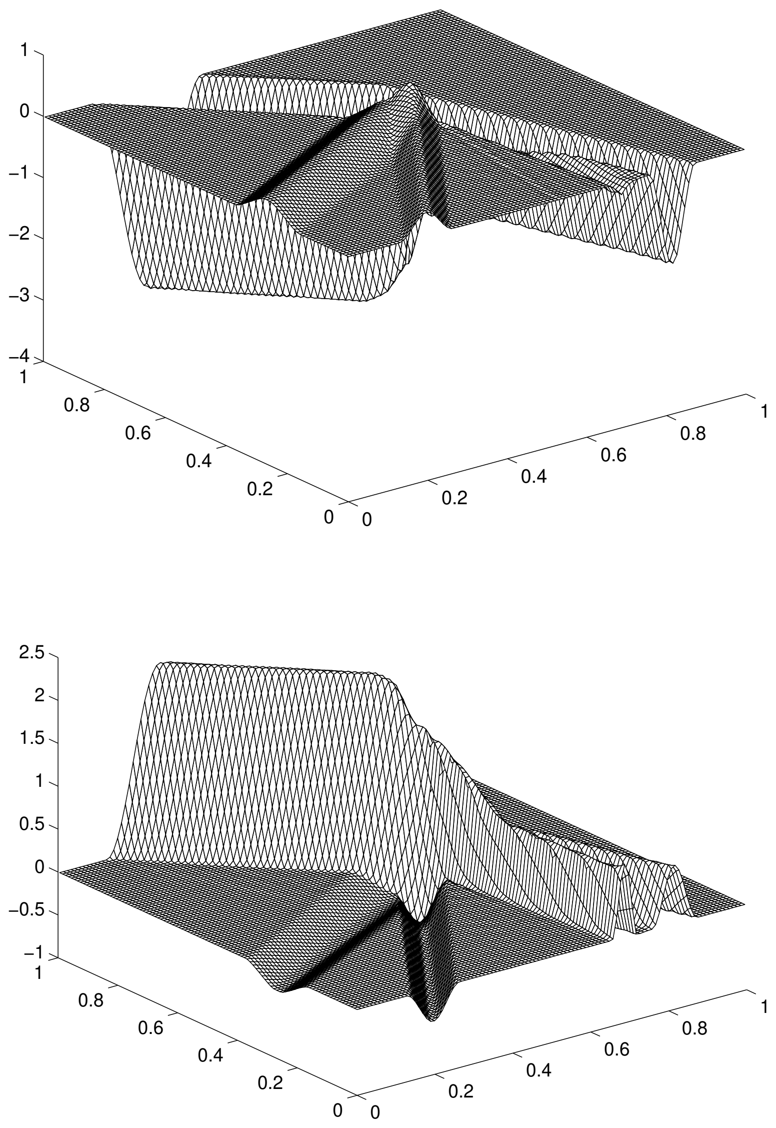

Figure 6.3: Oscillatory plane P-wave hump hitting a linear interface, creating four waves: reflected and transmitted P-waves and S-waves. Shown on the top is the mesh plot of σ_{22} and on the bottom is that of y-velocity v_2. All the five waves are clearly shown.

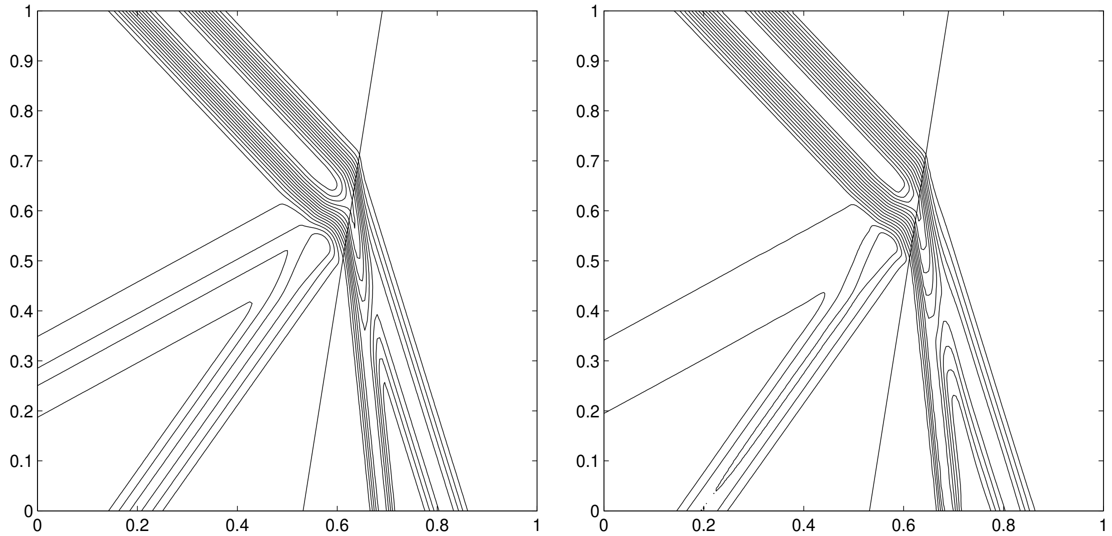

Figure 6.4: Oscillatory plane P-wave hump hitting a linear interface, creating four waves: reflected and transmitted P-waves and S-waves. Shown on the left is the contour plot of the exact solution of y-velocity v and on the right is that of computed v.

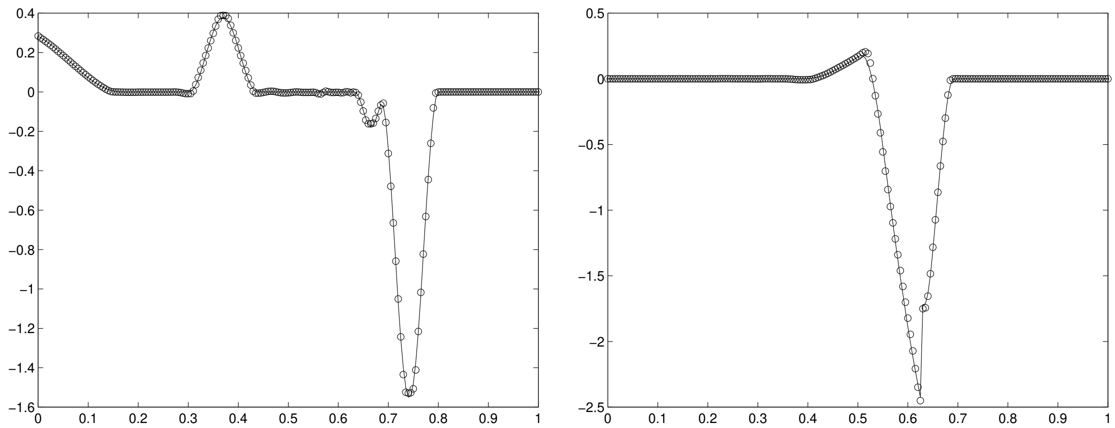

Figure 6.5: Oscillatory plane P-wave hump hitting a linear interface. Slice plot of σ_{22} at $y = 0.25$ and $y = 0.6$, the former of which shows four waves; the latter is discontinuous at the interface. Solid lines denote the exact solutions; the 'o' symbol denote the computed solutions.

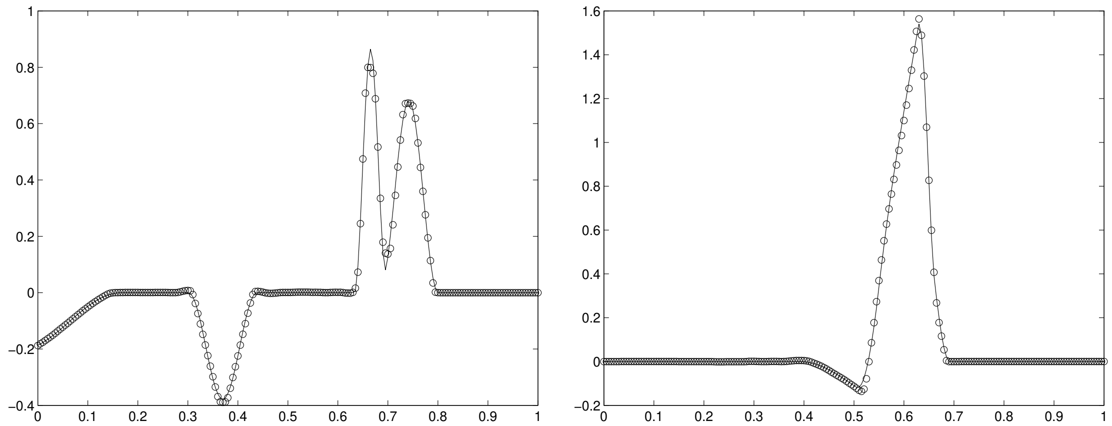

Figure 6.6: Oscillatory plane P-wave hump hitting a linear interface. Slice plots of y-velocity v at $y = 0.25$ and $y = 0.6$. The solid lines denote the exact solutions; 'o' symbol denote the computed solutions.

Table 6.1: Errors in σ_{22} at Slice $y = 0.6$

grid	1-norm	rate	max-norm	rate
100	0.0395435		0.189106	
120	0.0279489	1.90	0.148206	1.34
150	0.0187347	1.79	0.111040	1.29
180	0.0135133	1.79	0.088271	1.26
200	0.0112128	1.77	0.077510	1.23
250	0.0074677	1.82	0.059286	1.20
300	0.0053325	1.85	0.047464	1.22

Table 6.2: Errors in σ_{22} at Slice $y = 0.25$

grid	1-norm	rate	max-norm	rate
100	0.0438440		0.347881	
120	0.0331450	1.53	0.287250	1.05
150	0.0226886	1.70	0.210640	1.39
180	0.0163196	1.81	0.158750	1.55
200	0.0134246	1.85	0.135808	1.48
250	0.0087151	1.94	0.092511	1.72
300	0.0063273	1.76	0.066606	1.80

Table 6.3: Errors in v_2 at Slice $y = 0.6$

grid	1-norm	rate	max-norm	rate
100	0.0262741		0.199218	
120	0.0187689	1.84	0.149492	1.58
150	0.0125525	1.80	0.097985	1.89
180	0.0090498	1.79	0.069156	1.91
200	0.0074736	1.82	0.057018	1.83
250	0.0050880	1.72	0.036598	1.99
300	0.0037014	1.75	0.025591	1.96

Table 6.4: Errors in v_2 at Slice $y = 0.25$

grid	1-norm	rate	max-norm	rate
100	0.0419067		0.3851581	
120	0.0330534	1.30	0.3389520	0.70
150	0.0234914	1.53	0.2587020	1.21
180	0.0173938	1.65	0.1947550	1.56
200	0.0142987	1.86	0.1677230	1.42
250	0.0095031	1.83	0.1010830	2.27
300	0.0069198	1.74	0.0606283	2.80

Table 6.5 shows three computational costs, C_{prep}, C_{irr} and C_{total}, for this problem with different grid sizes. All are measured in seconds on a DEC 3000/650 with 32 MB (hyak) workstation. Here C_{prep} is the cost for preprocessing step (one time cost for computing the Γ's), C_{irr} is the cost for updating solutions at irregular points near the interface using the special finite difference formula, and C_{total} is the total cost for the entire computation. We compute the solutions at the same stopping time with different grid sizes. Note that with fixed CFL number, time steps will be proportional to $m = 1/h$, where h is the grid size. For example, if we compute a solution at $n_1 = 100$ time steps with $m = 100$ (grid size $h_1 = 1/100$), then we need to compute the same solution for $n_2 = 2n_1 = 200$ time steps with $m_2 = 2m_1 = 200$. We start with $m = 50$ and $n = 50$ in this table.

This table confirms that cost C_{prep} is proportional to $C_1 m + C_2 m^2$, where $C_1 \gg C_2$, cost C_{irr} is proportional to mn, and cost C_{total} is proportional to $m^2 n$. It shows that both C_{prep} and C_{irr} are very small compared with the total cost of the entire computation. When we refine the grid, the computational cost for using the Immersed Interface Method is relatively negligible. This advantage is very important, especially when one applies this method to solve inverse problems or moving interface problems.

A comparison of acoustics and elasticity problems is interesting. From Tables 4.5 and 6.5, we can estimate that cost C_{prep} for the elasticity problem is roughly 12-20 times larger than that for the acoustics problem due to the fact that larger systems must be solved. Nevertheless, the cost of the preprocessing and also the updating at irregular points is still negligible relative to the overall cost of time-stepping.

Table 6.5: Computational Cost Comparison

grid m	C_{prep} (sec)	C_{irr} (sec)	C_{total} (sec)
50	0.5449	0.7695	18.00
100	1.0898	3.1123	123.31
150	1.5986	7.1514	405.03
200	2.1298	12.7617	951.00
250	2.7138	19.9307	1772.39
300	3.2470	28.6025	2783.62

6.7.1 Plane S-wave

Example 6.7.2. The second example is a plane S-wave hitting a linear interface of $\xi = 0$ at an incident angle of $\pi/10$, where ξ is the first component of the ξ-η coordinate system given by

$$\begin{aligned} \xi &= (x - 0.8)\cos(\pi/10) + (y + 0.2)\sin(\pi/10) \\ \eta &= -(x - 0.8)\sin(\pi/10) + (y + 0.2)\cos(\pi/10). \end{aligned}$$

The initial data is

$$
\begin{aligned}
\sigma_{11} &= 0 \\
\sigma_{12} &= -f(\xi) \\
\sigma_{22} &= 0 \\
v_1 &= 0 \\
v_2 &= f(\xi)/(\rho c_s)
\end{aligned}
$$

under the ξ-η coordinate system, and $f(\xi)$ is a single hump plane S-wave given by

$$
f(\xi) = \begin{cases} \frac{1}{2}(1-\cos(\omega\xi)) & \text{if } -0.2 \le \xi \le 0, \\ 0 & \text{otherwise.} \end{cases}
$$

The coefficients are $\lambda_1 = 2$, $\mu_1 = 1.5$, and $\rho_1 = 0.5$ (for $\xi < 0$) and $\lambda_1 = 1$, $\mu_1 = 1$, and $\rho_2 = 1$ (for $\xi > 0$).

CLAWPACK with no limiter is used for the regular points away from the interface. Solutions are computed and plotted at $t = 1$. Figure 6.7 shows contour plots of the exact solution (left) and the computed solution (right). Transmitted and reflected P-waves and S-waves are captured well after the incident wave hits the interface of the discontinuity.

Figure 6.8 shows slices of σ_{12} at $y = 0.2$ (left), where the reflected and transmitted P-waves and S-waves are shown, and at $y = 0.75$ (right), where the solution is discontinuous at the interface.

Figure 6.9 shows the mesh plot of σ_{12} (top) and the y-velocity v_2. In the former, the reflected and transmitted P-waves and S-waves are displayed as well as the incident wave. For the latter, the view of the transmitted P-wave is blocked by the transmitted S-wave.

Tables 6.6 and 6.7 show the 1-norm and max-norm errors at slice $y = 0.75$ and $y = 0.2$ respectively. For the former the solution is discontinuous at the interface, while for the latter the reflected and transmitted P-waves and S-waves are captured. Second order pointwise accuracy is verified.

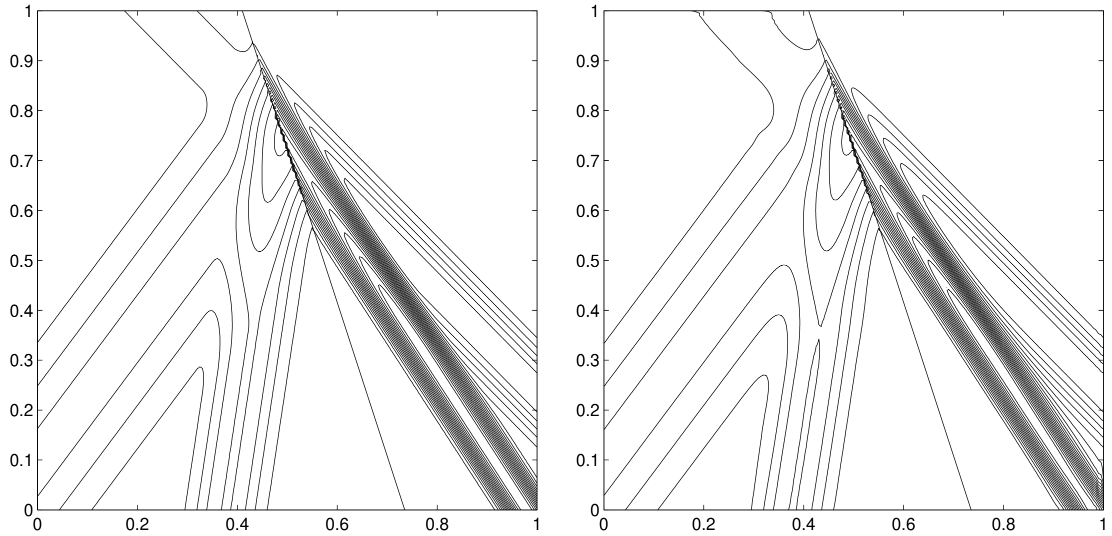

Figure 6.7: Oscillatory plane S-wave hump hitting a linear interface, creating four waves: reflected and transmitted P-waves and S-waves. Shown on the left is the contour plot of the exact solution of σ_{12} and on the right that of computed σ_{12}.

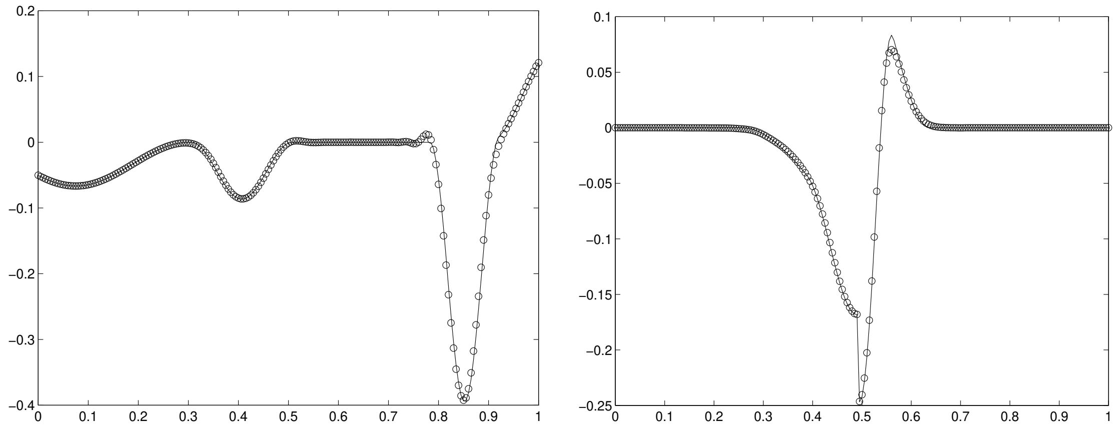

Figure 6.8: Slice plot of σ_{12} for an oscillatory plane S-wave hump hitting a linear interface. Four waves are captured at $y = 0.2$ (left), and at $y = 0.75$ (right), the solution is discontinuous at the interface. Solid lines denote the exact solutions, 'o' symbols denote computed solutions.

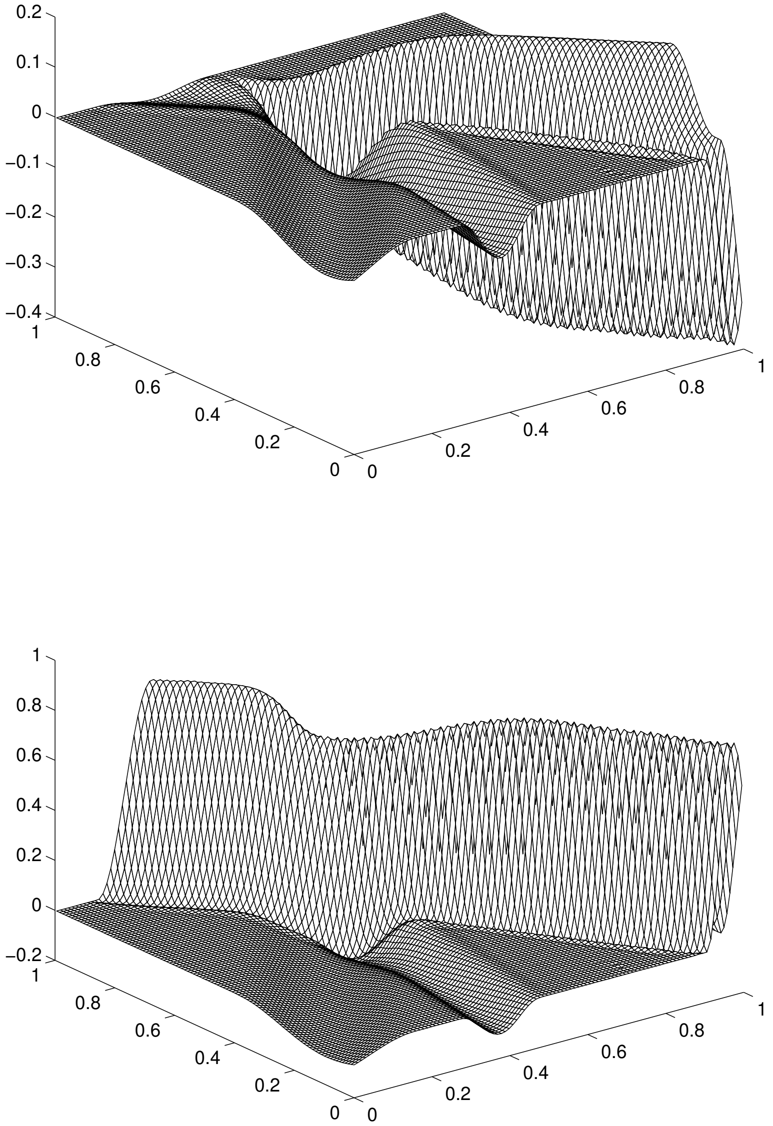

Figure 6.9: Oscillatory plane S-wave hump hitting a linear interface. Mesh plots of σ_{22} (top) and y-velocity v_2 (bottom), where for the latter the view for the transmitted P-wave is blocked by the transmitted S-wave.

Table 6.6: Errors in σ_{12} at Slice $y = 0.75$

grid	1-norm	rate	max-norm	rate
100	0.00325418		0.0266990	
120	0.00237119	1.74	0.0209451	1.33
150	0.00159376	1.78	0.0140678	1.78
180	0.00114724	1.80	0.0101048	1.81
200	0.00094536	1.84	0.0081763	2.01
250	0.00062021	1.89	0.0052414	1.99
300	0.00044147	1.86	0.0037038	1.90

Table 6.7: Errors in σ_{12} at Slice $y = 0.2$

grid	1-norm	rate	max-norm	rate
100	0.00726180		0.059264	
120	0.00526575	1.76	0.046253	1.36
150	0.00350206	1.83	0.032030	1.65
180	0.00248312	1.89	0.023254	1.76
200	0.00205146	1.81	0.019235	1.80
250	0.00136841	1.81	0.012398	1.97
300	0.00097360	1.87	0.008618	1.99

Figure 6.10 and 6.11 give plots for y-velocity v_2 similar to Figure 6.7 and 6.8, with the same locations for the slices.

As a comparison, solutions are computed with the Lax-Wendroff method on regular points, combined with the Immersed Interface Method on irregular points near the interface. Figure 6.12 shows the contour plots of σ_{12} (left) and y-velocity v_2 (right), and Figure 6.13 shows their slices at $y = 0.2$. The Immersed Interface Method can be used together with any standard solver, and the plots show that using CLAWPACK as the solver for the regular points (even when no limiter is used) helps to dampen the oscillation. It is more visible in the σ_{12} plots.

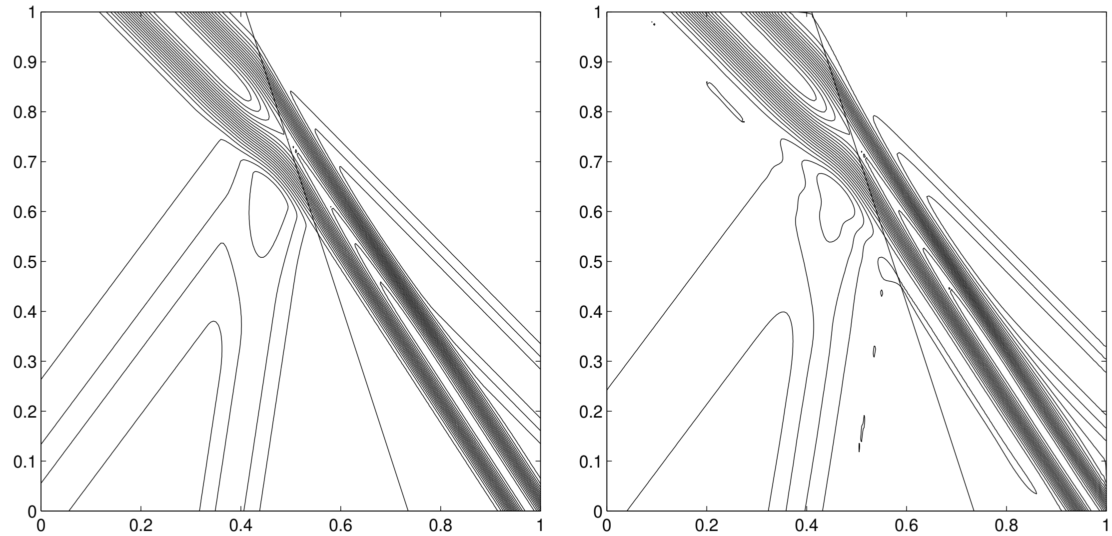

Figure 6.10: Oscillatory plane S-wave hump hitting a linear interface, creating four waves: reflected and transmitted P-waves and S-waves. Shown on the left is the contour plot of the exact solution of y-velocity v_2 and on the right is that of computed v_2.

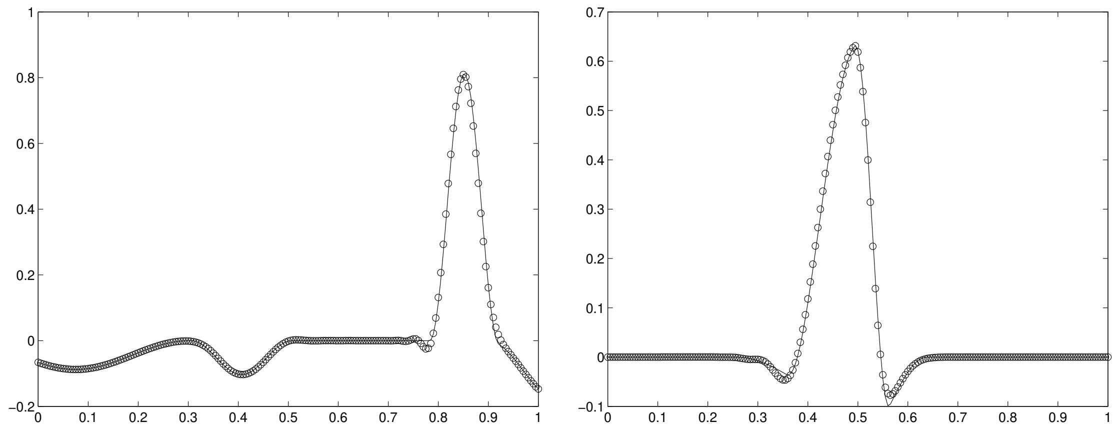

Figure 6.11: Oscillatory plane S-wave hump hitting a linear interface. Slice plot of y-velocity v_2 at $y = 0.2$ (left) and $y = 0.75$ (right). Solid lines denote the exact solution; 'o' symbols denote computed solutions.

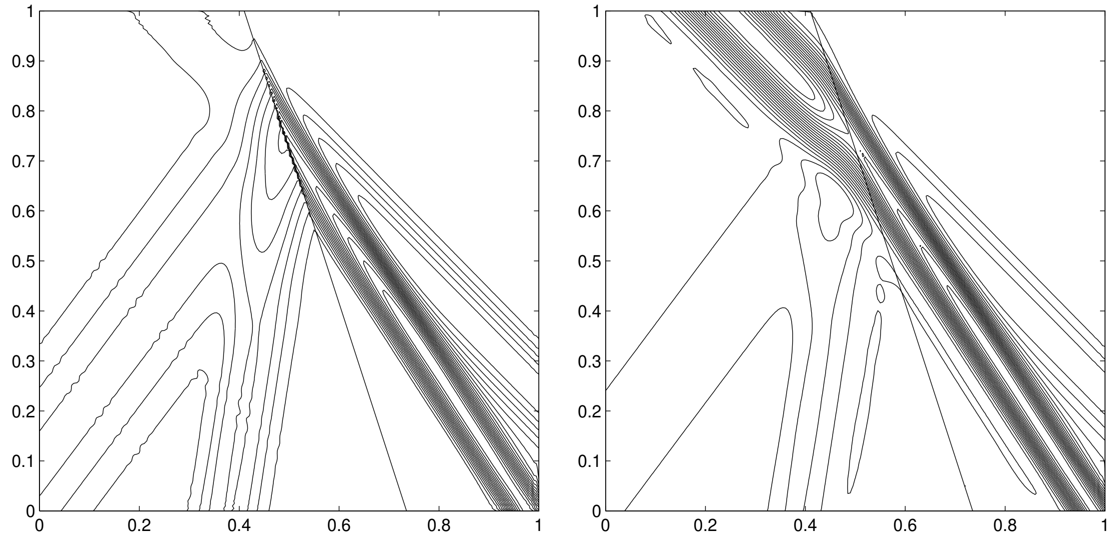

Figure 6.12: Oscillatory plane S-wave hump hitting a linear interface, creating four waves: reflected and transmitted P-waves and S-waves. Solutions are obtained with the Lax-Wendroff method on regular points away from the interface. Shown on the left is the contour plot of σ_{12} and on the right is that of y-velocity v_2.

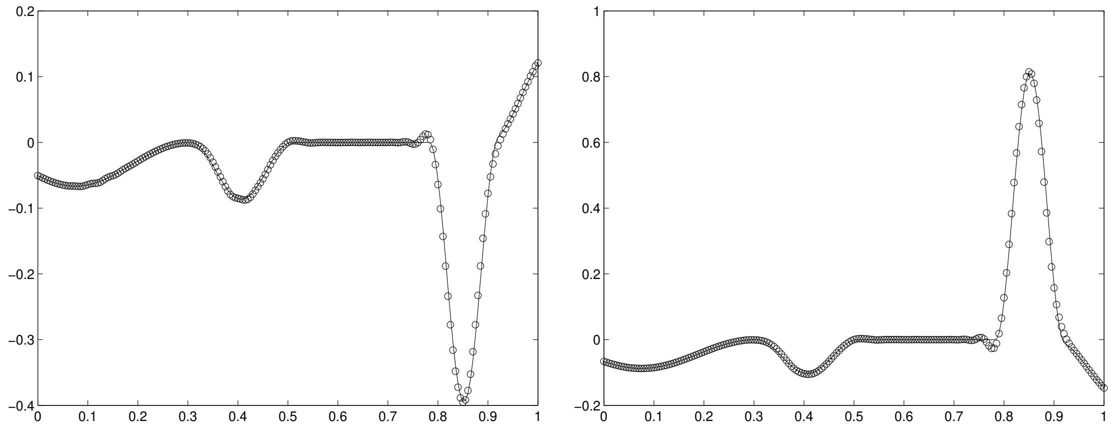

Figure 6.13: Oscillatory plane S-wave hump hitting a linear interface, creating four waves: reflected and transmitted P-waves and S-waves. Solutions are obtained with the Lax-Wendroff method on regular points away from the interface. Shown on the left is the slice plot of σ_{12} at $y = 0.2$ and on the right is that of y-velocity v_2.

6.7.2 *Circular Interface Problem*

Example 6.7.3. The third example is plane wave hitting a circular interface given by

$$(x - 0.5)^2 + (y - 0.5)^2 = 0.25^2$$

The initial data is

$$\begin{aligned} \sigma_{11} &= -(\lambda + 2\mu) f(x) \\ \sigma_{12} &= 0 \\ \sigma_{22} &= -\lambda f(x) \\ v_1 &= c_p f(x) \\ v_2 &= 0 \end{aligned}$$

where

$$f(x) = \begin{cases} \dfrac{1}{2}(1 - \cos(\omega x)) & \text{if } \ 0.04 \le x \le 0.24, \\ 0 & \text{otherwise} \end{cases}$$

with $\omega = 10\pi$. The coefficients for the problem is given as $\lambda_1 = 1$, $\mu_1 = 1$ and $\rho_1 = 1$ inside the circle, and $\lambda_2 = 2.4$, $\mu_2 = 1.2$ and $\rho_2 = 0.8$ outside of it. The solution is at time $t = 0.4$.

Figure 6.14 shows the contour plots of σ_{12} (left) and of σ_{22}, and figure 6.15 shows the x-velocity v_1 and y-velocity v_2. The solution is symmetric along $y = 0.5$. The transmitted and reflected waves are captured well.

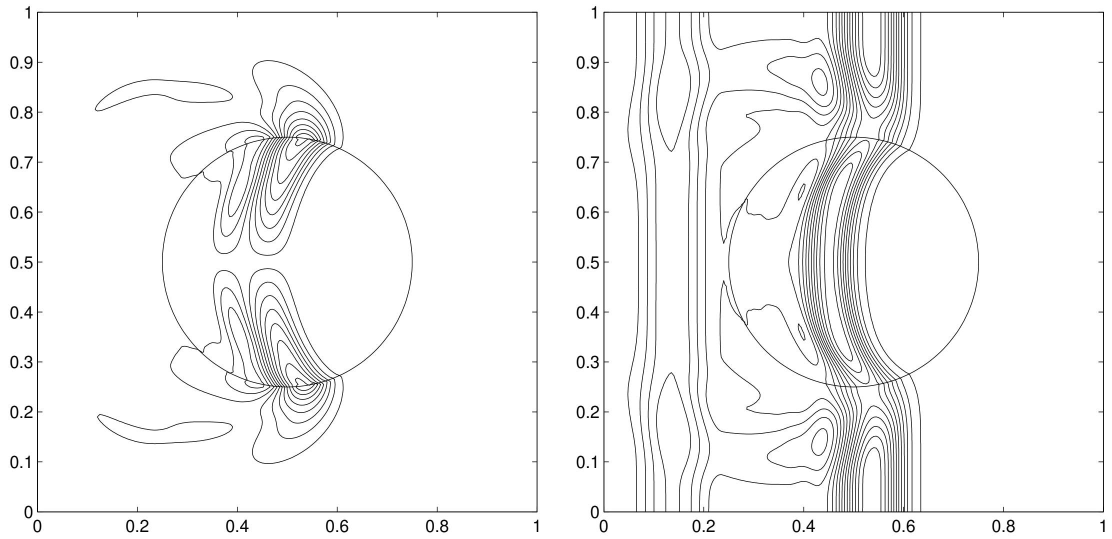

Figure 6.14: Oscillatory plane wave of a hump hitting a circular interface. Shown on the left is the contour plot of σ_{12} and on the right is that of σ_{22}.

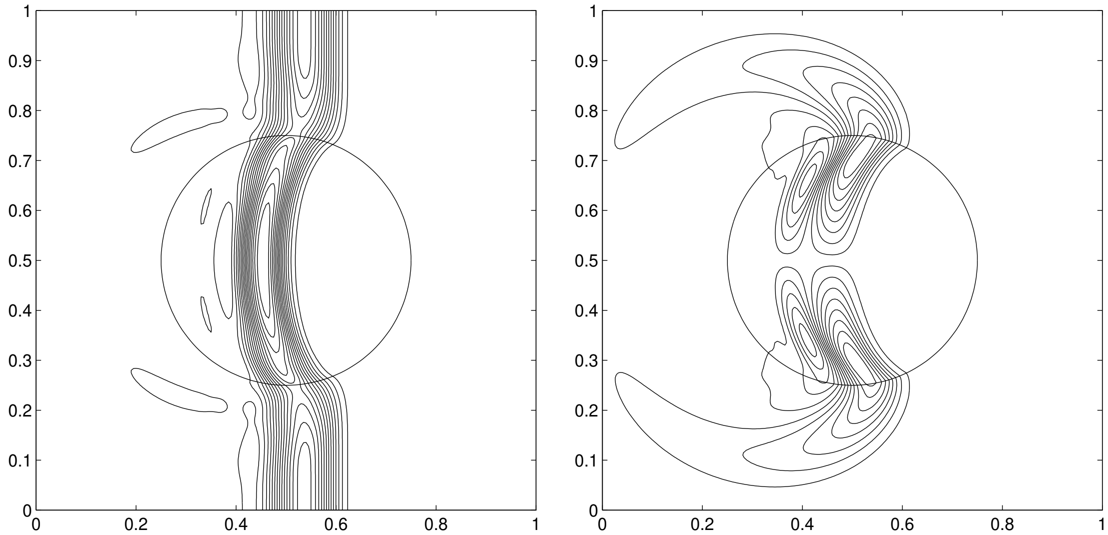

Figure 6.15: Oscillatory plane wave of a hump hitting a circular interface. Shown on the left is the contour plot of x-velocity u and on the right is that of y-velocity v.

Chapter 7

JUMP CONDITIONS AT THE INTERFACE FOR ELASTICITY

The jump conditions for vector variable U and its first and second derivatives are extremely important for the formulation of the special finite difference scheme at irregular points near the interface of discontinuity. Here we will derive those jump conditions for a linear interface in two space dimensions first, then we will derive those for curved interface.

7.1 Linear Interface

Consider the wave equations for elasticity

$$\begin{aligned} v_{1t} &= \frac{1}{\rho}\left(\sigma_{11\xi} + \sigma_{12\eta}\right) \\ v_{2t} &= \frac{1}{\rho}\left(\sigma_{12\xi} + \sigma_{22\eta}\right) \\ \sigma_{11t} &= (\lambda + 2\mu)v_{1\xi} + \lambda v_{2\eta} \\ \sigma_{12t} &= \mu(v_{1\eta} + v_{2\xi}) \\ \sigma_{22t} &= \lambda v_{1\xi} + (\lambda + 2\mu)v_{2\eta}, \end{aligned} \tag{7.1}$$

where ξ and η are coordinate directions normal and tangential to the interface at a point on the interface. Note that the last three equations are derived, by differentiating with respect to t, from

$$\begin{aligned}\sigma_{11} &= (\lambda+2\mu)u_{1\xi} + \lambda u_{2\eta} \\ \sigma_{12} &= \mu(u_{1\eta} + u_{2\xi}) \\ \sigma_{22} &= \lambda u_{1\xi} + (\lambda+2\mu)u_{2\eta}.\end{aligned} \tag{7.2}$$

The given jump conditions are

$$[v_1] = [v_2] = [\sigma_{11}] = [\sigma_{12}] = 0. \tag{7.3}$$

Recall that the jump conditions for the v_1 and v_2 are actually derived from those for u_1 and u_2:

$$[u_1] = [u_2] = 0. \tag{7.4}$$

Equations (7.3) and (7.4) give

$$\begin{aligned}&\left[u_{1\eta}\right] = \left[u_{2\eta}\right] = \left[v_{1\eta}\right] = \left[v_{1\eta}\right] = \left[\sigma_{11\eta}\right] = \left[\sigma_{12\eta}\right] = 0 \\ &\left[u_{1\eta\eta}\right] = \left[u_{2\eta\eta}\right] = \left[v_{1\eta\eta}\right] = \left[v_{2\eta\eta}\right] = [\sigma_{11}\eta\eta] = \left[\sigma_{12\eta\eta}\right] = 0 \\ &[u_{1t}] = [u_{2t}] = [v_{1t}] = [v_{2t}] = [\sigma_{11t}] = [\sigma_{12t}] = 0 \\ &[u_{1tt}] = [u_{2tt}] = [v_{1tt}] = [v_{2tt}] = [\sigma_{11tt}] = [\sigma_{12tt}] = 0,\end{aligned}$$

which will be frequently used in the derivations in this section. We can express $u_{1\xi}$ and $u_{2\eta}$ in terms of σ_{11} and σ_{22} by using (7.2):

$$\begin{aligned}u_{1\xi} &= \alpha_1\sigma_{11} + \alpha_2\sigma_{22} \\ u_{2\eta} &= \alpha_2\sigma_{11} + \alpha_1\sigma_{22},\end{aligned} \tag{7.5}$$

where

$$\begin{aligned}\alpha_1 &= \frac{\lambda+2\mu}{4\mu\,(\lambda+\mu)} \\ \alpha_2 &= -\frac{\lambda}{4\mu\,(\lambda+\mu)}.\end{aligned}$$

Then since

$$\left[u_{2\eta}\right] = 0 \quad\Longrightarrow\quad [\alpha_2\sigma_{11} + \alpha_1\sigma_{22}] = 0,$$

we get the jump condition for σ_{22}

$$\sigma_{22}^{+} = \frac{\alpha_1^-}{\alpha_1^+}\sigma_{22}^- + \frac{1}{\alpha_1^+}\left(\alpha_2^- - \alpha_2^+\right)\sigma_{11}^-. \tag{7.6}$$

Combining (7.3) and (7.6) we get

$$U^+ = Q_1 U^-, \tag{7.7}$$

where

$$Q_1 = \begin{pmatrix} 1 & 0 & 0 & 0 & 0 \\ 0 & 1 & 0 & 0 & 0 \\ 0 & 0 & 1 & 0 & 0 \\ 0 & 0 & 0 & 1 & 0 \\ 0 & 0 & q_{1,53} & 0 & q_{1,55} \end{pmatrix}, \tag{7.8}$$

with

$$q_{1,53} = \frac{\alpha_2^- - \alpha_2^+}{\alpha_1^+}, \quad q_{1,55} = \frac{\alpha_1^-}{\alpha_1^+}.$$

It follows by differentiating (7.7) twice with respect to η that

$$\begin{aligned} U_\eta^+ &= Q_1 U_\eta^- \\ U_{\eta\eta}^+ &= Q_1 U_{\eta\eta}^-. \end{aligned} \tag{7.9}$$

As for U_ξ^+, it is straight-forward to obtain $\sigma_{11\xi}$, $\sigma_{12\xi}$, $v_{1\xi}$ and $v_{2\xi}$. Starting with the first equation in (7.1), we get

$$[v_{1t}] = 0 \quad \Longrightarrow \quad \left[\frac{1}{\rho}\left(\sigma_{11\xi} + \sigma_{12\eta}\right)\right] = 0,$$

or, noting that $\sigma_{12\eta}^{+} = \sigma_{12\eta}^{-}$, we have

$$\sigma_{11\xi}^{+} = \frac{\rho^+}{\rho^-}\sigma_{11\xi}^{-} + \left(\frac{\rho^+}{\rho^-} - 1\right)\sigma_{12\eta}^{-}. \tag{7.10}$$

Similarly, by using the second equation in (7.1), we get

$$\sigma_{12\xi}^{+} = \frac{\rho^+}{\rho^-}\left(\sigma_{12\xi}^{-} + \sigma_{22\eta}^{-}\right) - \sigma_{22\eta}^{+}.$$

Eliminating $\sigma_{22\eta}^{+}$ by using (7.9), we have

$$\sigma_{12\xi}^{+} = \frac{\rho^{+}}{\rho^{-}}\sigma_{12\xi}^{-} + \frac{1}{\alpha_1^{+}}\left(\alpha_2^{+} - \alpha_2^{-}\right)\sigma_{11\eta}^{-} + \left(\frac{\rho^{+}}{\rho^{-}} - \frac{\alpha_1^{-}}{\alpha_1^{+}}\right)\sigma_{22\eta}^{-}. \tag{7.11}$$

The third and fourth equations of (7.1), together with $[\sigma_{11t}] = 0$ and $[\sigma_{12t}] = 0$, give us

$$\begin{aligned} v_{1\xi}^{+} &= \frac{(\lambda+2\mu)^{-}}{(\lambda+2\mu)^{+}}v_{1\xi}^{-} + \frac{(\lambda^{-}-\lambda^{+})}{(\lambda+2\mu)^{+}}v_{2\eta}^{-} \\ v_{2\xi}^{+} &= \frac{\mu^{-}}{\mu^{+}}v_{2\xi}^{-} + \left(\frac{\mu^{-}}{\mu^{+}} - 1\right)v_{1\eta}^{-}. \end{aligned} \tag{7.12}$$

Differentiating the second equation in (7.2) with respect to η yields

$$\sigma_{12\eta} = \mu(u_{1\eta\eta} + u_{2\xi\eta}).$$

Replacing $u_{2\eta}$ in this equation by the second expression in (7.5), we get

$$\sigma_{12\eta} = \mu(u_{1\eta\eta} + \alpha_2\sigma_{11\xi} + \alpha_1\sigma_{22\xi}). \tag{7.13}$$

Notice that

$$\left[u_{1\eta\eta}\right] = 0 \quad \Longrightarrow \quad \left[\frac{1}{\mu}\sigma_{12\eta}\right] = \left[\alpha_2\sigma_{11\xi} + \alpha_1\sigma_{22\xi}\right],$$

or,

$$\sigma_{22\xi}^{+} = \frac{\alpha_1^{-}}{\alpha_1^{+}}\sigma_{22\xi}^{-} + \frac{1}{\alpha_1^{+}}\left(\alpha_2^{-}\sigma_{11\xi}^{-} - \alpha_2^{+}\sigma_{11\xi}^{+} + \left(\frac{1}{\mu^{+}} - \frac{1}{\mu^{-}}\right)\sigma_{12\eta}^{-}\right).$$

Eliminating $\sigma_{11\xi}^{+}$ by using (7.10), we obtain

$$\begin{aligned} \sigma_{22\xi}^{+} \;=\; & \frac{\alpha_1^{-}}{\alpha_1^{+}}\sigma_{22\xi}^{-} + \frac{1}{\alpha_1^{+}}\left(\alpha_2^{-} - \alpha_2^{+}\frac{\rho^{+}}{\rho^{-}}\right)\sigma_{11\xi}^{-} \\ & + \left(\frac{\alpha_2^{+}}{\alpha_1^{+}}\left(1 - \frac{\rho^{+}}{\rho^{-}}\right) + \frac{1}{\alpha_1^{+}}\left(\frac{1}{\mu^{+}} - \frac{1}{\mu^{-}}\right)\right)\sigma_{12\eta}^{-}. \end{aligned} \tag{7.14}$$

Combining equations (7.10), (7.11), (7.12) and (7.14), we get

$$U_{\xi}^{+} = Q_2U_{\xi}^{-} + Q_3U_{\eta}^{-}, \tag{7.15}$$

where,

$$Q_2 = \begin{pmatrix} q_{2,11} & 0 & 0 & 0 & 0 \\ 0 & q_{2,22} & 0 & 0 & 0 \\ 0 & 0 & q_{2,33} & 0 & 0 \\ 0 & 0 & 0 & q_{2,44} & 0 \\ 0 & 0 & q_{2,53} & 0 & q_{2,55} \end{pmatrix}$$

$$Q_3 = \begin{pmatrix} 0 & q_{3,12} & 0 & 0 & 0 \\ q_{3,21} & 0 & 0 & 0 & 0 \\ 0 & 0 & 0 & q_{3,34} & 0 \\ 0 & 0 & q_{3,43} & 0 & q_{3,45} \\ 0 & 0 & 0 & q_{3,54} & 0 \end{pmatrix}, \tag{7.16}$$

with

$$q_{2,11} = \frac{(\lambda+2\mu)^-}{(\lambda+2\mu)^+}, \quad q_{2,22} = \frac{\mu^-}{\mu^+}, \quad q_{2,33} = q_{2,44} = \frac{\rho^+}{\rho^-},$$

$$q_{2,53} = \frac{1}{\alpha_1^+}\left(\alpha_2^- - \alpha_2^+ q_{2,33}\right), \quad q_{2,55} = q_{1,55}, \quad q_{3,12} = \frac{\lambda^- - \lambda^+}{(\lambda+2\mu)^+},$$

$$q_{3,21} = q_{2,22} - 1, \quad q_{3,34} = q_{2,33} - 1, \quad q_{3,43} = -q_{1,53},$$

$$q_{3,45} = q_{2,33} - q_{2,55}, \quad q_{3,54} = \frac{1}{\alpha_1^+}\left(\frac{1}{\mu^+} - \frac{1}{\mu^-}\right) - \frac{\alpha_2^+}{\alpha_1^+} q_{3,34}.$$

Differentiating (7.15) with respect to η gives

$$U^+_{\xi\eta} = Q_2 U^-_{\xi\eta} + Q_3 U^-_{\eta\eta}. \tag{7.17}$$

The only remaining unknown jump condition is that for $U_{\xi\xi}$. We start by differentiating the first equation in (7.1) with respect to t:

$$v_{1tt} = \frac{1}{\rho}\left(\sigma_{11t\xi} + \sigma_{12t\eta}\right).$$

Substituting σ_{11t} and σ_{12t} in the third and fourth equations in (7.1), we get

$$v_{1tt} = \frac{1}{\rho}\left((\lambda+2\mu)v_{1\xi\xi} + \mu v_{1\eta\eta} + (\lambda+\mu)v_{2\xi\eta}\right).$$

Knowing that $[v_{1tt}] = 0$ and $v_{1\eta\eta}^{+} = v_{1\eta\eta}^{-}$, we obtain

$$\begin{aligned} v_{1\xi\xi}^{+} &= \frac{\rho^{+}}{(\lambda+2\mu)^{+}} \left(\frac{(\lambda+2\mu)^{-}}{\rho^{-}} v_{1\xi\xi}^{-} + \left(\frac{\mu^{-}}{\rho^{-}} - \frac{\mu^{+}}{\rho^{+}} \right) v_{1\eta\eta}^{-} \right. \\ &\quad \left. + \frac{(\lambda+\mu)^{-}}{\rho^{-}} v_{2\xi\eta}^{-} - \frac{(\lambda+\mu)^{+}}{\rho^{+}} v_{2\xi\eta}^{+} \right). \end{aligned}$$

Eliminating $v_{2\xi\eta}^{+}$ using (7.17), we obtain

$$\begin{aligned} v_{1\xi\xi}^{+} &= \frac{\rho^{+}}{(\lambda+2\mu)^{+}} \left\{ \left(\frac{\mu^{-}}{\rho^{+}} \left(\frac{\rho^{+}}{\rho^{-}} - 1 \right) + \frac{\lambda^{+}}{\rho^{+}} \left(\frac{\mu^{-}}{\mu^{+}} - 1 \right) \right) v_{1\eta\eta}^{-} \right. \\ &\quad \left. + \frac{(\lambda+2\mu)^{-}}{\rho^{-}} v_{1\xi\xi}^{-} + \left(\frac{(\lambda+\mu)^{-}}{\rho^{-}} - \frac{\mu^{-}(\lambda+\mu)^{+}}{\mu^{+}\rho^{+}} \right) v_{2\xi\eta}^{-} \right\}. \end{aligned} \tag{7.18}$$

Similarly, we can get

$$\begin{aligned} v_{2tt} &= \frac{1}{\rho} \Big((\lambda+\mu) v_{1\xi\eta} + \mu v_{2\xi\xi} + (\lambda+2\mu) v_{2\eta\eta} \Big) \\ \sigma_{11tt} &= \frac{1}{\rho} \Big((\lambda+2\mu)\sigma_{11\xi\xi} + 2(\lambda+\mu)\sigma_{12\xi\eta} + \lambda \sigma_{22\eta\eta} \Big) \\ \sigma_{12tt} &= \frac{\mu}{\rho} \Big(\sigma_{11\xi\eta} + \sigma_{12\eta\eta} + \sigma_{12\xi\xi} + \sigma_{22\xi\eta} \Big), \end{aligned}$$

which, with $[v_{2tt}] = [\sigma_{11tt}] = [\sigma_{12tt}] = 0$ and $v_{2\eta\eta}^{+} = v_{2\eta\eta}^{-}$ and $\sigma_{12\eta\eta}^{+} = \sigma_{12\eta\eta}^{-}$, leads to

$$\begin{aligned} v_{2\xi\xi}^{+} &= \frac{\rho^{+}}{\mu^{+}} \left\{ \frac{\mu^{-}}{\rho^{-}} v_{2\xi\xi}^{-} + \frac{(\lambda+\mu)^{-}}{\rho^{-}} v_{1\xi\eta}^{-} - \frac{(\lambda+\mu)^{+}}{\rho^{+}} v_{1\xi\eta}^{+} \right. \\ &\quad \left. + \left(\frac{(\lambda+2\mu)^{-}}{\rho^{-}} - \frac{(\lambda+2\mu)^{+}}{\rho^{+}} \right) v_{2\eta\eta}^{-} \right\} \\ \sigma_{11\xi\xi}^{+} &= \frac{\rho^{+}}{(\lambda+2\mu)^{+}} \left\{ \frac{(\lambda+2\mu)^{-}}{\rho^{-}} \sigma_{11\xi\xi}^{-} + \frac{2(\lambda+\mu)^{-}}{\rho^{-}} \sigma_{12\xi\eta}^{-} \right. \\ &\quad \left. - \frac{2(\lambda+\mu)^{+}}{\rho^{+}} \sigma_{12\xi\eta}^{+} + \frac{\lambda^{-}}{\rho^{-}} \sigma_{22\eta\eta}^{-} - \frac{\lambda^{+}}{\rho^{+}} \sigma_{22\eta\eta}^{+} \right\} \\ \sigma_{12\xi\xi}^{+} &= \frac{\rho^{+}\mu^{-}}{\rho^{-}\mu^{+}} \Big(\sigma_{12\xi\xi}^{-} + \sigma_{11\xi\eta}^{-} + \sigma_{22\xi\eta}^{-} + \sigma_{12\eta\eta}^{-} \Big) - \Big(\sigma_{11\xi\eta}^{+} + \sigma_{22\xi\eta}^{+} + \sigma_{12\eta\eta}^{-} \Big). \end{aligned}$$

Using (7.9) and (7.17) to eliminate $v_{1\xi\eta}^{+}$, $\sigma_{12\xi\eta}^{+}$, $\sigma_{22\eta\eta}^{+}$, $\sigma_{11\xi\eta}^{+}$ and $\sigma_{22\xi\eta}^{+}$ on the right hand sides of the above equations, we obtain

$$\begin{aligned}
v_{2\xi\xi}^{+} &= \frac{\rho^{+}}{\mu^{+}}\left\{\frac{\mu^{-}}{\rho^{-}}v_{2\xi\xi}^{-}+\left(\frac{(\lambda+\mu)^{-}}{\rho^{-}}-\frac{(\lambda+\mu)^{+}(\lambda+2\mu)^{-}}{\rho^{+}(\lambda+2\mu)^{+}}\right)v_{1\xi\eta}^{-}\right.\\
&\quad\left.+\left(\left(\frac{\lambda+2\mu}{\rho}\right)^{-}-\left(\frac{\lambda+2\mu}{\rho}\right)^{+}+\frac{(\lambda+\mu)^{+}(\lambda^{+}-\lambda^{-})}{\rho^{+}(\lambda+2\mu)^{+}}\right)v_{2\eta\eta}^{-}\right\}\\
\sigma_{11\xi\xi}^{+} &= \frac{\rho^{+}}{(\lambda+2\mu)^{+}}\left\{\frac{(\lambda+2\mu)^{-}}{\rho^{-}}\sigma_{11\xi\xi}^{-}+\frac{2\left((\lambda+\mu)^{-}-(\lambda+\mu)^{+}\right)}{\rho^{-}}\sigma_{12\xi\eta}^{-}\right.\\
&\quad\left.+\left(\frac{\lambda^{-}}{\rho^{-}}-\frac{\lambda^{+}\alpha_1^{-}}{\rho^{+}\alpha_1^{+}}+\frac{2(\lambda+\mu)^{+}}{\rho^{+}}\left(\frac{\alpha_1^{-}}{\alpha_1^{+}}-\frac{\rho^{+}}{\rho^{-}}\right)\right)\sigma_{22\eta\eta}^{-}\right\}\\
&\quad+\frac{(\alpha_2^{-}-\alpha_2^{+})}{\alpha_1^{+}}\sigma_{11\eta\eta}^{-}\\
\sigma_{12\xi\xi}^{+} &= \left(\frac{\rho^{+}}{\rho^{-}}\left(\frac{\mu^{-}}{\mu^{+}}-1\right)-\frac{1}{\alpha_1^{+}}\left(\alpha_2^{-}-\alpha_2^{+}\frac{\rho^{+}}{\rho^{-}}\right)\right)\sigma_{11\xi\eta}^{-}\\
&\quad+\left(\frac{\rho^{+}}{\rho^{-}}\left(\frac{\mu^{-}}{\mu^{+}}-1\right)+\frac{\alpha_2^{+}}{\alpha_1^{+}}\left(\frac{\rho^{+}}{\rho^{-}}-1\right)-\frac{1}{\alpha_1^{+}}\left(\frac{1}{\mu^{+}}-\frac{1}{\mu^{-}}\right)\right)\sigma_{12\eta\eta}^{-}\\
&\quad\frac{\rho^{+}\mu^{-}}{\rho^{-}\mu^{+}}\sigma_{12\xi\xi}^{-}+\left(\frac{\rho^{+}\mu^{-}}{\rho^{-}\mu^{+}}-\frac{\alpha_1^{-}}{\alpha_1^{+}}\right)\sigma_{22\xi\eta}^{-}.
\end{aligned}\tag{7.19}$$

In order to solve for $\sigma_{22\xi\xi}^{+}$, we differentiate (7.13) with respect to ξ and get

$$\sigma_{12\xi\eta}=\mu(u_{1\xi\eta\eta}+\alpha_2\sigma_{11\xi\xi}+\alpha_1\sigma_{22\xi\xi}).$$

Substituting $u_{1\xi}$ obtained from (7.5) gives

$$\sigma_{12\xi\eta}=\mu\left(\alpha_1\sigma_{11\eta\eta}+\alpha_2\sigma_{22\eta\eta}+\alpha_2\sigma_{11\xi\xi}+\alpha_1\sigma_{22\xi\xi}\right),\tag{7.20}$$

which, together with $\sigma_{11\eta\eta}^{+}=\sigma_{11\eta\eta}^{-}$, leads to

$$\begin{aligned}
\sigma_{22\xi\xi}^{+} &= \frac{1}{\alpha_1^{+}}\left\{\alpha_1^{-}\sigma_{22\xi\xi}^{-}+\alpha_2^{-}\sigma_{11\xi\xi}^{-}-\alpha_2^{+}\sigma_{11\xi\xi}^{+}+\frac{1}{\mu^{+}}\sigma_{12\xi\eta}^{+}\right.\\
&\quad\left.-\frac{1}{\mu^{-}}\sigma_{12\xi\eta}^{-}+(\alpha_1^{-}-\alpha_1^{+})\sigma_{11\eta\eta}^{-}+\alpha_2^{-}\sigma_{22\eta\eta}^{-}-\alpha_2^{+}\sigma_{22\eta\eta}^{+}\right\}.
\end{aligned}$$

Eliminating $\sigma_{11}{}^{+}_{\xi\xi}$, $\sigma_{12}{}^{+}_{\xi\eta}$ and $\sigma_{22}{}^{+}_{\eta\eta}$ by using (7.9), (7.17) and (7.19), we get

$$\begin{aligned}
\sigma_{22}{}^{+}_{\xi\xi} \;=\; & \frac{1}{\alpha_1^+}\Bigg\{\alpha_1^-\sigma_{22}{}^{-}_{\xi\xi} + \left(\alpha_2^- - \alpha_2^+\frac{\rho^+(\lambda+2\mu)^-}{\rho^-(\lambda+2\mu)^+}\right)\sigma_{11}{}^{-}_{\xi\xi} \\
& + \left(\frac{2\alpha_2^+\rho^+\left((\lambda+\mu)^+ - (\lambda+\mu)^-\right)}{\rho^-(\lambda+2\mu)^+} + \frac{\rho^+}{\mu^+\rho^-} - \frac{1}{\mu^-}\right)\sigma_{12}{}^{-}_{\xi\eta} \\
& + \left(\frac{\alpha_2^+\rho^+}{(\lambda+2\mu)^+}\left(\frac{2(\lambda+\mu)^+}{\rho^+}\left(\frac{\rho^+}{\rho^-} - \frac{\alpha_1^-}{\alpha_1^+}\right) - \frac{\lambda^-}{\rho^-} + \frac{\lambda^+\alpha_1^-}{\rho^+\alpha_1^+}\right)\right. \\
& \left. + \frac{1}{\mu^+}\left(\frac{\rho^+}{\rho^-} - \frac{\alpha_1^-}{\alpha_1^+}\right) + \alpha_2^- - \frac{\alpha_2^+\alpha_1^-}{\alpha_1^+}\right)\sigma_{22}{}^{-}_{\eta\eta} \\
& + \left(\alpha_1^- - \alpha_1^+ + \frac{(\alpha_2^+ - \alpha_2^-)}{\alpha_1^+}\left(2\alpha_2^+ + \frac{1}{\mu^+}\right)\right)\sigma_{11}{}^{-}_{\eta\eta}\Bigg\}.
\end{aligned} \tag{7.21}$$

Combining equations (7.18), (7.19) and (7.21), we obtain

$$U^+_{\xi\xi} = Q_4 U^-_{\xi\xi} + Q_5 U^-_{\xi\eta} + Q_6 U^-_{\eta\eta}, \tag{7.22}$$

where,

$$Q_4 = \begin{pmatrix} q_{4,11} & 0 & 0 & 0 & 0 \\ 0 & q_{4,22} & 0 & 0 & 0 \\ 0 & 0 & q_{4,33} & 0 & 0 \\ 0 & 0 & 0 & q_{4,44} & 0 \\ 0 & 0 & q_{4,53} & 0 & q_{4,55} \end{pmatrix} \tag{7.23}$$

$$Q_5 = \begin{pmatrix} 0 & q_{5,12} & 0 & 0 & 0 \\ q_{5,21} & 0 & 0 & 0 & 0 \\ 0 & 0 & 0 & q_{5,34} & 0 \\ 0 & 0 & q_{5,43} & 0 & q_{5,45} \\ 0 & 0 & 0 & q_{5,54} & 0 \end{pmatrix} \tag{7.24}$$

$$Q_6 = \begin{pmatrix} q_{6,11} & 0 & 0 & 0 & 0 \\ 0 & q_{6,22} & 0 & 0 & 0 \\ 0 & 0 & q_{6,33} & 0 & q_{6,35} \\ 0 & 0 & 0 & q_{6,44} & 0 \\ 0 & 0 & q_{6,53} & 0 & q_{6,55} \end{pmatrix}, \tag{7.25}$$

with

$$q_{4,11}=q_{4,33}=\frac{\rho^+(\lambda+2\mu)^-}{\rho^-(\lambda+2\mu)^+},\quad q_{4,22}=q_{4,44}=\frac{\rho^+\mu^-}{\rho^-\mu^+},\quad q_{4,53}=\frac{\alpha_2^-}{\alpha_1^+}-\frac{\alpha_2^+}{\alpha_1^+}q_{4,11},$$

$$q_{4,55}=\frac{\alpha_1^-}{\alpha_1^+},\quad q_{5,12}=\frac{1}{(\lambda+2\mu)^+}\left(\frac{\rho^+(\lambda+\mu)^-}{\rho^-}-\frac{\mu^-(\lambda+\mu)^+}{\mu^+}\right),$$

$$q_{5,21}=\frac{\rho^+}{\mu^+}\left(\frac{(\lambda+\mu)^-}{\rho^-}-\frac{(\lambda+\mu)^+(\lambda+2\mu)^-}{\rho^+(\lambda+2\mu)^+}\right),$$

$$q_{5,34}=\frac{2\rho^+((\lambda+\mu)^--(\lambda+\mu)^+)}{\rho^-(\lambda+2\mu)^+},$$

$$q_{5,43}=\frac{\rho^+}{\rho^-}\left(\frac{\mu^-}{\mu^+}-1\right)-\frac{1}{\alpha_1^+}\left(\alpha_2^--\alpha_2^+\frac{\rho^+}{\rho^-}\right),$$

$$q_{5,45}=\frac{\rho^+\mu^-}{\rho^-\mu^+}-\frac{\alpha_1^-}{\alpha_1^+},$$

$$q_{5,54}=\frac{1}{\alpha_1^+}\left(\frac{2\alpha_2^+\rho^+\left((\lambda+\mu)^+-(\lambda+\mu)^-\right)}{\rho^-(\lambda+2\mu)^+}+\frac{\rho^+}{\mu^+\rho^-}-\frac{1}{\mu^-}\right),$$

$$q_{6,11}=\frac{1}{(\lambda+2\mu)^+}\left(\mu^-\left(\frac{\rho^+}{\rho^-}-1\right)+\lambda^+\left(\frac{\mu^-}{\mu^+}-1\right)\right),$$

$$q_{6,22}=\frac{\rho^+}{\mu^+}\left(\left(\frac{\lambda+2\mu}{\rho}\right)^--\left(\frac{\lambda+2\mu}{\rho}\right)^++\frac{(\lambda+\mu)^+(\lambda^+-\lambda^-)}{\rho^+(\lambda+2\mu)^+}\right),$$

$$q_{6,33}=\frac{\alpha_2^--\alpha_2^+}{\alpha_1^+},\quad q_{6,35}=\frac{1}{(\lambda+2\mu)^+}\left(2(\lambda+\mu)^+\left(\frac{\alpha_1^-}{\alpha_1^+}-\frac{\rho^+}{\rho^-}\right)+\frac{\lambda^-\rho^+}{\rho^-}-\frac{\lambda^+\alpha_1^-}{\alpha_1^+}\right),$$

$$q_{6,44}=\frac{\rho^+}{\rho^-}\left(\frac{\mu^-}{\mu^+}-1\right)+\frac{\alpha_2^+}{\alpha_1^+}\left(\frac{\rho^+}{\rho^-}-1\right)-\frac{1}{\alpha_1^+}\left(\frac{1}{\mu^+}-\frac{1}{\mu^-}\right),$$

$$q_{6,53}=\frac{\alpha_1^-}{\alpha_1^+}-1+\frac{(\alpha_2^+-\alpha_2^-)}{(\alpha_1^+)^2}\left(2\alpha_2^++\frac{1}{\mu^+}\right),$$

$$\begin{aligned}q_{6,55}=&\frac{\alpha_2^+}{\alpha_1^+(\lambda+2\mu)^+}\left(2(\lambda+\mu)^+\left(\frac{\rho^+}{\rho^-}-\frac{\alpha_1^-}{\alpha_1^+}\right)-\frac{\lambda^-\rho^+}{\rho^-}+\frac{\lambda^+\alpha_1^-}{\alpha_1^+}\right)\\&+\frac{1}{\alpha_1^+\mu^+}\left(\frac{\rho^+}{\rho^-}-\frac{\alpha_1^-}{\alpha_1^+}\right)+\frac{1}{\alpha_1^+}\left(\alpha_2^--\frac{\alpha_2^+\alpha_1^-}{\alpha_1^+}\right),\end{aligned}$$

or,

$$
\begin{aligned}
q_{4,11} &= q_{4,33} = q_{2,11}q_{2,33}, \quad q_{4,22} = q_{4,44} = q_{2,22}q_{2,33}, \\
q_{4,53} &= \frac{\alpha_2^-}{\alpha_1^+} - \frac{\alpha_2^+}{\alpha_1^+}q_{4,11}, \quad q_{4,55} = q_{1,55}, \\
q_{5,12} &= \frac{1}{(\lambda+2\mu)^+}\left(\frac{\rho^+(\lambda+\mu)^-}{\rho^-} - \frac{\mu^-(\lambda+\mu)^+}{\mu^+}\right), \\
q_{5,21} &= \frac{\rho^+}{\mu^+}\left(\frac{(\lambda+\mu)^-}{\rho^-} - \frac{(\lambda+\mu)^+}{\rho^+}q_{2,11}\right), \\
q_{5,34} &= \frac{2\rho^+((\lambda+\mu)^- - (\lambda+\mu)^+)}{\rho^-(\lambda+2\mu)^+}, \quad q_{5,43} = q_{2,33}q_{3,21} - q_{2,53}, \\
q_{5,45} &= q_{4,22} - q_{1,55}, \quad q_{5,54} = \frac{1}{\alpha_1^+}\left(\frac{1}{\mu^+}q_{2,33} - \frac{1}{\mu^-} - \alpha_2^+ q_{5,34}\right), \\
q_{6,11} &= \frac{1}{(\lambda+2\mu)^+}\left(\mu^- q_{3,34} + \lambda^+ q_{3,21}\right), \\
q_{6,22} &= \frac{\rho^+}{\mu^+}\left(\left(\frac{\lambda+2\mu}{\rho}\right)^- - \left(\frac{\lambda+2\mu}{\rho}\right)^+ - \frac{(\lambda+\mu)^+}{\rho^+}q_{3,12}\right), \\
q_{6,33} &= q_{1,53}, \quad q_{6,35} = \frac{1}{(\lambda+2\mu)^+}\left(\frac{\lambda^-\rho^+}{\rho^-} - \frac{\lambda^+\alpha_1^-}{\alpha_1^+} - 2(\lambda+\mu)^+ q_{3,45}\right), \\
q_{6,44} &= q_{2,33}q_{3,21} - q_{3,54}, \quad q_{6,53} = q_{1,55} - 1 - \frac{1}{\alpha_1^+}\left(2\alpha_2^+ + \frac{1}{\mu^+}\right)q_{1,53}, \\
q_{6,55} &= \frac{1}{\alpha_1^+\mu^+}\left(\frac{\rho^+}{\rho^-} - \frac{\alpha_1^-}{\alpha_1^+}\right) + \frac{1}{\alpha_1^+}\left(q_{2,53} - \alpha_2^+ q_{6,53}\right).
\end{aligned}
$$

In summary, here are the jump conditions that are needed:

$$
\begin{aligned}
U^+ &= Q_1 U^- \\
U_\eta^+ &= Q_1 U_\eta^- \\
U_{\eta\eta}^+ &= Q_1 U_{\eta\eta}^- \\
U_\xi^+ &= Q_2 U_\xi^- + Q_3 U_\eta^- \\
U_{\xi\eta}^+ &= Q_2 U_{\xi\eta}^- + Q_3 U_{\eta\eta}^- \\
U_{\xi\xi}^+ &= Q_4 U_{\xi\xi}^- + Q_5 U_{\xi\eta}^- + Q_6 U_{\eta\eta}^-,
\end{aligned}
\tag{7.26}
$$

with the Q's given in (7.8), (7.16), (7.23), (7.24), and (7.25).

7.2 Curved Interfaces

We now consider a curved interface. Let the interface be parametrically expressed locally by

$$\xi = \chi(\eta)$$

$$\eta = \eta,$$

then with the choice of the local coordinate system used in Chapter 6, i.e., the origin is at a point on the interface, and ξ and η are in the directions normal and perpendicular to the interface, we have

$$\chi(0) = 0$$

$$\chi'(0) = 0.$$

Equation (7.7) is still valid, i.e.

$$U^+ = Q_1 U^-, \tag{7.27}$$

with Q_1 defined in (7.8). Since we have

$$[u_{1\eta}] = [u_{2\eta}] = [\sigma_{11\eta}] = [\sigma_{12\eta}] = 0, \tag{7.28}$$

the jump condition for U_η^+ only changes for the component of $\sigma_{22\eta}$. The second equation in (7.5) gives

$$u_{2\eta\eta} = \alpha_2 \sigma_{11\eta} + \alpha_1 \sigma_{22\eta}.$$

We get

$$\sigma_{22}{}_\eta^+ = \frac{\alpha_1^-}{\alpha_1^+} \sigma_{22}{}_\eta^- + \frac{1}{\alpha_1^+} \left(\alpha_2^- - \alpha_2^+ \right) \sigma_{11}{}_\eta^- + \frac{1}{\alpha_1^+} [u_{2\eta\eta}]. \tag{7.29}$$

In order to eliminate $[u_{2\eta\eta}]$, we start with a general form. For any quantity $f(\xi, \eta)$ satisfying $[f(\xi, \eta)] = 0$ at the interface, differentiate it twice with respect to η, we get

$$[f_{\xi\xi} \chi'^2 + 2 f_{\xi\eta} \chi' + f_\xi \chi'' + f_{\eta\eta}] = 0. \tag{7.30}$$

Setting $\eta = 0$, and noting that $\chi'(0) = 0$, we obtain

$$[f_{\eta\eta}] = -\chi''(0)[f_\xi]. \tag{7.31}$$

In particular, we have

$$[u_{2\eta\eta}] = -\chi''(0)[u_{2\xi}]. \tag{7.32}$$

The second equation of (7.2), together with $[u_{1\eta}] = 0$, yields

$$[u_{2\xi}] = \left[\frac{1}{\mu}\sigma_{12}\right] = \left(\frac{1}{\mu^+} - \frac{1}{\mu^-}\right)\sigma_{12}^-.$$

Equation (7.29) becomes

$$\sigma_{22\eta}^+ = \frac{\alpha_1^-}{\alpha_1^+}\sigma_{22\eta}^- + \frac{1}{\alpha_1^+}\left(\alpha_2^- - \alpha_2^+\right)\sigma_{11\eta}^- - \frac{\chi''(0)}{\alpha_1^+}\left(\frac{1}{\mu^+} - \frac{1}{\mu^-}\right)\sigma_{12}^-. \tag{7.33}$$

Combining (7.28) and (7.33), we get

$$U_\eta^+ = Q_1 U_\eta^- + R_1 U^-, \tag{7.34}$$

where Q_1 is again given by (7.8), and

$$R_1 = \begin{pmatrix} 0 & 0 & 0 & 0 & 0 \\ 0 & 0 & 0 & 0 & 0 \\ 0 & 0 & 0 & 0 & 0 \\ 0 & 0 & 0 & 0 & 0 \\ 0 & 0 & 0 & r_{1,54} & 0 \end{pmatrix}, \tag{7.35}$$

with

$$r_{1,54} = -\frac{\chi''(0)}{\alpha_1^+}\left(\frac{1}{\mu^+} - \frac{1}{\mu^-}\right).$$

The derivation of jump condition for U_ξ for $v_{1\xi}^+$, $v_{2\xi}^+$, and $\sigma_{11\xi}^+$ does not depend on the interface information and therefore is still valid. Equations (7.12) and (7.10) give

$$\begin{aligned} v_{1\xi}^+ &= \frac{(\lambda+2\mu)^-}{(\lambda+2\mu)^+}v_{1\xi}^- + \frac{(\lambda^- - \lambda^+)}{(\lambda+2\mu)^+}v_{2\eta}^- \\ v_{2\xi}^+ &= \frac{\mu^-}{\mu^+}v_{2\xi}^- + \left(\frac{\mu^-}{\mu^+} - 1\right)v_{1\eta}^- \\ \sigma_{11\xi}^+ &= \frac{\rho^+}{\rho^-}\sigma_{11\xi}^- + \left(\frac{\rho^+}{\rho^-} - 1\right)\sigma_{12\eta}^-. \end{aligned} \tag{7.36}$$

By using the second equation of (7.1) and noting that $[v_{2t}] = 0$, we get

$$\sigma_{12\xi}^{+} = \frac{\rho^{+}}{\rho^{-}}\left(\sigma_{12\xi}^{-} + \sigma_{22\eta}^{-}\right) - \sigma_{22\eta}^{+}.$$

Substituting in $\sigma_{22\eta}^{+}$ from (7.32), we have

$$\begin{aligned}\sigma_{12\xi}^{+} &= \frac{\rho^{+}}{\rho^{-}}\sigma_{12\xi}^{-} + \frac{1}{\alpha_1^{+}}\left(\alpha_2^{+} - \alpha_2^{-}\right)\sigma_{11\eta}^{-} + \left(\frac{\rho^{+}}{\rho^{-}} - \frac{\alpha_1^{-}}{\alpha_1^{+}}\right)\sigma_{22\eta}^{-} \\ &\quad + \frac{\chi''(0)}{\alpha_1^{+}}\left(\frac{1}{\mu^{+}} - \frac{1}{\mu^{-}}\right)\sigma_{12}^{-}.\end{aligned} \tag{7.37}$$

For $\sigma_{22\xi}^{+}$, again we use (7.13),

$$\sigma_{12\eta} = \mu(u_{1\eta\eta} + \alpha_2\sigma_{11\xi} + \alpha_1\sigma_{22\xi}),$$

which gives

$$\left[\frac{1}{\mu}\sigma_{12\eta}\right] = \left[u_{1\eta\eta} + \alpha_2\sigma_{11\xi} + \alpha_1\sigma_{22\xi}\right],$$

or,

$$\sigma_{22\xi}^{+} = \frac{\alpha_1^{-}}{\alpha_1^{+}}\sigma_{22\xi}^{-} + \frac{1}{\alpha_1^{+}}\left(\alpha_2^{-}\sigma_{11\xi}^{-} - \alpha_2^{+}\sigma_{11\xi}^{+} + \left(\frac{1}{\mu^{+}} - \frac{1}{\mu^{-}}\right)\sigma_{12\eta}^{-}\right) - \frac{1}{\alpha_1^{+}}\left[u_{1\eta\eta}\right].$$

Eliminating $\sigma_{11\xi}^{+}$ by using (7.36), we get

$$\begin{aligned}\sigma_{22\xi}^{+} &= \frac{\alpha_1^{-}}{\alpha_1^{+}}\sigma_{22\xi}^{-} + \frac{1}{\alpha_1^{+}}\left(\alpha_2^{-} - \alpha_2^{+}\frac{\rho^{+}}{\rho^{-}}\right)\sigma_{11\xi}^{-} - \frac{1}{\alpha_1^{+}}\left[u_{1\eta\eta}\right] \\ &\quad + \left(\frac{\alpha_2^{+}}{\alpha_1^{+}}\left(1 - \frac{\rho^{+}}{\rho^{-}}\right) + \frac{1}{\alpha_1^{+}}\left(\frac{1}{\mu^{+}} - \frac{1}{\mu^{-}}\right)\right)\sigma_{12\eta}^{-}.\end{aligned} \tag{7.38}$$

By using equation (7.31) and (7.5), we get

$$[u_{1\eta\eta}] = -\chi''(0)[u_{1\xi}] = -\chi''(0)\left[\alpha_1\sigma_{11} + \alpha_2\sigma_{22}\right],$$

or,

$$[u_{1\eta\eta}] = -\chi''(0)\left(\alpha_1^{+} - \alpha_1^{-}\right)\sigma_{11}^{-} - \chi''(0)\left(\alpha_2^{+}\sigma_{22}^{+} - \alpha_2^{-}\sigma_{22}^{-}\right).$$

Eliminating σ_{22}^{+} with equation (7.6), we get

$$[u_{1\eta\eta}] = -\chi''(0)\left(\left(\alpha_1^{+} - \alpha_1^{-} + \frac{\alpha_2^{+}}{\alpha_1^{+}}\left(\alpha_2^{-} - \alpha_2^{+}\right)\right)\sigma_{11}^{-} + \left(\frac{\alpha_2^{+}\alpha_1^{-}}{\alpha_1^{+}} - \alpha_2^{-}\right)\sigma_{22}^{-}\right). \tag{7.39}$$

Substituting (7.39) into (7.38), we obtain

$$\begin{aligned}
\sigma_{22}{}_{\xi}^{+} \;=\; & \frac{\alpha_1^-}{\alpha_1^+}\sigma_{22}{}_{\xi}^{-} + \frac{1}{\alpha_1^+}\left(\alpha_2^- - \alpha_2^+\frac{\rho^+}{\rho^-}\right)\sigma_{11}{}_{\xi}^{-} \\
& + \left(\frac{\alpha_2^+}{\alpha_1^+}\left(1-\frac{\rho^+}{\rho^-}\right) + \frac{1}{\alpha_1^+}\left(\frac{1}{\mu^+}-\frac{1}{\mu^-}\right)\right)\sigma_{12}{}_{\eta}^{-} \\
& + \frac{\chi''(0)}{\alpha_1^+}\left(\left(\alpha_1^+ - \alpha_1^- + \frac{\alpha_2^+}{\alpha_1^+}\left(\alpha_2^- - \alpha_2^+\right)\right)\sigma_{11}^- \right. \\
& \left. + \left(\frac{\alpha_2^+\alpha_1^-}{\alpha_1^+} - \alpha_2^-\right)\sigma_{22}^-\right).
\end{aligned} \tag{7.40}$$

Combining equations (7.36), (7.37) and (7.40), we get the jump condition

$$U_\xi^+ = Q_2 U_\xi^- + Q_3 U_\eta^- + R_2 U^-, \tag{7.41}$$

where, Q_2 and Q_3 are the same as before, and

$$R_2 = \begin{pmatrix} 0 & 0 & 0 & 0 & 0 \\ 0 & 0 & 0 & 0 & 0 \\ 0 & 0 & 0 & 0 & 0 \\ 0 & 0 & 0 & r_{2,44} & 0 \\ 0 & 0 & r_{2,53} & 0 & r_{2,55} \end{pmatrix}, \tag{7.42}$$

with

$$\begin{aligned}
r_{2,44} &= -r_{1,54} \\
r_{2,53} &= \frac{\chi''(0)}{\alpha_1^+}\left(\alpha_1^+ - \alpha_1^- + \frac{\alpha_2^+}{\alpha_1^+}\left(\alpha_2^- - \alpha_2^+\right)\right) \\
r_{2,55} &= \frac{\chi''(0)}{\alpha_1^+}\left(\frac{\alpha_2^+\alpha_1^-}{\alpha_1^+} - \alpha_2^-\right).
\end{aligned}$$

As in (7.32), we have

$$\begin{aligned}
[v_{1\eta\eta}] &= -\chi''(0)[v_{1\xi}] \\
[v_{2\eta\eta}] &= -\chi''(0)[v_{2\xi}] \\
[\sigma_{11\eta\eta}] &= -\chi''(0)[\sigma_{11\xi}] \\
[\sigma_{12\eta\eta}] &= -\chi''(0)[\sigma_{12\xi}].
\end{aligned}$$

Which, combined with (7.36) and (7.37), leads to

$$\begin{aligned}
v_{1\eta\eta}^{+} &= v_{1\eta\eta}^{-} - \chi''(0)\left(\left(\frac{(\lambda+2\mu)^-}{(\lambda+2\mu)^+}-1\right)v_{1\xi}^{-} + \frac{(\lambda^- - \lambda^+)}{(\lambda+2\mu)^+}v_{2\eta}^{-}\right)\\
v_{2\eta\eta}^{+} &= v_{2\eta\eta}^{-} - \chi''(0)\left(\frac{\mu^-}{\mu^+}-1\right)\left(v_{2\xi}^{-} + v_{1\eta}^{-}\right)\\
\sigma_{11\eta\eta}^{+} &= \sigma_{11\eta\eta}^{-} - \chi''(0)\left(\frac{\rho^+}{\rho^-}-1\right)\left(\sigma_{11\xi}^{-} + \sigma_{12\eta}^{-}\right) \qquad (7.43)\\
\sigma_{12\eta\eta}^{+} &= \sigma_{12\eta\eta}^{-} - \chi''(0)\left(\left(\frac{\rho^+}{\rho^-}-1\right)\sigma_{12\xi}^{-} + \frac{1}{\alpha_1^+}(\alpha_2^+ - \alpha_2^-)\sigma_{11\eta}^{-}\right.\\
&\left. + \left(\frac{\rho^+}{\rho^-} - \frac{\alpha_1^-}{\alpha_1^+}\right)\sigma_{22\eta}^{-} + \frac{\chi''(0)}{\alpha_1^+}\left(\frac{1}{\mu^+}-\frac{1}{\mu^-}\right)\sigma_{12}^{-}\right).
\end{aligned}$$

From equation (7.5), we have

$$\left[u_{2\eta\eta\eta}\right] = \left[\alpha_2\sigma_{11\eta\eta} + \alpha_1\sigma_{22\eta\eta}\right],$$

or,

$$\sigma_{22\eta\eta}^{+} = \frac{\alpha_1^-}{\alpha_1^+}\sigma_{22\eta\eta}^{-} + \frac{1}{\alpha_1^+}\left(\alpha_2^-\sigma_{11\eta\eta}^{-} - \alpha_2^+\sigma_{11\eta\eta}^{+}\right) + \frac{1}{\alpha_1^+}\left[u_{2\eta\eta\eta}\right]. \qquad (7.44)$$

In order to get $\left[u_{2\eta\eta\eta}\right]$, differentiating equation (7.30), we get

$$\left[\left(f_{\xi\xi}\chi'^2 + 2f_{\xi\eta}\chi' + f_\xi\chi'' + f_{\eta\eta}\right)_\xi\chi' + \left(f_{\xi\xi}\chi'^2 + 2f_{\xi\eta}\chi' + f_\xi\chi'' + f_{\eta\eta}\right)_\eta\right] = 0.$$

Setting $\eta = 0$, with $\chi'(0) = 0$, we get

$$[3f_{\xi\eta}\chi''(0) + f_\xi\chi'''(0) + f_{\eta\eta\eta}] = 0$$

or,

$$[f_{\eta\eta\eta}] = -3\chi''(0)\,[f_{\xi\eta}] - \chi'''(0)\,[f_\xi]\,. \qquad (7.45)$$

In particular, we have

$$\left[u_{2\eta\eta\eta}\right] = -3\chi''(0)\left[u_{2\xi\eta}\right] - \chi'''(0)\left[u_{2\xi}\right]. \qquad (7.46)$$

Note that from equation (7.2) we have $u_{2\xi} = \dfrac{1}{\mu}\sigma_{12} - u_{1\eta}$, therefore we get

$$\left[u_{2\eta\eta\eta}\right] = -3\chi''(0)\left[\frac{1}{\mu}\sigma_{12\eta} - u_{1\eta\eta}\right] - \chi'''(0)\left[\frac{1}{\mu}\sigma_{12} - u_{1\eta}\right],$$

or,

$$\begin{aligned}\left[u_{2\eta\eta\eta}\right] &= -3\chi''(0)\left(\tfrac{1}{\mu^+}-\tfrac{1}{\mu^-}\right)\sigma_{12\eta}^- + 3\chi''(0)\left[u_{1\eta\eta}\right]\\ &\quad -\chi'''(0)\left(\frac{1}{\mu^+}-\frac{1}{\mu^-}\right)\sigma_{12}^-.\end{aligned}$$

Substituting in $\left[u_{1\eta\eta}\right]$ by using equation (7.39), we get

$$\begin{aligned}\left[u_{2\eta\eta\eta}\right] &= -3\chi''(0)\left(\frac{1}{\mu^+}-\frac{1}{\mu^-}\right)\sigma_{12\eta}^- - \chi'''(0)\left(\frac{1}{\mu^+}-\frac{1}{\mu^-}\right)\sigma_{12}^-\\ &\quad -3\chi''^2(0)\left(\left(\alpha_1^+-\alpha_1^-+\frac{\alpha_2^+}{\alpha_1^+}\left(\alpha_2^--\alpha_2^+\right)\right)\sigma_{11}^-\right.\\ &\quad \left.+\left(\frac{\alpha_2^+\alpha_1^-}{\alpha_1^+}-\alpha_2^-\right)\sigma_{22}^-\right).\end{aligned} \tag{7.47}$$

Replacing $\sigma_{11\eta\eta}^+$ and $\left[u_{2\eta\eta\eta}\right]$ in equation (7.44) by using equations (7.43) and (7.47), we get

$$\begin{aligned}\sigma_{22\eta\eta}^+ &= \frac{\alpha_1^-}{\alpha_1^+}\sigma_{22\eta\eta}^- + \frac{1}{\alpha_1^+}\left(\alpha_2^--\alpha_2^+\right)\sigma_{11\eta\eta}^-\\ &\quad +\chi''(0)\frac{\alpha_2^+}{\alpha_1^+}\left(\frac{\rho^+}{\rho^-}-1\right)\left(\sigma_{11\xi}^-+\sigma_{12\eta}^-\right)\\ &\quad -\frac{3\chi''(0)}{\alpha_1^+}\left(\frac{1}{\mu^+}-\frac{1}{\mu^-}\right)\sigma_{12\eta}^- - \frac{\chi'''(0)}{\alpha_1^+}\left(\frac{1}{\mu^+}-\frac{1}{\mu^-}\right)\sigma_{12}^-\\ &\quad -\frac{3\chi''^2(0)}{\alpha_1^+}\left(\left(\alpha_1^+-\alpha_1^-+\frac{\alpha_2^+}{\alpha_1^+}\left(\alpha_2^--\alpha_2^+\right)\right)\sigma_{11}^-\right.\\ &\quad \left.+\left(\frac{\alpha_2^+\alpha_1^-}{\alpha_1^+}-\alpha_2^-\right)\sigma_{22}^-\right).\end{aligned} \tag{7.48}$$

Equations (7.43) and (7.48), together with (7.41), give us

$$U_{\eta\eta}^+ = Q_1U_{\eta\eta}^- + R_3U_\xi^- + R_4U_\eta^- + R_5U^-, \tag{7.49}$$

where,

$$R_3 = \begin{pmatrix} r_{3,11} & 0 & 0 & 0 & 0\\ 0 & r_{3,22} & 0 & 0 & 0\\ 0 & 0 & r_{3,33} & 0 & 0\\ 0 & 0 & 0 & r_{3,44} & 0\\ 0 & 0 & r_{3,53} & 0 & 0\end{pmatrix}, \tag{7.50}$$

$$R_4 = \begin{pmatrix} 0 & r_{4,12} & 0 & 0 & 0 \\ r_{4,21} & 0 & 0 & 0 & 0 \\ 0 & 0 & 0 & r_{4,34} & 0 \\ 0 & 0 & r_{4,43} & 0 & r_{4,45} \\ 0 & 0 & 0 & r_{4,54} & 0 \end{pmatrix}, \tag{7.51}$$

$$R_5 = \begin{pmatrix} 0 & 0 & 0 & 0 & 0 \\ 0 & 0 & 0 & 0 & 0 \\ 0 & 0 & 0 & 0 & 0 \\ 0 & 0 & 0 & r_{5,44} & 0 \\ 0 & 0 & r_{5,53} & r_{5,54} & r_{5,55} \end{pmatrix}, \tag{7.52}$$

with

$$\begin{aligned}
r_{3,11} &= \chi''(0)\left(1 - \frac{(\lambda+2\mu)^-}{(\lambda+2\mu)^+}\right), \quad r_{3,22} = \chi''(0)\left(1 - \frac{\mu^-}{\mu^+}\right), \\
r_{3,33} &= r_{3,44} = \chi''(0)\left(1 - \frac{\rho^+}{\rho^-}\right), \quad r_{3,53} = \chi''(0)\frac{\alpha_2^+}{\alpha_1^+}\left(\frac{\rho^+}{\rho^-} - 1\right), \\
r_{4,12} &= \chi''(0)\frac{(\lambda^+ - \lambda^-)}{(\lambda+2\mu)^+}, \quad r_{4,21} = r_{3,22}, \quad r_{4,34} = r_{3,33}, \\
r_{4,43} &= \frac{\chi''(0)}{\alpha_1^+}(\alpha_2^- - \alpha_2^+), \quad r_{4,45} = \chi''(0)\left(\frac{\alpha_1^-}{\alpha_1^+} - \frac{\rho^+}{\rho^-}\right), \\
r_{4,54} &= \frac{\chi''(0)}{\alpha_1^+}\left(\alpha_2^+\left(\frac{\rho^+}{\rho^-} - 1\right) - 3\left(\frac{1}{\mu^+} - \frac{1}{\mu^-}\right)\right), \\
r_{5,44} &= \frac{\chi''(0)^2}{\alpha_1^+}\left(\frac{1}{\mu^-} - \frac{1}{\mu^+}\right), \\
r_{5,53} &= \frac{3\chi''^2(0)}{\alpha_1^+}\left(\alpha_1^- - \alpha_1^+ + \frac{\alpha_2^+}{\alpha_1^+}\left(\alpha_2^+ - \alpha_2^-\right)\right), \\
r_{5,54} &= \frac{\chi'''(0)}{\alpha_1^+}\left(\frac{1}{\mu^-} - \frac{1}{\mu^+}\right), \quad r_{5,55} = \frac{3\chi''^2(0)}{\alpha_1^+}\left(\alpha_2^- - \frac{\alpha_2^+\alpha_1^-}{\alpha_1^+}\right),
\end{aligned}$$

or,

$$
\begin{aligned}
&r_{3,11} = \chi''(0)\left(1 - q_{2,11}\right), \quad r_{3,22} = -\chi''(0) q_{3,21}, \quad r_{3,33} = -\chi''(0) q_{3,34}, \\
&r_{3,44} = r_{3,33}, \quad r_{3,53} = -\frac{\alpha_2^+}{\alpha_1^+} r_{3,33}, \quad r_{4,12} = -\chi''(0) q_{3,12}, \quad r_{4,21} = r_{3,22}, \\
&r_{4,34} = r_{3,33}, \quad r_{4,43} = \chi''(0) q_{1,53}, \quad r_{4,45} = \chi''(0)\left(q_{1,55} - q_{2,33}\right), \\
&r_{4,54} = r_{3,53} + 3r_{1,54}, \quad r_{5,44} = \chi''(0) r_{1,54}, \quad r_{5,53} = -3\chi''(0) r_{2,53}, \\
&r_{5,54} = \frac{\chi'''(0)}{\alpha_1^+}\left(\frac{1}{\mu^-} - \frac{1}{\mu^+}\right), \quad r_{5,55} = -3\chi'' r_{2,55}.
\end{aligned}
$$

For $U_{\xi\eta}$, from $\left[\sigma_{11t\eta}\right] = \left[\sigma_{12t\eta}\right] = \left[v_{1t\eta}\right] = \left[v_{2t\eta}\right] = 0$, we get

$$
\begin{aligned}
&\left[(\lambda + 2\mu) v_{1\xi\eta} + \lambda v_{2\eta\eta}\right] = 0 \\
&\left[\mu (v_{1\eta\eta} + v_{2\xi\eta})\right] = 0 \\
&\left[\frac{1}{\rho}(\sigma_{11\xi\eta} + \sigma_{12\eta\eta})\right] = 0 \\
&\left[\frac{1}{\rho}(\sigma_{12\xi\eta} + \sigma_{22\eta\eta})\right] = 0,
\end{aligned}
$$

or,

$$
\begin{aligned}
v_{1\xi\eta}^{+} &= \frac{(\lambda + 2\mu)^-}{(\lambda + 2\mu)^+} v_{1\xi\eta}^{-} + \frac{\lambda^-}{(\lambda + 2\mu)^+} v_{2\eta\eta}^{-} - \frac{\lambda^+}{(\lambda + 2\mu)^+} v_{2\eta\eta}^{+} \\
v_{2\xi\eta}^{+} &= \frac{\mu^-}{\mu^+} v_{2\xi\eta}^{-} + \frac{\mu^-}{\mu^+} v_{1\eta\eta}^{-} - v_{1\eta\eta}^{+} \\
\sigma_{11\xi\eta}^{+} &= \frac{\rho^+}{\rho^-} \sigma_{11\xi\eta}^{-} + \frac{\rho^+}{\rho^-} \sigma_{12\eta\eta}^{-} - \sigma_{12\eta\eta}^{+} \\
\sigma_{12\xi\eta}^{+} &= \frac{\rho^+}{\rho^-} \sigma_{12\xi\eta}^{-} + \frac{\rho^+}{\rho^-} \sigma_{22\eta\eta}^{-} - \sigma_{22\eta\eta}^{+}.
\end{aligned}
$$

Eliminating $v_{2\eta\eta}^{+}$, $v_{1\eta\eta}^{+}$, $\sigma_{12\eta\eta}^{+}$ and $\sigma_{22\eta\eta}^{+}$ by using (7.43) and (7.48), we get

$$\begin{aligned}
v_{1\xi\eta}^{+} &= \frac{(\lambda+2\mu)^{-}}{(\lambda+2\mu)^{+}}v_{1\xi\eta}^{-} + \frac{\lambda^{-}-\lambda^{+}}{(\lambda+2\mu)^{+}}v_{2\eta\eta}^{-} \\
&+\frac{\lambda^{+}\chi''(0)}{(\lambda+2\mu)^{+}}\left(\frac{\mu^{-}}{\mu^{+}}-1\right)\left(v_{2\xi}^{-}+v_{1\eta}^{-}\right) \\
v_{2\xi\eta}^{+} &= \frac{\mu^{-}}{\mu^{+}}v_{2\xi\eta}^{-} + \left(\frac{\mu^{-}}{\mu^{+}}-1\right)v_{1\eta\eta}^{-} \\
&+\chi''(0)\left(\left(\frac{(\lambda+2\mu)^{-}}{(\lambda+2\mu)^{+}}-1\right)v_{1\xi}^{-} + \frac{(\lambda^{-}-\lambda^{+})}{(\lambda+2\mu)^{+}}v_{2\eta}^{-}\right) \\
\sigma_{11\xi\eta}^{+} &= \frac{\rho^{+}}{\rho^{-}}\sigma_{11\xi\eta}^{-} + \left(\frac{\rho^{+}}{\rho^{-}}-1\right)\sigma_{12\eta\eta}^{-} \\
&+\chi''(0)\left(\left(\frac{\rho^{+}}{\rho^{-}}-1\right)\sigma_{12\xi}^{-} + \frac{1}{\alpha_1^{+}}(\alpha_2^{+}-\alpha_2^{-})\sigma_{11\eta}^{-}\right. \\
&\left.+\left(\frac{\rho^{+}}{\rho^{-}}-\frac{\alpha_1^{-}}{\alpha_1^{+}}\right)\sigma_{22\eta}^{-} + \frac{\chi''(0)}{\alpha_1^{+}}\left(\frac{1}{\mu^{+}}-\frac{1}{\mu^{-}}\right)\sigma_{12}^{-}\right) \\
\sigma_{12\xi\eta}^{+} &= \frac{\rho^{+}}{\rho^{-}}\sigma_{12\xi\eta}^{-} + \left(\frac{\rho^{+}}{\rho^{-}}-\frac{\alpha_1^{-}}{\alpha_1^{+}}\right)\sigma_{22\eta\eta}^{-} + \frac{1}{\alpha_1^{+}}\left(\alpha_2^{+}-\alpha_2^{-}\right)\sigma_{11\eta\eta}^{-} \\
&+\frac{\chi''(0)}{\alpha_1^{+}}\left(3\left(\frac{1}{\mu^{+}}-\frac{1}{\mu^{-}}\right)-\alpha_2^{+}\left(\frac{\rho^{+}}{\rho^{-}}-1\right)\right)\sigma_{12\eta}^{-} \\
&-\chi''(0)\frac{\alpha_2^{+}}{\alpha_1^{+}}\left(\frac{\rho^{+}}{\rho^{-}}-1\right)\sigma_{11\xi}^{-} + \frac{\chi'''(0)}{\alpha_1^{+}}\left(\frac{1}{\mu^{+}}-\frac{1}{\mu^{-}}\right)\sigma_{12}^{-} \\
&+\frac{3\chi''^{2}(0)}{\alpha_1^{+}}\left(\left(\alpha_1^{+}-\alpha_1^{-}+\frac{\alpha_2^{+}}{\alpha_1^{+}}\left(\alpha_2^{-}-\alpha_2^{+}\right)\right)\sigma_{11}^{-}\right. \\
&\left.+\left(\frac{\alpha_2^{+}\alpha_1^{-}}{\alpha_1^{+}}-\alpha_2^{-}\right)\sigma_{22}^{-}\right).
\end{aligned} \tag{7.53}$$

From equation (7.13), we obtain

$$\sigma_{12\eta\eta} = \mu(u_{1\eta\eta\eta} + \alpha_2\sigma_{11\xi\eta} + \alpha_1\sigma_{22\xi\eta}),$$

or,

$$\begin{aligned}
\sigma_{22\xi\eta}^{+} &= \frac{\alpha_1^{-}}{\alpha_1^{+}}\sigma_{22\xi\eta}^{-} + \frac{1}{\alpha_1^{+}}\left(\alpha_2^{-}\sigma_{11\xi\eta}^{-} - \alpha_2^{+}\sigma_{11\xi\eta}^{+}\right. \\
&\left.+\frac{1}{\mu^{+}}\sigma_{12\eta\eta}^{+} - \frac{1}{\mu^{-}}\sigma_{12\eta\eta}^{-}\right) - \frac{1}{\alpha_1^{+}}\left[u_{1\eta\eta\eta}\right].
\end{aligned} \tag{7.54}$$

Equation (7.45) gives us

$$\left[u_{1\eta\eta\eta}\right] = -3\chi''(0)\left[u_{1\xi\eta}\right] - \chi'''(0)\left[u_{1\xi}\right].$$

Using (7.5), we get

$$\left[u_{1\eta\eta\eta}\right] = -3\chi''(0)\left[\alpha_1\sigma_{11\eta} + \alpha_2\sigma_{22\eta}\right] - \chi'''(0)\left[\alpha_1\sigma_{11} + \alpha_2\sigma_{22}\right],$$

or,

$$\begin{aligned}\left[u_{1\eta\eta\eta}\right] \quad = \quad & -3\chi''(0)\left\{\left(\alpha_1^+ - \alpha_1^-\right)\sigma_{11\eta}^- \right.\\ & +\alpha_2^+\left(\frac{\alpha_1^-}{\alpha_1^+}\sigma_{22\eta}^- + \frac{1}{\alpha_1^+}\left(\alpha_2^- - \alpha_2^+\right)\sigma_{11\eta}^- \right.\\ & \left.\left. -\frac{\chi''(0)}{\alpha_1^+}\left(\frac{1}{\mu^+} - \frac{1}{\mu^-}\right)\sigma_{12}^-\right) - \alpha_2^-\sigma_{22\eta}^-\right\} \\ & -\chi'''(0)\left\{\left(\alpha_1^+ - \alpha_1^-\right)\sigma_{11}^- + \alpha_2^+\left(\frac{\alpha_1^-}{\alpha_1^+}\sigma_{22}^- \right.\right.\\ & \left.\left. +\frac{1}{\alpha_1^+}\left(\alpha_2^- - \alpha_2^+\right)\sigma_{11}^-\right) - \alpha_2^-\sigma_{22}^-\right\}.\end{aligned} \tag{7.55}$$

Eliminating $\sigma_{11\xi\eta}^+$, $\sigma_{12\eta\eta}^+$ and $\left[u_{1\eta\eta\eta}\right]$ in (7.54) from (7.53), (7.43) and (7.55) respectively, we get

$$\begin{aligned}\sigma_{22\xi\eta}^+ \quad = \quad & \frac{\alpha_1^-}{\alpha_1^+}\sigma_{22\xi\eta}^- + \frac{1}{\alpha_1^+}\left(\alpha_2^- - \frac{\alpha_2^+\rho^+}{\rho^-}\right)\sigma_{11\xi\eta}^- + \left(\frac{\alpha_2^+}{\alpha_1^+}\left(1 - \frac{\rho^+}{\rho^-}\right)\right.\\ & \left. +\frac{1}{\alpha_1^+}\left(\frac{1}{\mu^+} - \frac{1}{\mu^-}\right)\right)\sigma_{12\eta\eta}^- + \frac{\chi''(0)}{\alpha_1^+}\left(1 - \frac{\rho^+}{\rho^-}\right)\left(\alpha_2^+ + \frac{1}{\mu^+}\right)\sigma_{12\xi}^- \\ & +\frac{\chi''(0)}{\alpha_1^+}\left(3(\alpha_1^+ - \alpha_1^-) + \frac{1}{\alpha_1^+}\left(\alpha_2^- - \alpha_2^+\right)\left(4\alpha_2^+ + \frac{1}{\mu^+}\right)\right)\sigma_{11\eta}^- \\ & +\frac{\chi''(0)}{\alpha_1^+}\left(3\left(\frac{\alpha_1^-\alpha_2^+}{\alpha_1^+} - \alpha_2^-\right) - \left(\frac{\rho^+}{\rho^-} - \frac{\alpha_1^-}{\alpha_1^+}\right)\left(\frac{1}{\mu^+} + \alpha_2^+\right)\right)\sigma_{22\eta}^- \\ & +\frac{\chi'''(0)}{\alpha_1^+}\left(\left(\alpha_1^+ - \alpha_1^- + \frac{\alpha_2^+}{\alpha_1^+}(\alpha_2^- - \alpha_2^+)\right)\sigma_{11}^- + \left(\frac{\alpha_1^-\alpha_2^+}{\alpha_1^+} - \alpha_2^-\right)\sigma_{22}^-\right) \\ & -\left(\frac{\chi''(0)}{\alpha_1^+}\right)^2\left(\frac{1}{\mu^+} - \frac{1}{\mu^-}\right)\left(\frac{1}{\mu^+} + 4\alpha_2^+\right)\sigma_{12}^-.\end{aligned} \tag{7.56}$$

Combining equations (7.53) and (7.56), we obtain

$$U_{\xi\eta}^+ = Q_2U_{\xi\eta}^- + Q_3U_{\eta\eta}^- + R_6U_\xi^- + R_7U_\eta^- + R_8U^-, \tag{7.57}$$

where,

$$R_6 = \begin{pmatrix} 0 & r_{6,12} & 0 & 0 & 0 \\ r_{6,21} & 0 & 0 & 0 & 0 \\ 0 & 0 & 0 & r_{6,34} & 0 \\ 0 & 0 & r_{6,43} & 0 & 0 \\ 0 & 0 & 0 & r_{6,54} & 0 \end{pmatrix} \tag{7.58}$$

$$R_7 = \begin{pmatrix} r_{7,11} & 0 & 0 & 0 & 0 \\ 0 & r_{7,22} & 0 & 0 & 0 \\ 0 & 0 & r_{7,33} & 0 & r_{7,35} \\ 0 & 0 & 0 & r_{7,44} & 0 \\ 0 & 0 & r_{7,53} & 0 & r_{7,55} \end{pmatrix} \tag{7.59}$$

$$R_8 = \begin{pmatrix} 0 & 0 & 0 & 0 & 0 \\ 0 & 0 & 0 & 0 & 0 \\ 0 & 0 & 0 & r_{8,34} & 0 \\ 0 & 0 & r_{8,43} & r_{8,44} & r_{8,45} \\ 0 & 0 & r_{8,53} & r_{8,54} & r_{8,55} \end{pmatrix}, \tag{7.60}$$

with

$$\begin{aligned}
r_{6,12} &= -\frac{\lambda^+\chi''(0)}{(\lambda+2\mu)^+}\left(1-\frac{\mu^-}{\mu^+}\right), \quad r_{6,21} = \chi''(0)\left(\frac{(\lambda+2\mu)^-}{(\lambda+2\mu)^+}-1\right), \\
r_{6,34} &= \chi''(0)\left(\frac{\rho^+}{\rho^-}-1\right), \quad r_{6,43} = -\frac{\alpha_2^+}{\alpha_1^+}r_{6,34}, \\
r_{6,54} &= \frac{\chi''(0)}{\alpha_1^+}\left(1-\frac{\rho^+}{\rho^-}\right)\left(\alpha_2^+ + \frac{1}{\mu^+}\right), \quad r_{7,11} = r_{6,12}, \\
r_{7,22} &= \chi''(0)\frac{(\lambda^- - \lambda^+)}{(\lambda+2\mu)^+}, \quad r_{7,33} = \frac{\chi''(0)}{\alpha_1^+}(\alpha_2^- - \alpha_2^+),
\end{aligned}$$

$$
\begin{aligned}
r_{7,35} &= \chi''(0)\left(\frac{\rho^+}{\rho^-} - \frac{\alpha_1^-}{\alpha_1^+}\right),\\
r_{7,44} &= \frac{\chi''(0)}{\alpha_1^+}\left(3\left(\frac{1}{\mu^+} - \frac{1}{\mu^-}\right) - \alpha_2^+\left(\frac{\rho^+}{\rho^-} - 1\right)\right),\\
r_{7,53} &= \frac{\chi''(0)}{\alpha_1^+}\left(3(\alpha_1^+ - \alpha_1^-) + \frac{1}{\alpha_1^+}\left(\alpha_2^- - \alpha_2^+\right)\left(4\alpha_2^+ + \frac{1}{\mu^+}\right)\right),\\
r_{7,55} &= \frac{\chi''(0)}{\alpha_1^+}\left(3\left(\frac{\alpha_1^-\alpha_2^+}{\alpha_1^+} - \alpha_2^-\right) - \left(\frac{\rho^+}{\rho^-} - \frac{\alpha_1^-}{\alpha_1^+}\right)\left(\frac{1}{\mu^+} + \alpha_2^+\right)\right),
\end{aligned}
$$

$$
\begin{aligned}
r_{8,34} &= \frac{\chi''(0)}{\alpha_1^+}\left(\frac{1}{\mu^+} - \frac{1}{\mu^-}\right),\\
r_{8,43} &= \frac{3\chi''^2(0)}{\alpha_1^+}\left(\alpha_1^+ - \alpha_1^- + \frac{\alpha_2^+}{\alpha_1^+}(\alpha_2^- - \alpha_2^+)\right),\\
r_{8,44} &= \frac{\chi'''(0)}{\alpha_1^+}\left(\frac{1}{\mu^+} - \frac{1}{\mu^-}\right), \quad r_{8,45} = \frac{3\chi''^2(0)}{\alpha_1^+}\left(\frac{\alpha_2^+\alpha_1^-}{\alpha_1^+} - \alpha_2^-\right),\\
r_{8,53} &= \frac{\chi'''(0)}{\alpha_1^+}\left(\alpha_1^+ - \alpha_1^- + \frac{\alpha_2^+}{\alpha_1^+}(\alpha_2^- - \alpha_2^+)\right),\\
r_{8,54} &= -\left(\frac{\chi''(0)}{\alpha_1^+}\right)^2\left(\frac{1}{\mu^+} - \frac{1}{\mu^-}\right)\left(\frac{1}{\mu^+} + 4\alpha_2^+\right),\\
r_{8,55} &= \frac{\chi'''(0)}{\alpha_1^+}\left(\frac{\alpha_1^-\alpha_2^+}{\alpha_1^+} - \alpha_2^-\right).
\end{aligned}
$$

or,

$$
\begin{aligned}
& r_{6,12} = -\frac{\lambda^+}{(\lambda+2\mu)^+}r_{3,22}, \quad r_{6,21} = -r_{3,11}, \quad r_{6,34} = -r_{3,33},\\
& r_{6,43} = -r_{3,53}, \quad r_{6,54} = \frac{1}{\alpha_1^+}\left(\alpha_2^+ + \frac{1}{\mu^+}\right)r_{3,33}, \quad r_{7,11} = r_{6,12},\\
& r_{7,22} = -r_{4,12}, \quad r_{7,33} = r_{4,43}, \quad r_{7,35} = -r_{4,45}, \quad r_{7,44} = -r_{4,54},\\
& r_{7,53} = \frac{\chi''(0)}{\alpha_1^+}\left(3(\alpha_1^+ - \alpha_1^-) + \frac{1}{\alpha_1^+}\left(\alpha_2^- - \alpha_2^+\right)\left(4\alpha_2^+ + \frac{1}{\mu^+}\right)\right),\\
& r_{7,55} = 3r_{2,55} - \frac{1}{\alpha_1^+}\left(\frac{1}{\mu^+} + \alpha_2^+\right)r_{7,35}, \quad r_{8,34} = r_{1,54}, \quad r_{8,43} = -r_{5,53},\\
& r_{8,44} = -r_{5,54}, \quad r_{8,45} = -r_{5,55}, \quad r_{8,53} = \frac{\chi'''(0)}{\alpha_1^+}\left(\alpha_1^+ - \alpha_1^- + \frac{\alpha_2^+}{\alpha_1^+}(\alpha_2^- - \alpha_2^+)\right),\\
& r_{8,54} = \frac{\chi''(0)}{\alpha_1^+}\left(4\alpha_2^+ + \frac{1}{\mu^+}\right)r_{1,54}, \quad r_{8,55} = \frac{\chi'''(0)}{\alpha_1^+}\left(\frac{\alpha_1^-\alpha_2^+}{\alpha_1^+} - \alpha_2^-\right).
\end{aligned}
$$

Now, the first four equations of (7.1) yields

$$
\begin{aligned}
v_{1tt} &= \frac{1}{\rho}\Big((\lambda+2\mu)v_{1\xi\xi}+\mu v_{1\eta\eta}+(\lambda+\mu)v_{2\xi\eta}\Big)\\
v_{2tt} &= \frac{1}{\rho}\Big((\lambda+\mu)v_{1\xi\eta}+\mu v_{2\xi\xi}+(\lambda+2\mu)v_{2\eta\eta}\Big)\\
\sigma_{11tt} &= \frac{1}{\rho}\Big((\lambda+2\mu)\sigma_{11\xi\xi}+2(\lambda+\mu)\sigma_{12\xi\eta}+\lambda\sigma_{22\eta\eta}\Big)\\
\sigma_{12tt} &= \frac{\mu}{\rho}\Big(\sigma_{11\xi\eta}+\sigma_{12\eta\eta}+\sigma_{12\xi\xi}+\sigma_{22\xi\eta}\Big),
\end{aligned}
$$

then $[v_{1tt}]=[v_{2tt}]=[\sigma_{11tt}]=[\sigma_{12tt}]=0$ leads to

$$
\begin{aligned}
v_{1\overset{+}{\xi\xi}} &= \frac{\rho^+}{(\lambda+2\mu)^+}\left(\frac{(\lambda+2\mu)^-}{\rho^-}v_{1\overset{-}{\xi\xi}}+\frac{\mu^-}{\rho^-}v_{1\overset{-}{\eta\eta}}-\frac{\mu^+}{\rho^+}v_{1\overset{+}{\eta\eta}}\right.\\
&\qquad\left.+\frac{(\lambda+\mu)^-}{\rho^-}v_{2\overset{-}{\xi\eta}}-\frac{(\lambda+\mu)^+}{\rho^+}v_{2\overset{+}{\xi\eta}}\right)\\
v_{2\overset{+}{\xi\xi}} &= \frac{\rho^+}{\mu^+}\left(\frac{\mu^-}{\rho^-}v_{2\overset{-}{\xi\xi}}+\frac{(\lambda+\mu)^-}{\rho^-}v_{1\overset{-}{\xi\eta}}-\frac{(\lambda+\mu)^+}{\rho^+}v_{1\overset{+}{\xi\eta}}\right.\\
&\qquad\left.+\frac{(\lambda+2\mu)^-}{\rho^-}v_{2\overset{-}{\eta\eta}}-\frac{(\lambda+2\mu)^+}{\rho^+}v_{2\overset{+}{\eta\eta}}\right)\\
\sigma_{11\overset{+}{\xi\xi}} &= \frac{\rho^+}{(\lambda+2\mu)^+}\left(\frac{(\lambda+2\mu)^-}{\rho^-}\sigma_{11\overset{-}{\xi\xi}}+\frac{2(\lambda+\mu)^-}{\rho^-}\sigma_{12\overset{-}{\xi\eta}}\right.\\
&\qquad\left.-\frac{2(\lambda+\mu)^+}{\rho^+}\sigma_{12\overset{+}{\xi\eta}}+\frac{\lambda^-}{\rho^-}\sigma_{22\overset{-}{\eta\eta}}-\frac{\lambda^+}{\rho^+}\sigma_{22\overset{+}{\eta\eta}}\right)\\
\sigma_{12\overset{+}{\xi\xi}} &= \frac{\rho^+\mu^-}{\rho^-\mu^+}\Big(\sigma_{12\overset{-}{\xi\xi}}+\sigma_{11\overset{-}{\xi\eta}}+\sigma_{22\overset{-}{\xi\eta}}+\sigma_{12\overset{-}{\eta\eta}}\Big)-\Big(\sigma_{11\overset{+}{\xi\eta}}+\sigma_{22\overset{+}{\xi\eta}}+\sigma_{12\overset{+}{\eta\eta}}\Big),
\end{aligned}
$$

or, by using (7.49) and (7.57), we have

$$
\begin{aligned}
v_{1\overset{+}{\xi\xi}} &= \frac{\rho^+}{(\lambda+2\mu)^+}\left\{\frac{(\lambda+2\mu)^-}{\rho^-}v_{1\overset{-}{\xi\xi}}\right.\\
&\quad+\left(\frac{\mu^-}{\rho^+}\left(\frac{\rho^+}{\rho^-}-1\right)+\frac{\lambda^+}{\rho^+}\left(\frac{\mu^-}{\mu^+}-1\right)\right)v_{1\overset{-}{\eta\eta}}\\
&\quad\left.+\left(\frac{(\lambda+\mu)^-}{\rho^-}-\frac{\mu^-(\lambda+\mu)^+}{\mu^+\rho^+}\right)v_{2\overset{-}{\xi\eta}}\right\}.\\
&\quad-\frac{\chi''(0)\lambda^+}{(\lambda+2\mu)^+}\left(\left(\frac{(\lambda+2\mu)^-}{(\lambda+2\mu)^+}-1\right)v_{1\overset{-}{\xi}}+\frac{(\lambda^--\lambda^+)}{(\lambda+2\mu)^+}v_{2\overset{-}{\eta}}\right)
\end{aligned}
\tag{7.61}
$$

$$
\begin{aligned}
v_{2\xi\xi}^{+} \;=\;& \frac{\rho^+}{\mu^+}\left\{\frac{\mu^-}{\rho^-}v_{2\xi\xi}^{-} + \left(\frac{(\lambda+\mu)^-}{\rho^-} - \frac{(\lambda+\mu)^+(\lambda+2\mu)^-}{\rho^+(\lambda+2\mu)^+}\right)v_{1\xi\eta}^{-}\right.\\
&\left. + \left(\left(\frac{\lambda+2\mu}{\rho}\right)^- - \left(\frac{\lambda+2\mu}{\rho}\right)^+ + \frac{(\lambda+\mu)^+(\lambda^+-\lambda^-)}{\rho^+(\lambda+2\mu)^+}\right)v_{2\eta\eta}^{-}\right\}\\
& + \chi''(0)\frac{(3\lambda+4\mu)^+}{(\lambda+2\mu)^+}\left(\frac{\mu^-}{\mu^+}-1\right)\left(v_{2\xi}^{-} + v_{1\eta}^{-}\right)
\end{aligned} \tag{7.62}
$$

$$
\begin{aligned}
\sigma_{11\xi\xi}^{+} \;=\;& \frac{\rho^+}{(\lambda+2\mu)^+}\left\{\frac{(\lambda+2\mu)^-}{\rho^-}\sigma_{11\xi\xi}^{-} + \frac{2\left((\lambda+\mu)^- - (\lambda+\mu)^+\right)}{\rho^-}\sigma_{12\xi\eta}^{-}\right.\\
&\left. + \left(\frac{\lambda^-}{\rho^-} - \frac{\lambda^+\alpha_1^-}{\rho^+\alpha_1^+} + \frac{2(\lambda+\mu)^+}{\rho^+}\left(\frac{\alpha_1^-}{\alpha_1^+} - \frac{\rho^+}{\rho^-}\right)\right)\sigma_{22\eta\eta}^{-}\right\}\\
& + \frac{(\alpha_2^- - \alpha_2^+)}{\alpha_1^+}\sigma_{11\eta\eta}^{-} + \frac{\chi''(0)}{\alpha_1^+}\left(\alpha_2^+\left(\frac{\rho^+}{\rho^-}-1\right)\right.\\
&\left. + 3\left(\frac{1}{\mu^-} - \frac{1}{\mu^+}\right)\right)\sigma_{12\eta}^{-} + \frac{\chi''(0)\alpha_2^+}{\alpha_1^+}\left(\frac{\rho^+}{\rho^-}-1\right)\sigma_{11\xi}^{-}\\
& - \frac{3\chi''^2(0)}{\alpha_1^+}\left(\left(\alpha_1^+ - \alpha_1^- + \frac{\alpha_2^+}{\alpha_1^+}\left(\alpha_2^- - \alpha_2^+\right)\right)\sigma_{11}^{-}\right.\\
&\left. + \left(\frac{\alpha_2^+\alpha_1^-}{\alpha_1^+} - \alpha_2^-\right)\sigma_{22}^{-}\right) + \frac{\chi'''(0)}{\alpha_1^+}\left(\frac{1}{\mu^-} - \frac{1}{\mu^+}\right)\sigma_{12}^{-}
\end{aligned} \tag{7.63}
$$

$$
\begin{aligned}
\sigma_{12\xi\xi}^{+} \;=\;& \frac{\rho^+\mu^-}{\rho^-\mu^+}\sigma_{12\xi\xi}^{-} + \left(\frac{\rho^+}{\rho^-}\left(\frac{\mu^-}{\mu^+}-1\right) + \frac{\alpha_2^+}{\alpha_1^+}\left(\frac{\rho^+}{\rho^-}-1\right) - \frac{1}{\alpha_1^+}\left(\frac{1}{\mu^+} - \frac{1}{\mu^-}\right)\right)\sigma_{12\eta\eta}^{-}\\
& + \left(\frac{\rho^+}{\rho^-}\left(\frac{\mu^-}{\mu^+}-1\right) - \frac{1}{\alpha_1^+}\left(\alpha_2^- - \alpha_2^+\frac{\rho^+}{\rho^-}\right)\right)\sigma_{11\xi\eta}^{-} + \left(\frac{\rho^+\mu^-}{\rho^-\mu^+} - \frac{\alpha_1^-}{\alpha_1^+}\right)\sigma_{22\xi\eta}^{-}\\
& - \frac{\chi''(0)}{\alpha_1^+}\left(1 - \frac{\rho^+}{\rho^-}\right)\left(\alpha_2^+ + \frac{1}{\mu^+}\right)\sigma_{12\xi}^{-}\\
& - \frac{\chi''(0)}{\alpha_1^+}\left(3(\alpha_1^+ - \alpha_1^-) + \frac{1}{\alpha_1^+}\left(\alpha_2^- - \alpha_2^+\right)\left(4\alpha_2^+ + \frac{1}{\mu^+}\right)\right)\sigma_{11\eta}^{-}\\
& - \frac{\chi''(0)}{\alpha_1^+}\left(3\left(\frac{\alpha_1^-\alpha_2^+}{\alpha_1^+} - \alpha_2^-\right) - \left(\frac{\rho^+}{\rho^-} - \frac{\alpha_1^-}{\alpha_1^+}\right)\left(\frac{1}{\mu^+} + \alpha_2^+\right)\right)\sigma_{22\eta}^{-}\\
& - \frac{\chi'''(0)}{\alpha_1^+}\left(\left(\alpha_1^+ - \alpha_1^- + \frac{\alpha_2^+}{\alpha_1^+}(\alpha_2^- - \alpha_2^+)\right)\sigma_{11}^{-} + \left(\frac{\alpha_1^-\alpha_2^+}{\alpha_1^+} - \alpha_2^-\right)\sigma_{22}^{-}\right)\\
& + \left(\frac{\chi''(0)}{\alpha_1^+}\right)^2\left(\frac{1}{\mu^+} - \frac{1}{\mu^-}\right)\left(\frac{1}{\mu^+} + 4\alpha_2^+\right)\sigma_{12}^{-}.
\end{aligned} \tag{7.64}
$$

For $\sigma_{22\xi\xi}$, recall equation (7.20):

$$\sigma_{12\xi\eta} = \mu\left(\alpha_1\sigma_{11\eta\eta} + \alpha_2\sigma_{22\eta\eta} + \alpha_2\sigma_{11\xi\xi} + \alpha_1\sigma_{22\xi\xi}\right),$$

which yields

$$\begin{aligned}\sigma_{22\xi\xi}^{+} &= \frac{1}{\alpha_1^+}\left(\alpha_1^-\sigma_{22\xi\xi}^- + \alpha_2^-\sigma_{11\xi\xi}^- - \alpha_2^+\sigma_{11\xi\xi}^+ + \frac{1}{\mu^+}\sigma_{12\xi\eta}^+\right.\\ &\quad\left.-\frac{1}{\mu^-}\sigma_{12\xi\eta}^- + \alpha_1^-\sigma_{11\eta\eta}^- - \alpha_1^+\sigma_{11\eta\eta}^+ + \alpha_2^-\sigma_{22\eta\eta}^- - \alpha_2^+\sigma_{22\eta\eta}^+\right).\end{aligned}$$

Eliminating $\sigma_{11\xi\xi}^+$, $\sigma_{12\xi\eta}^+$, $\sigma_{11\eta\eta}^+$ and $\sigma_{22\eta\eta}^+$ by using (7.49), (7.57), (7.61), (7.62), (7.63) and (7.64) we get

$$\begin{aligned}\sigma_{22\xi\xi}^{+} &= \frac{1}{\alpha_1^+}\left\{\alpha_1^-\sigma_{22\xi\xi}^- + \left(\alpha_2^- - \alpha_2^+\frac{\rho^+(\lambda+2\mu)^-}{\rho^-(\lambda+2\mu)^+}\right)\sigma_{11\xi\xi}^-\right.\\ &\quad+\left(\frac{2\alpha_2^+\rho^+\left((\lambda+\mu)^+-(\lambda+\mu)^-\right)}{\rho^-(\lambda+2\mu)^+} + \frac{\rho^+}{\mu^+\rho^-} - \frac{1}{\mu^-}\right)\sigma_{12\xi\eta}^-\\ &\quad+\left(\frac{\alpha_2^+\rho^+}{(\lambda+2\mu)^+}\left(\frac{2(\lambda+\mu)^+}{\rho^+}\left(\frac{\rho^+}{\rho^-} - \frac{\alpha_1^-}{\alpha_1^+}\right) - \frac{\lambda^-}{\rho^-} + \frac{\lambda^+\alpha_1^-}{\rho^+\alpha_1^+}\right)\right.\\ &\quad\left.+\frac{1}{\mu^+}\left(\frac{\rho^+}{\rho^-} - \frac{\alpha_1^-}{\alpha_1^+}\right) + \alpha_2^- - \frac{\alpha_2^+\alpha_1^-}{\alpha_1^+}\right)\sigma_{22\eta\eta}^-\\ &\quad\left.+\left(\alpha_1^- - \alpha_1^+ + \frac{(\alpha_2^+ - \alpha_2^-)}{\alpha_1^+}\left(2\alpha_2^+ + \frac{1}{\mu^+}\right)\right)\sigma_{11\eta\eta}^-\right\}. \\ &\quad+\chi''(0)\left(\frac{\rho^+}{\rho^-} - 1\right)\left(1 - \frac{\alpha_2^+}{(\alpha_1^+)^2}\left(2\alpha_2 + \frac{1}{\mu}\right)^+\right)\left(\sigma_{11\xi}^- + \sigma_{12\eta}^-\right)\\ &\quad+\frac{1}{\alpha_1^+}\left(2\alpha_2 + \frac{1}{\mu}\right)^+\left\{\frac{3\chi''(0)}{\alpha_1^+}\left(\frac{1}{\mu^+} - \frac{1}{\mu^-}\right)\sigma_{12\eta}^-\right.\\ &\quad+\frac{3\chi''^2(0)}{\alpha_1^+}\left(\left(\alpha_1^+ - \alpha_1^- + \frac{\alpha_2^+}{\alpha_1^+}\left(\alpha_2^- - \alpha_2^+\right)\right)\sigma_{11}^-\right.\\ &\quad\left.\left.+\left(\frac{\alpha_2^+\alpha_1^-}{\alpha_1^+} - \alpha_2^-\right)\sigma_{22}^-\right)\right\} + \frac{\chi'''(0)}{\alpha_1^+}\left(\frac{1}{\mu^+} - \frac{1}{\mu^-}\right)\sigma_{12}^-.\end{aligned} \tag{7.65}$$

Combining equations (7.61),(7.62), (7.63),(7.64) and (7.65), we obtain

$$U_{\xi\xi}^+ = Q_4U_{\xi\xi}^- + Q_5U_{\xi\eta}^- + Q_6U_{\eta\eta}^- + R_9U_\xi^- + R_{10}U_\eta^- + R_{11}U^-, \tag{7.66}$$

where

$$R_9 = \begin{pmatrix} r_{9,11} & 0 & 0 & 0 & 0 \\ 0 & r_{9,22} & 0 & 0 & 0 \\ 0 & 0 & r_{9,33} & 0 & 0 \\ 0 & 0 & 0 & r_{9,44} & 0 \\ 0 & 0 & r_{9,53} & 0 & 0 \end{pmatrix} \tag{7.67}$$

$$R_{10} = \begin{pmatrix} 0 & r_{10,12} & 0 & 0 & 0 \\ r_{10,21} & 0 & 0 & 0 & 0 \\ 0 & 0 & 0 & r_{10,34} & 0 \\ 0 & 0 & r_{10,43} & 0 & r_{10,45} \\ 0 & 0 & 0 & r_{10,54} & 0 \end{pmatrix} \tag{7.68}$$

$$R_{11} = \begin{pmatrix} 0 & 0 & 0 & 0 & 0 \\ 0 & 0 & 0 & 0 & 0 \\ 0 & 0 & r_{11,33} & r_{11,34} & r_{11,35} \\ 0 & 0 & r_{11,43} & r_{11,44} & r_{11,45} \\ 0 & 0 & r_{11,53} & r_{11,54} & r_{11,55} \end{pmatrix}, \tag{7.69}$$

with

$$\begin{aligned}
r_{9,11} &= -\frac{\chi''(0)\lambda^+}{(\lambda+2\mu)^+}\left(\frac{(\lambda+2\mu)^-}{(\lambda+2\mu)^+} - 1\right), \\
r_{9,22} &= \chi''(0)\frac{(3\lambda+4\mu)^+}{(\lambda+2\mu)^+}\left(\frac{\mu^-}{\mu^+} - 1\right), \\
r_{9,33} &= \frac{\chi''(0)\alpha_2^+}{\alpha_1^+}\left(\frac{\rho^+}{\rho^-} - 1\right), \quad r_{9,44} = \frac{\chi''(0)}{\alpha_1^+}\left(\frac{\rho^+}{\rho^-} - 1\right)\left(\alpha_2^+ + \frac{1}{\mu^+}\right), \\
r_{9,53} &= \chi''(0)\left(\frac{\rho^+}{\rho^-} - 1\right)\left(1 - \frac{\alpha_2^+}{\alpha_1^+}\left(2\alpha_2 + \frac{1}{\mu}\right)^+\right),
\end{aligned}$$

$$r_{10,12} = -\frac{\chi''(0)\lambda^+(\lambda^- - \lambda^+)}{((\lambda+2\mu)^+)^2},$$
$$r_{10,21} = r_{9,22}, \quad r_{10,34} = \frac{\chi''(0)}{\alpha_1^+}\left(\alpha_2^+\left(\frac{\rho^+}{\rho^-} - 1\right) + 3\left(\frac{1}{\mu^-} - \frac{1}{\mu^+}\right)\right),$$
$$r_{10,43} = -\frac{\chi''(0)}{\alpha_1^+}\left(3(\alpha_1^+ - \alpha_1^-) + \frac{1}{\alpha_1^+}\left(\alpha_2^- - \alpha_2^+\right)\left(4\alpha_2^+ + \frac{1}{\mu^+}\right)\right),$$

$$r_{10,45} = -\frac{\chi''(0)}{\alpha_1^+}\left(3\left(\frac{\alpha_1^-\alpha_2^+}{\alpha_1^+} - \alpha_2^-\right) - \left(\frac{\rho^+}{\rho^-} - \frac{\alpha_1^-}{\alpha_1^+}\right)\left(\frac{1}{\mu^+} + \alpha_2^+\right)\right),$$
$$r_{10,54} = r_{9,53} + \frac{3\chi''(0)}{(\alpha_1^+)^2}\left(2\alpha_2 + \frac{1}{\mu}\right)^+\left(\frac{1}{\mu^+} - \frac{1}{\mu^-}\right),$$
$$r_{11,33} = -\frac{3\chi''^2(0)}{\alpha_1^+}\left(\alpha_1^+ - \alpha_1^- + \frac{\alpha_2^+}{\alpha_1^+}\left(\alpha_2^- - \alpha_2^+\right)\right),$$

$$r_{11,34} = \frac{\chi'''(0)}{\alpha_1^+}\left(\frac{1}{\mu^-} - \frac{1}{\mu^+}\right), \quad r_{11,35} = -\frac{3\chi''^2(0)}{\alpha_1^+}\left(\frac{\alpha_2^+\alpha_1^-}{\alpha_1^+} - \alpha_2^-\right),$$
$$r_{11,43} = -\frac{\chi'''(0)}{\alpha_1^+}\left(\alpha_1^+ - \alpha_1^- + \frac{\alpha_2^+}{\alpha_1^+}(\alpha_2^- - \alpha_2^+)\right),$$
$$r_{11,44} = \left(\frac{\chi''(0)}{\alpha_1^+}\right)^2\left(\frac{1}{\mu^+} - \frac{1}{\mu^-}\right)\left(\frac{1}{\mu^+} + 4\alpha_2^+\right),$$

$$r_{11,45} = -\frac{\chi'''(0)}{\alpha_1^+}\left(\frac{\alpha_1^-\alpha_2^+}{\alpha_1^+} - \alpha_2^-\right),$$
$$r_{11,53} = \frac{3\chi''^2(0)}{\alpha_1^+}\left(\alpha_1^+ - \alpha_1^- + \frac{\alpha_2^+}{\alpha_1^+}\left(\alpha_2^- - \alpha_2^+\right)\right),$$
$$r_{11,54} = \frac{\chi'''(0)}{\alpha_1^+}\left(\frac{1}{\mu^+} - \frac{1}{\mu^-}\right), \quad r_{11,55} = \frac{3\chi''^2(0)}{\alpha_1^+}\left(\frac{\alpha_2^+\alpha_1^-}{\alpha_1^+} - \alpha_2^-\right).$$

or,

$$r_{9,11} = \frac{\lambda^+}{(\lambda+2\mu)^+}r_{3,11}, \quad r_{9,22} = -\frac{(3\lambda+4\mu)^+}{(\lambda+2\mu)^+}r_{3,22},$$
$$r_{9,33} = r_{3,53}, \quad r_{9,44} = -r_{6,55},$$
$$r_{9,53} = \left(1 - \frac{\alpha_2^+}{\alpha_1^+}\left(2\alpha_2 + \frac{1}{\mu}\right)^+\right)r_{6,34},$$

$$r_{10,12} = -\frac{\lambda^+}{(\lambda+2\mu)^+} r_{7,22}, \quad r_{10,21} = r_{9,22},$$

$$r_{10,34} = -r_{7,44}, \quad r_{10,43} = -r_{7,53}, \quad r_{10,45} = -r_{7,55},$$

$$r_{10,54} = r_{9,53} - \frac{3}{\alpha_1^+}\left(2\alpha_2 + \frac{1}{\mu}\right)^+ r_{1,54},$$

$$r_{11,33} = r_{5,53}, \qquad r_{11,34} = r_{5,54}, \qquad r_{11,35} = r_{5,55},$$

$$r_{11,43} = -r_{8,53}, \quad r_{11,44} = -r_{8,54}, \quad r_{11,45} = -r_{8,55},$$

$$r_{11,53} = -r_{5,53}, \quad r_{11,54} = -r_{5,54}, \quad r_{11,55} = -r_{5,55}.$$

Combining equations (7.27), (7.34), (7.41), (7.49), (7.57) and (7.66), we obtain the jump conditions we used in Chapter 6:

$$\begin{aligned}
U^+ &= Q_1 U^- \\
U^+_\eta &= Q_1 U^-_\eta + R_1 U^- \\
U^+_\xi &= Q_2 U^-_\xi + Q_3 U^-_\eta + R_2 U^- \\
U^+_{\eta\eta} &= Q_1 U^-_{\eta\eta} + R_3 U^-_\xi + R_4 U^-_\eta + R_5 U^- \\
U^+_{\xi\eta} &= Q_2 U^-_{\xi\eta} + Q_3 U^-_{\eta\eta} + R_6 U^-_\xi + R_7 U^-_\eta + R_8 U^- \\
U^+_{\xi\xi} &= Q_4 U^-_{\xi\xi} + Q_5 U^-_{\xi\eta} + Q_6 U^-_{\eta\eta} + R_9 U^-_\xi + R_{10} U^-_\eta + R_{11} U^-,
\end{aligned} \tag{7.70}$$

with the Q's and R's given in (7.8), (7.16), (7.23), (7.24), (7.25), (7.35), (7.42), (7.50), (7.51), (7.52), (7.58), (7.59), (7.60), (7.67), (7.68) and (7.69). Note that for a linear interface, $\chi''(0) = \chi'''(0) = 0$, This gives rise to the special case (7.26) where all R's are zero.

Chapter 8

CONCLUSIONS

8.1 Current Work

We have developed a method of solving a linear hyperbolic system with discontinuous coefficients across arbitrary interfaces on uniform grids. The method is applied to acoustic and elastic wave equations in two spatial dimensions. Standard numerical schemes can be used at regular points away from the interface, and a special formula involving a six-point stencil is developed to modify the finite difference scheme at irregular points near the interface. The coefficients Γ, for our special difference scheme near the interface, are computed taking into account the jump conditions at the interface. For the forward problem we solved, the Γ's depend only on the geometry, the material properties and the jump conditions, but not on the solutions themselves. Therefore we only need to compute them once as a pre-processing step before time stepping. The computations of the Γ's at different irregular points are independent of each other, suggesting that the method could be naturally parallelized. These special formulas can also be used with other numerical schemes to handle interface problems. In particular, this method has been successfully merged with a high-resolution multi-dimensional finite volume algorithm for solving the acoustic or elasticity equations in regions away from the interface.

Working on a first order system of equations enables us to solve simultaneously for many physical quantities, such as the components of velocity vector and stress tensor. In order to get the coefficients used for the special formula near the interface of a discontinuity, the jump conditions for the variables and their first and second order derivatives need to be derived based on the physical jump conditions at the interface. Then we solve a linear system of matrix equations to obtain the coefficients of the formula at one irregular point. The fact that the number of physical jump conditions is less than the number of variables for wave equations in two space dimensions makes the derivation of the jump conditions for the system much more difficult, especially with a curved interface.

Test calculations have confirmed that the special finite difference formulas are pointwise second order accurate. Actually, it also gives second order accuracy in the local truncation errors. Solutions to wave equations obtained in this work give sharp discontinuities without smearing, regardless of the orientation, location, and complexity of the interface. (provided that the grid is fine enough to resolve the interface.)

This method has also been extended to handle some non-smooth interfaces. This is the first such extension for Immersed Interface Methods. Piecewise smooth interface problems, such as the acoustic lens problem, have been solved (see Chapter 4). Furthermore, this method is capable of solving problems with multiple interfaces intersecting each other, yielding the possibility of solving very interesting problems, such as the "pinch-out" problem in seismology (also see Chapter 4). Examples in Section 4.2 show that the transmitted and reflected waves are well modeled in the case where interfaces have kinks or where they intersect each other.

Furthermore, the computational work involved is relatively low for several reasons. First, explicit time stepping is preserved. Second, our modified coefficients are applied only to the irregular points, which number far less than the total number of computational points. Third, we only need to compute them once as a pre-processing step before time-stepping. Moreover, the treatment of the interface is local. This means that at each irregular point, the size of the system we need to solve in order to obtain the Γ's does not depend on the mesh size. Furthermore, this pre-processing step has been made more efficient by using decomposition. Also it was pointed out that because the computation of Γ's at one irregular point is independent of that at any other point, the method can be parallelized.

These same ideas could apply to other linear systems of hyperbolic equations. In principle it would also be possible to derive higher order accurate interface methods for use with more accurate solvers.

8.2 Future Work

In this thesis the Immersed Interface Method has been used to solve wave equations with discontinuous coefficients, with the focus on the acoustics and elasticity in two space dimensions. This work can be extended in many directions and applied to other applications.

8.2.1 Three Dimensional Problem

A direct extension of the current work is to the problems of acoustic and elasticity waves in three space dimensions. Standard solvers are available for regular points away from the interface of discontinuity; e.g. the three-dimensional version of CLAWPACK. Near the interface, a scheme using a ten-point stencil could be used to eliminate the coefficients of U, U_x, U_y, U_z, U_{xx}, U_{yy}, U_{zz}, U_{xy}, U_{xz}, and U_{yz}. The ten points can be chosen as the seven standard points plus three other points (at corners or edges). Working out the jump conditions at the interface up to second order derivatives may be challenging, and keeping track of the irregular points near the interface of discontinuity in three space dimensions will be a major component of the implementation.

8.2.2 Problems with Variable Coefficients

The coefficients in the problems we solved are piecewise constant. We can solve similar problems with discontinuous variable coefficients equally effectively. Standard solvers for problems with variable coefficients can be used away from the interface of the discontinuities. (CLAWPACK is also capable of handling variable coefficients.) In the special formulas for irregular points near the interface, the differences in the implementation will be seen mainly in the derivation of the jump conditions.

8.2.3 Adaptive Grid Refinement Method

Combining the adaptive grid refinement method with the Immersed Interface Method to solve hyperbolic equations with discontinuous coefficients will be another important project. In addition to the conventional reasons for using the adaptive grid refinement method, e.g. particular interest in some of the subregions, an efficient treatment of multiple interfaces of different curvatures and sizes also needs the use of the adaptive method. The Cartesian grid should be fine enough to resolve the interfaces, therefore we need different resolutions for different parts of the interfaces. CLAWPACK with an adaptive method is already available for regular points [6], and the remaining implementation of combining the adaptive method and immersed interface method will mainly be to compute the Γ's on different Cartesian grids.

8.2.4 Higher Order Method

The Immersed Interface Method can be combined with a higher order method for regular points to get higher order accuracy. A higher order method is especially useful in relatively high frequency waves, where we need to resolve the wave well with limited grid points. Once the jump conditions for higher order derivatives are worked out, the basic idea can be applied.

8.2.5 Maxwell's Equation and Nonlinear Hyperbolic Equations

Another interesting problem is Maxwell's equation with discontinuous coefficients. This gives a much larger system. We can solve the problem of the form $\dfrac{\partial^2 \mathbf{E}}{\partial t^2} = c^2\nabla^2\mathbf{E}$, where $\mathbf{E}$ = electric intensity, and then solve for the rest of the unknowns from Maxwell's equation.

Also, applying these methods to nonlinear hyperbolic conservation equations would be a worthwhile challenge. Good solvers are already available, so the key will be to develop the special formulas near the interface. Because the derived jump conditions at the interface depend on the wave equations themselves, the nonlinearity makes the derivation of the jump conditions very complicated.

8.2.6 Inverse Problem

Inverse problems that require solutions to wave equations represent a very important application. The present forward method that I have developed is an important piece for inverse problems. For each iteration of an inverse problem, one needs to solve a forward problem. Because of the complexity of inverse problems, this will be a long term project.

BIBLIOGRAPHY

[1] E. F. Kaasschieter A. C. Berkenbosch and J. H. M. ten Thije Boonkkamp. Finite-difference methods for one-dimensional hyperbolic conservation laws. *Numerical Methods for Partial Differential Equations*, (10):225–269, 1994.

[2] L. Adams. A multigrid algorithm for immersed interface problems. In *Copper Mountain Multigrid Conference*. NASA, available anonymous ftp from mgnet, 1995.

[3] Z. S. Alterman and F. C. Karal. Propagation of elastic wave in layered media by finite difference method. *Bull. Seism. Soc. Am.*, 58:367–398, 1968.

[4] Garth A. Baker. Error estimates for the finite element methods for second order hyperbolic equations. *SIAM J. Num. Anal.*, 13:564, 1976.

[5] A. Bayliss, K. E. Jordan, B. J. LeMesurier, and E. Turkel. A fourth-order accurate finite difference scheme for the computation of elastic waves. *Bull. Seis. Soc. Amer.*, 76:1115–1132, 1986.

[6] M. J. Berger and R. J. LeVeque. Adaptive mesh refinement for two-dimensional hyperbolic systems and the AMRCLAW software. in preparation.

[7] R. P. Beyer and R. J. LeVeque. Analysis of a one-dimensional model for the immersed boundary method. *SIAM J. Num. Anal.*, 29:332–364, 1992.

[8] D. M. Boore. Finite-difference methods for seismic wave propagation in heterogeneous materials. II ed. Bolt B.A., Academic Press, London, 1972.

[9] Max Born and Emil Wolf. *Principles of Optics.* Pergamon Press, Great Britain, 1980.

[10] M. Bouchon, M. Campillo, and S. Gaffet. A boundary integral equation – discrete wavenumber representation method to study wave propagation in multilayered media having irregular interfaces. *Geophysics*, 54:1134–1140, 1989.

[11] D. L. Brown. A note on the numerical solution of the wave equation with piecewise smooth coefficients. *Math. Comput.*, 42:369–391, 1984.

[12] Shunhua Cao and Stewart Greenhalgh. Finite-difference simulation of p-sv-wave propagation : A displacement-potential approach. *Geophys. J. Int.*, 109:525–535, 1992.

[13] C. L. Card and M. B. Allen. Difference approximations for wave equations via finite elements: I. Construction and performance. *Numer. Meth. PDE*, 11:127–146, 1995.

[14] C. L. Card and M. B. Allen. Difference approximations for wave equations via finite elements: II. Error analysis. *Numer. Meth. PDE*, 11:147–163, 1995.

[15] A. Q. Filho E. Tessmer A. Behle D. Kosloff, D. Kessler and R. Strahilevitz. Solution of the equations of dynamic elasticity by a chebychev spectral method. *Geophys. J. Int.*, 55:734–748, 1990.

[16] J. L Davis. *Wave Propagation in Solids and Fluids.* Springer, New York, 1988.

[17] P. P. Delsanto, R. S. Schecter, H. H. Chaskelis, R. B. Mignogna, and R. Kline. Connection machine simulation of ultrasonic wave propagation in materials. ii: the two-dimensional case. *Wave Motion*, 20:295–314, 1994.

[18] Todd Dupont. l^2-estimates for galerkin methods for second order hyperbolic equations. *SIAM J. Num. Anal.*, 10:880, 1973.

[19] M. B. Porter F. B. Jensen, W. A. Kuperman and H. Schmidt. *Computational Ocean Acoustics.* American Institute of Physics, New York, 1994.

[20] B. Fornberg. The pseudospectral method: accurate representation of interfaces in elastic wave calculations. *Geophysics*, 53:625–637, 1988.

[21] M. H. Freeman. *Optics.* Butterworths, London, 1990.

[22] Y. C. Fung. *Fundation of Solid Mechanics.* Prentice-Hall, 1965.

[23] David Gubbins. *Seismology and Plate Tectonics.* Cambridge University Press, 1992.

[24] R. E. Ewing J. S. Sochacki, J. H. George and S. B. Smithson. Interface conditions for acoustic and elastic wave propagation. *Geophys. J. Int.*, 56(2):168–181, 1991.

[25] G. A. McMechan J. Wen and M. W. Booth. Three-dimensional modeling and migration of seismic data using fourier transforms. *Geophys. J. Int.*, 53:1194–1201, 1988.

[26] F. B. Jensen, W. A. Kuperman, M. B. Porter, and H. Schmidt. *Computational Ocean Acoustics.* American Institute of Physics, New York, 1993.

[27] K. R. Kelly, R. W. Ward, S. Treitel, and R. M. Alford. Synthetic seismograms: a finite difference approach. *Geophysics*, 41:2–27, 1976.

[28] J. Kevorkian. *Partial Differential Equations.* Wadsworth & Brooks/Cole, 1990.

[29] R. G. Keys. Absorbing boundary conditions for acoustic media. *Geophys. J. Int.*, 50:892–902, 1985.

[30] D. Kosloff and E. Baysal. Forward modeling by a fourier method. *Geophys. J. Int.*, 47:1402–1412, 1982.

[31] W. J. Lamb, X. Zhu, G. A. McMechan, M. L. Greenberg, and J. P. Castagna. Elastic wave propagation in composite media. *Geophysics*, 57:1155–1165, 1992.

[32] A. R. Levander. Fourth-order finite-difference p–sv seismograms. *Geophysics*, 53:1425–1436, 1988.

[33] R. J. LeVeque. CLAWPACK software. available from `netlib.att.com` in `netlib/pdes/claw` or on the Web at the URL `http://www.amath.washington.edu/~rjl/clawpack.html`.

[34] R. J. LeVeque. CLAWPACK User Notes. available from `netlib.att.com` in `netlib/pdes/claw/doc` or on the Web at the URL `http://www.amath.washington.edu/~rjl/clawpack.html`.

[35] R. J. LeVeque. *Numerical Methods for Conservation Laws.* Birkhäuser-Verlag, 1990.

[36] R. J. LeVeque. CLAWPACK — a software package for solving multi-dimensional conservation laws. In *Proc. 5'th Int'l Conf. Hyperbolic Problems*, 1994. (`ftp://amath.washington.edu/pub/rjl/papers/hyp94.ps.Z`).

[37] R. J. LeVeque. High-resolution conservative algorithms for advection in incompressible flow. *SIAM J. Numer. Anal.*, to appear, 1995. (UW Applied Math Tech Report 93-03, `ftp://amath.washington.edu/pub/rjl/papers/advection.ps.Z`).

[38] R. J. LeVeque. Wave propagation algorithms for multi-dimensional hyperbolic systems. submitted, 1995.

[39] R. J. LeVeque. Wave propagation algorithms for multi-dimensional hyperbolic systems. submitted, 1995. (ftp://amath.washington.edu/pub/rjl/papers/rjl:wpalg.ps.Z).

[40] R. J. LeVeque and Z. Li. Immersed interface methods for Stokes flow with elastic boundaries or surface tension. to appear in SIAM J. Sci. Comput. (ftp://amath.washington.edu/pub/rjl/papers/rjl-li:stokes.ps.Z).

[41] R. J. LeVeque and Z. Li. The immersed interface method for elliptic equations with discontinuous coefficients and singular sources. *SIAM J. Num. Anal.*, 31:1019–1044, 1994.

[42] R. J. LeVeque and C. Zhang. Immersed interface methods for wave equations with discontinuous coefficients. submitted. (ftp://amath.washington.edu/pub/rjl/papers/rjl-zhang:acou.ps.Z).

[43] R. J. LeVeque and C. Zhang. Finite difference methods for wave equations with discontinuous coefficients. In S. Sture, editor, *Proc. 1995 ASCE Conference*, to appear. (ftp://amath.washington.edu/pub/rjl/papers/rjl-zhang:asce95).

[44] Z. Li. *The Immersed Interface Method — A Numerical Approach for Partial Differential Equations with Interfaces.* PhD thesis, University of Washington, 1994. (ftp://math.ucla.edu/pub/zhilin/Papers/thesis.ps.Z).

[45] Z. Li. Immersed interface methods for one-dimensional moving interface problems. CAM Report #95-01, UCLA, (submitted), 1995. (ftp://math.ucla.edu/pub/zhilin/Papers/1d.ps.Z).

[46] Z. Li. A note on immersed interface methods for three dimensional elliptic equations. *Computers Math. Appl.*, to appear. (`ftp://math.ucla.edu/pub/zhilin/Papers/3d.ps.Z`).

[47] Z. Li and A. Mayo. ADI methods for heat equations with discontinuties along an arbitrary interface. *Proc. Symp. Appl. Math.*, 48:311–316, 1994.

[48] John Lysmer and Lawrence A. Drake. A finite element for seismology. Methods of Computational Physics, II , B.A. Bolt, Ed. Academic Press, New York, 1972.

[49] M. Edwards M. Reshef, D. kosloff and C. Hsiung. Three-dimensional elastic modeling by the fourier method. *Geophys. J. Int.*, 53:1184–1193, 1988.

[50] R. Madariaga. Dynamics of an expanding circular fault. *Bull. Seism. Soc. Am.*, 66:163–182, 1976.

[51] A. Mayo. On the rapid evaluation of heat potentials on general regions. IBM Technical report 14305.

[52] F. Muir, J. Dellinger, J. Etgen, and D. Nichols. Modeling elastic fields across irregular boundaries. *Geophysics*, 57:1189–1193, 1992.

[53] C. S. Peskin. Numerical analysis of blood flow in the heart. *J. Comput. Phys.*, 25:220–252, 1977.

[54] C. S. Peskin. Lectures on mathematical aspects of physiology. *Lectures in Appl. Math.*, 19:69–107, 1981.

[55] A. Sei. A family of numerical schemes for the computation of elastic waves. Technical Report TR93-07, Department of Computational and Applied Mathematics, Rice University, 1993.

[56] A. Sei and W. W. Symes. Error analysis of numerical schemes for the wave equation in heterogeneous media. *Appl. Numer. Meth.*, 15:465–480, 1994.

[57] W. D. Smith. The application of finite-element analysis to body wave. *Geophys. J. Royal Astronom. Soc.*, 42:747, 1975.

[58] J. S. Sochacki, J. H. George, R. E. Ewing, and S. B. Smithson. Interface conditions for acoustic and elastic wave propagation. *Geophysics*, 56:168–181, 1991.

[59] A. N. Tikhonov and A. A. Samarskii. Homogeneous difference schemes. *USSR Comput. Math. and Math. Phys.*, 1:5–67, 1962.

[60] Jukka Tuomela. Fourth-order schemes for the wave equations, maxwell equations, and linerized elastodynamic equations. *Numerical Methods for Partial Differential Equations*, (10):33–63, 1994.

[61] J. Virieux. P-SV wave propagation in heterogeneous media: velocity-stress finite-difference method. *Geophysics*, 51:889–901, 1986.

[62] A. Wiegmann and K. P. Bube. The immersed interface method for nonlinear differential equations with discontinuous coefficients and singular sources. Submitted to SIAM J. Numer. Anal.

[63] G. Wojcik, J. Mould, Jr., R. Ferguson, and K. K. Low. Some image modeling issues for I-line, 5x phase shifting masks. In *SPIE Proceedings Vol 2197: Optical/Laser Microlithography VII*. SPIE, 1994.

[64] G. L Wojcik, D. K. Vaughan, N. Abboud, and J. Mould, Jr. Electromechanical modeling using explicit time-domain finite elements. In *IEEE Ultrasonics Symposium Proceedings*. IEEE, 1993.

Appendix A

EQUATIONS OF ACOUSTICS

A.1 Equations of Acoustics

The derivation of the acoustic wave equation can be obtained as a special case of elastic wave equation, which is given in Section 6.1. We start with equation (6.11) of the elasticity

$$\begin{aligned}
v_{1t} &= \frac{1}{\rho}\Big(\sigma_{11x} + \sigma_{12y}\Big) \\
v_{2t} &= \frac{1}{\rho}\Big(\sigma_{12x} + \sigma_{22y}\Big) \\
\sigma_{11t} &= (\lambda + 2\mu)v_{1x} + \lambda v_{2y} \\
\sigma_{12t} &= \mu(v_{1y} + v_{2x}) \\
\sigma_{22t} &= \lambda v_{1x} + (\lambda + 2\mu)v_{2y}.
\end{aligned}$$

In the special case of $\mu = 0$, from equation (6.8) we have $\sigma_{11} = \sigma_{22}$, and $\sigma_{12} = 0$, (i.e., no shear tensor). Then the third and fifth equations are identical, while the fourth equation becomes an identity. Setting

$$p = -\sigma_{11}$$

and using $\kappa = \lambda + \frac{2}{3}\mu = \lambda$ instead of λ, we get the acoustic wave equation

$$\begin{aligned}
&\rho u_t + p_x = 0 \\
&\rho v_t + p_y = 0 \qquad\qquad (A.1) \\
&p_t + \kappa(u_x + v_y) = 0,
\end{aligned}$$

where u and v have been used in place of v_1 and v_2 respectively. Independent of the coordinate system, equation (A.1) becomes

$$\begin{aligned} \rho\vec{v}_t + \bigtriangledown p &= 0 \\ p_t + \kappa \bigtriangledown \cdot \vec{v} &= 0, \end{aligned} \tag{A.2}$$

These vector equations for acoustics are valid for three spatial dimensions as well.

Appendix B

CONSERVATION LAWS PACKAGE

B.1 High resolution methods

The procedure described in this paper yields a 6-point stencil which can be used at the irregular points where a standard finite difference method would break down. Away from the interface, any standard method with second order accuracy can be used. We have discussed the simple Lax-Wendroff method, but in the examples given in Chapter 4 and 6 we have instead used a high resolution multi-dimensional flux limiter method of the sort developed for multi-dimensional nonlinear systems of conservation laws, particularly in the field of gas dynamics (*e.g.*, [35]). The particular algorithm used is the wave-propagation method described in [36, 39] and implemented in the CLAWPACK (Conservation LAWs PACKage) software available from `netlib` [33]. A description of these algorithms, including applications to acoustic equations, can be found in [39], which includes a discussion of acoustic equations with discontinuous coefficients. See also the CLAWPACK User Notes[34].

For more general interfaces, CLAWPACK is coupled with the special methods developed in this paper. The CLAWPACK algorithm is a finite volume method, meaning that each value U_{ij} is viewed as a cell average over a grid cell of size h^2 centered at the point (x_i, y_j). Each cell average is updated due to waves that propagate into the cell, as determined by the solution of Riemann problems at the four edges of these cells, and also the eight edges between cells that are adjacent to cell (i, j). Hence the method has at least a 9-point stencil. In addition, a flux-limiter can be used to eliminate oscillations in the solution due to the dispersive nature of the second order method. The use of these limiters extends the stencil out one more point in each coordinate direction, giving a 13-point stencil.

In practice, however, we have found that it is necessary to use the special stencils derived in this paper only at grid points for which the 9-point stencil crosses the interface. If the limiter uses a point on the wrong side of the interface, it is not catastrophic provided that the limiter is not allowed to *increase* the magnitude of a jump based on information from the neighboring Riemann problem. In other words the limiter function must lie between 0 and 1. Thus, we have used the minmod limiter in these experiments. (See [37] and [39] for discussions of limiters.) A limiter such as superbee, which often gives sharper discontinuities in other problems, can lead to oscillations and poor performance near the interface in the present context.

Moreover, at a point where the 9-point stencil crosses the interface but the 5-point stencil used by the Lax-Wendroff formula (4.8) does not, we can use (4.8). Thus the special 6-point formulas developed in Chapter 4 are needed only at points where the standard Lax-Wendroff method cannot be used.

Using CLAWPACK rather than the standard Lax-Wendroff method over most of the grid has several advantages. It is more stable than Lax-Wendroff and allows a time step k for which $ck/h \leq 1$ (*i.e.*, up to Courant number 1). Lax-Wendroff is stable only for $ck/h < 0.7$ roughly (see [39]). The wave propagation approach is also slightly more accurate than Lax-Wendroff when no limiters are used, and gives a great reduction in dispersive oscillations and phase errors with the use of limiters. Finally, the wave propagation methods allow one to simply extrapolate the solution at computational boundaries where non-reflecting computational boundary conditions are desired. Though not perfect, this gives a very reasonable solution with very little work. This is discussed further in [34].

In practice we use the following approach to advance the solution by one time step. The time step is first taken with CLAWPACK, updating the solution at all points on the grid based on assuming that the coefficients are piecewise constant in each grid cell. Then, for any irregular cells as defined above, we recompute a value based on either (4.8), (6.31) (for the elasticity case) or the special 6-point stencil.

Appendix C

SOME DISCUSSION ABOUT THE IMPLEMENTATIONS

C.1 Six Point Stencil

For a scheme with a six point stencil, we have the freedom of choosing any one of the four corner points. We can choose the same corner (for example, the upper right corner point) as the sixth point for all the irregular points, or we can choose different corners for different irregular points. Any selection will give second order accuracy. Another possibility is to use four corners. Let us consider equation (4.9), again dropping the indices i, j and n on the right hand side for concreteness. The difference methods at an irregular point is given by

$$U_{ij}^{n+1} = U + \frac{k}{h}\sum_{l=1}^{6}\Gamma_l^{(s)}U_l^{(s)},$$

where the superscript s ($s = 1,\ \ldots,\ 4$) of Γ is introduced to indicate the four corner points as the possible choices of the sixth point. We can compute the Γ's for the four different selections, and use the weighted sum of Γ's to form the difference method. Let the weight functions be w_s, with $\sum_{s=1}^{4} w_s = 1$. Note that the choice of the other five points is not affected by the choice of the sixth point, then we have

$$U_{ij}^{n+1} = U + \frac{k}{h}\left(\sum_{s=1}^{4}\sum_{l=1}^{5} w_s\Gamma_l^{(s)}U_l + \sum_{s=1}^{4} w_s\Gamma_l^{(s)}U_6^{(s)}\right),$$

or

$$U_{ij}^{n+1} = U + \frac{k}{h}\left(\sum_{l=1}^{5}\left(\sum_{s=1}^{4} w_s\Gamma_l^{(s)}\right)U_l + \sum_{s=1}^{4} w_s\Gamma_l^{(s)}U_6^{(s)}\right).$$

Letting

$$\Gamma_l = \sum_{s=1}^{4} w_s\Gamma_l^{(s)} \qquad (l = 1,\ \ldots,\ 5),$$

we get

$$U_{ij}^{n+1} = U + \frac{k}{h}\sum_{l=1}^{5}\Gamma_l U_l + \sum_{s=1}^{4} w_s \Gamma_l^{(s)} U_6^{(s)}.$$

In particular, with an obvious choice of the weights $w_s = 1/4 \quad (\forall s)$, we can simplify the above expression to get

$$U_{ij}^{n+1} = U + \frac{k}{h}\sum_{l=1}^{5}\Gamma_l U_l + \frac{1}{4}\sum_{s=1}^{4} \Gamma_l^{(s)} U_6^{(s)},$$

where

$$\Gamma_l = \frac{1}{4}\sum_{s=1}^{4}\Gamma_l^{(s)} \qquad (l = 1,\ ...,\ 5).$$

We need to compute four sets of Γ's, but since this is computed only once before time stepping, it is a one-time cost. In each time step, we also need to have three more matrix multiplications for each irregular point. The advantage is that we get a symmetric stencil in the sense that we do not favor any particular corner point. This gives somewhat better solutions in general.

Another choice is to pick the sixth point from the four corners at random. For example, for the kth irregular point, the sixth point can be chosen as a random function $r(k)$ $(r(k) \in \{1,\ 2,\ 3,\ 4\})$. In this way no particular corner will be favored against any other. The advantage of this choice is that the computation cost will not increase at all while a kind of symmetry in the stencil is achieved.

A scheme with a nine-point stencil could be used. In addition to eliminating the terms of U and its first and second order derivatives, the inclusion of the other three corner points would allow us to get rid of three of the four third-order derivatives of U $(U_{\xi\xi\xi}, U_{\xi\xi\eta}, U_{\xi\eta\eta}$ and $U_{\eta\eta\eta})$. This would improve the accuracy. Actually it will be a different scheme, still giving a second order accuracy, but with the cost increasing significantly.

VITA

Name: Chaoming Zhang

Date of Birth: March 2, 1961

Place of Birth: Zhejiang Province, China

Education

Fudan University, Shanghai, China

B.S. in Mathematics, 1982.

Shanghai Jiaotong University, Shanghai, China

M.S. in Engineering Mechanics, 1985.

Employment

Beijing Control Device Institute, Beijing, China

Structural Engineer, 1985-1990.

Yanan Education Institute, Yanan, China

Visiting Lecturer, 1986-1987.